DOT/FAA/AR-04/40,P1

Office of Aviation Research
Washington, D.C. 20591

Explicit Finite Element Modeling of Multilayer Composite Fabric for Gas Turbine Engine Containment Systems

Part 1: Static Tests and Modeling

November 2004

Final Report

U.S. Department of Transportation
Federal Aviation Administration

NOTICE

Technical Report Documentation Page

1. Report No.	2. Government Accession No.	3. Recipient's Catalog No.
DOT/FAA/AR-04/40,P1		

4. Title and Subtitle	5. Report Date
EXPLICIT FINITE ELEMENT MODELING OF MULTILAYER COMPOSITE FABRIC FOR GAS TURBINE ENGINE CONTAINMENT SYSTEMS PART 1: STATIC TESTS AND MODELING	November 2004
	6. Performing Organization Code

7. Author(s)	8. Performing Organization Report No.
S. D. Rajan, Barzin Mobasher, Jignesh Sharda, Venkat Yanna, Chaitanya Deenadaylu, David Lau, and Dhaval Shah	

9. Performing Organization Name and Address	10. Work Unit No. (TRAIS)
Department of Civil & Environmental Engineering Arizona State University Tempe, AZ 85287-5306	11. Contract or Grant No. 01-C-AW-ASU

12. Sponsoring Agency Name and Address	13. Type of Report and Period Covered
U.S. Department of Transportation Federal Aviation Administration FAA William J. Hughes Technical Center Atlantic City International Airport, NJ 08405	Final Report 8/2001 – 5/2003
	14. Sponsoring Agency Code ANE-100

15. Supplementary Notes

The FAA William J. Hughes Technical Center COTR was Donald Altobelli.

16. Abstract

Under the Federal Aviation Administration's Airworthiness Assurance Center of Excellence and with support from the Aircraft Catastrophic Failure Prevention Program, the team consisting of Arizona State University, Honeywell Engines, Systems & Services, National Aeronautics and Space Administration Glenn Research Center, and SRI International collaborated to develop testing procedures and computational models for designing and evaluating ballistic fabric turbine engine containment structures. This report contains the details of the static tests and their finite element simulations carried out at Arizona State University.

17. Key Words	18. Distribution Statement
Aircraft engine fragments, Containment, Zylon, Kevlar, Finite element analysis, Ballistic testing, Static testing	This document is available to the public through the National Technical Information Service (NTIS) Springfield, Virginia 22161.

19. Security Classif. (of this report)	20. Security Classif. (of this page)	21. No. of Pages	22. Price
Unclassified	Unclassified	115	

ACKNOWLEDGEMENTS

The investigators wish to thank Mr. William Emmerling, Mr. Donald Altobelli, Mr. Chet Lewis, and Dr. Xiaogong Lee of the Federal Aviation Administration for their technical and financial support. In order to meet the objectives of this project we have relied heavily on the technical collaborations with several other organizations that include Honeywell Engines & Systems Phoenix, SRI International, and NASA Glenn Research Center. Some of the individuals who contributed immensely to this project include Dr. Shen Yeh Chen, Mr. Reha Gomuc, Mr. Wil Baker, and Mr. Jack Robinson of Honeywell; Dr. Don Shockey, Dr. Jeff Simons, and Mr. Dave Erlich of SRI International; and Mr. J. M. Pereira and Mr. Duane Revilock of NASA Glen Research Center. Their support and cooperation in meeting the research objectives was greatly appreciated.

TABLE OF CONTENTS

		Page
EXECUTIVE SUMMARY		xv
1.	INTRODUCTION	1-1
1.1	Purpose	1-1
1.2	Background	1-1
2.	TENSION TESTS	2-1
2.1	Objectives	2-1
2.2	Specimen Preparation Procedure	2-1
2.2.1	Area Properties	2-1
2.2.2	End Tabs	2-1
2.2.3	End Plates	2-2
2.3	Test Procedure and Results	2-3
3.	SPLICE TESTS	3-1
3.1	Objectives	3-1
3.2	Specimen Preparation Procedure	3-1
3.3	Test Procedure	3-1
3.4	Test Results	3-2
4.	STATIC TESTS	4-1
4.1	Objectives	4-1
4.2	Specimen Preparation Procedure	4-1
4.3	Test Setup	4-3
4.4	Test Procedure	4-7
4.5	Test Results	4-8
5.	FINITE ELEMENT MODELING	5-1
5.1	Objectives	5-1
5.2	Tension Test Models	5-2
5.3	Finite Element Analysis of Static Test Models	5-6
5.3.1	One-Layer Kevlar Model	5-9
5.3.2	Two-Layer Kevlar Model	5-12
5.3.3	Four-Layer Kevlar Model	5-14
5.3.4	Eight-Layer Kevlar Model	5-17

5.3.5 Twenty-Four-Layer Kevlar Model 5-19
5.3.6 One-Layer Zylon Model 5-22
5.3.7 Two-Layer Zylon Model 5-26
5.3.8 Four-Layer Zylon Model 5-30
5.3.9 Eight-Layer Zylon Model 5-34
5.3.10 Twenty-Four-Layer Zylon Model 5-38

5.4 Energy Absorption Comparisons 5-42

6. CONCLUSIONS 6-1

7. REFERENCES 7-1

APPENDIX A—STATIC TEST RESULTS

LIST OF FIGURES

Figure		Page
2-1	Zylon Specimens (T1)	2-2
2-2	Kevlar Specimens (T1)	2-2
2-3	Test Setup With Specimen	2-2
2-4a	End Plates for Gripping (T2)	2-3
2-4b	Side View (T2)	2-3
2-4c	Inner View of the Grip Assembly (T2)	2-3
2-5a	Load vs Actuator Stroke (KTest1) (Grip T1)	2-4
2-5b	Stress vs Strain Diagram (KTest1) (Grip T1)	2-4
2-6a	Load vs Actuator Stroke (KTest2) (Grip T1)	2-5
2-6b	Stress vs Strain Diagram (KTest2) (Grip T1)	2-5
2-7a	Load vs Actuator Stroke (KSwath1) (Grip T2)	2-6
2-7b	Stress vs Strain Diagram (KSwath1) (Grip T2)	2-6
2-8a	Load vs Actuator Stroke (KSwath2) (Grip T2)	2-7
2-8b	Stress vs Strain Diagram (KSwath2) (Grip T2)	2-7
2-9a	Load vs Actuator Stroke (ZTest1) (Grip T1)	2-8
2-9b	Stress vs Strain Diagram (ZTest1) (Grip T1)	2-8
2-10a	Load vs Actuator Stroke (ZTest2) (Grip T1)	2-9
2-10b	Stress vs Strain Diagram (ZTest2) (Grip T1)	2-9
2-11a	Load vs Actuator Stroke (ZSwath1) (Grip T2)	2-10
2-11b	Stress vs Strain Diagram (ZSwath1) (Grip T2)	2-10
2-12a	Load vs Actuator Stroke (ZSwath2) (Grip T2)	2-11
2-12b	Stress vs Strain Diagram (ZSwath2) (Grip T2)	2-11
2-13	Stress vs Strain Diagrams for All Kevlar Specimens	2-12

2-14	Stress vs Strain Diagrams for All Zylon Specimens	2-12
2-15	Kevlar Specimen (T2)	2-14
2-16	Failure at Center (T2)	2-14
2-17	Zylon Specimen (T2)	2-14
2-18	Failure at the Edge (T2)	2-14
3-1a	Load vs Deflection (GTestk4_oe) (LVDT)	3-3
3-1b	Stress vs Strain Diagram (GTestk4_oe) (LVDT)	3-3
3-2a	Load vs Deflection (GTestk4_ne) (LVDT)	3-4
3-2b	Stress vs Strain Diagram (GTestk4_ne) (LVDT)	3-4
3-3	Load vs Actuator Stroke (GTestk6_ne) (Actuator)	3-5
3-4a	Load vs Deflection (GTestz4_oe) (LVDT)	3-5
3-4b	Stress vs Strain Diagram (GTestz4_oe) (LVDT)	3-6
4-1	Test Setup	4-1
4-2a	Mandrel for Specimen Preparation	4-2
4-2b	Specimen Transfer Ring	4-2
4-3	Blunt Nose With Bearings	4-3
4-4	Attachment of C-Clamps to the Specimen	4-4
4-5	Top Plate With Bearings Orthogonal to Nose Bearings (Fixed-End Condition at Top)	4-5
4-6a	Schematic Diagram of the Test Setup	4-6
4-6b	Schematic of Test Setup With Clamps and Hinges to Remove Spurious Loads	4-6
4-6c	Revised Blunt Nose Housing Design (Fixed-Fixed Conditions)	4-7
4-7	Load-Deformation Response of Single-Layer Kevlar Specimens Prior to Slack Adjustment	4-8
4-8	Load-Deformation Response of Single-Layer Kevlar Samples After Slack Adjustment	4-9

4-9	Load-Deformation Response of 1-, 2-, 4-, 8-, and 24-Layer Kevlar Samples	4-10
4-10	Load-Deformation Response of 1-, 2-, 4-, 8-, and 24-Layer Zylon Samples	4-11
4-11	Energy-Absorbed/Areal Density Graphs of 1-, 2-, 4-, 8-, and 24-Layer Kevlar and Zylon Samples	4-12
4-12	Energy-Absorbed/Areal Density Graphs of 1-, 2-, 4-, 8-, and 24-Layer Kevlar and Zylon Samples Normalized by Number of Layers	4-12
4-13	Number of Layers vs Peak Load for All Tests	4-13
4-14	Number of Layers vs Normalized Peak Load for All Tests	4-13
4-15	Number of Layers vs Stiffness for All Tests (Actual and Linearly Extrapolated)	4-14
4-16	Number of Layers vs Normalized Stiffness for All Tests (Actual and Linearly Extrapolated)	4-14
5-1	User-Supplied Piecewise Linear Stress-Strain Curve for Kevlar (KTest1)	5-3
5-2a	Piecewise Linear Stress-Strain Curve for Zylon (ZTest1, Grip T1)	5-4
5-2b	Piecewise Linear Stress-Strain Curve for Zylon (ZSwath1, Grip T2)	5-5
5-3	Geometric Model Showing Quarter Model of the Static Test Setup	5-6
5-4	Finite Element Mesh	5-7
5-5	Details of the FE Mesh Showing the Blunt Nose, Steel Cylinder, and the Fabric	5-7
5-6a	Boundary Conditions Imposed on the Bottom of the Steel Cylinder and at the Position of the Clamps	5-8
5-6b	Boundary Conditions Imposed at the Bottom of the Blunt Nose	5-8
5-7	Comparison of the Load-Displacement Graphs for a One-Layer Kevlar Test	5-9
5-8	One-Layer Kevlar—Plot of In-Plane Strain ε_1 Superimposed on Deformation at the End of the Last Load Step	5-11
5-9	One-Layer Kevlar—Plot of in-Plane Strain ε_2 Superimposed on Deformation at the End of the Last Load Step	5-11
5-10	Comparison of the Load-Displacement Graphs for a Two-Layer Kevlar Test	5-12
5-11	Two-Layer Kevlar—Plot of in-Plane Strain ε_1 Superimposed on Deformation at the End of the Last Load Step	5-13

5-12 Two-Layer Kevlar—Plot of in-Plane Strain ε_2 Superimposed on Deformation at the End of the Last Load Step 5-14

5-13 Comparison of the Load-Displacement Graphs for a Four-Layer Kevlar Test 5-14

5-14 Four-Layer Kevlar—Plot of In-Plane Strain ε_1 Superimposed on Deformation at the End of the Last Load Step 5-16

5-15 Four-Layer Kevlar—Plot of In-Plane Strain ε_2 Superimposed on Deformation at the End of the Last Load Step 5-16

5-16 Comparison of the Load-Displacement Graphs for an Eight-Layer Kevlar Test 5-17

5-17 Eight-Layer Kevlar—Plot of In-Plane Strain ε_1 Superimposed on Deformation at the End of the Last Load Step 5-18

5-18 Eight-Layer Kevlar—Plot of In-Plane Strain ε_2 Superimposed on Deformation at the End of the Last Load Step 5-19

5-19 Comparison of the Load-Displacement Graphs for a 24-Layer Kevlar Test 5-19

5-20 Twenty-Four-Layer Kevlar—Plot of In-Plane Strain ε_1 Superimposed on Deformation at the End of the Last Load Step 5-21

5-21 Twenty-Four-Layer Kevlar—Plot of In-Plane Strain ε_2 Superimposed on Deformation at the End of the Last Load Step 5-21

5-22 Comparison of the Load-Displacement Graphs for a One-Layer Zylon Test 5-22

5-23 One-Layer Zylon—Plot of In-Plane Strain ε_1 Superimposed on Deformation at the End of the Last Load Step (Grip T1) 5-24

5-24 One-Layer Zylon—Plot of In-Plane Strain ε_2 Superimposed on Deformation at the End of the Last Load Step (Grip T1) 5-24

5-25 One-Layer Zylon—Plot of In-Plane Strain ε_1 Superimposed on Deformation at the End of the Last Load Step (Grip T2) 5-25

5-26 One-Layer Zylon—Plot of In-Plane Strain ε_2 Superimposed on Deformation at the End of the Last Load Step (Grip T2) 5-25

5-27 Comparison of the Load-Displacement Graphs for a Two-Layer Zylon Test 5-26

5-28 Two-Layer Zylon—Plot of In-Plane Strain ε_1 Superimposed on Deformation at the End of the Last Load Step (Grip T1) 5-28

5-29 Two-Layer Zylon—Plot of In-Plane Strain ε_2 Superimposed on Deformation at the End of the Last Load Step (Grip T1) 5-28

5-30 Two-Layer Zylon—Plot of In-Plane Strain ε_1 Superimposed on Deformation at the End of the Last Load Step (Grip T2) 5-29

5-31 Two-Layer Zylon—Plot of In-Plane Strain ε_2 Superimposed on Deformation at the End of the Last Load Step (Grip T2) 5-29

5-32 Comparison of the Load-Displacement Graphs for a Four-Layer Zylon Test 5-30

5-33 Four-Layer Zylon—Plot of In-Plane Strain ε_1 Superimposed on Deformation at the End of the Last Load Step (Grip T1) 5-32

5-34 Four-Layer Zylon—Plot of In-Plane Strain ε_2 Superimposed on Deformation at the End of the Last Load Step (Grip T1) 5-32

5-35 Four-Layer Zylon—Plot of In-Plane Strain ε_1 Superimposed on Deformation at the End of the Last Load Step (Grip T2) 5-33

5-36 Four-Layer Zylon—Plot of In-Plane Strain ε_2 Superimposed on Deformation at the End of the Last Load Step (Grip T2) 5-33

5-37 Comparison of the Load-Displacement Graphs for an Eight-Layer Zylon Test 5-34

5-38 Eight-Layer Zylon—Plot of In-Plane Strain ε_1 Superimposed on Deformation at the End of the Last Load Step (Grip T1) 5-36

5-39 Eight-Layer Zylon—Plot of In-Plane Strain ε_2 Superimposed on Deformation at the End of the Last Load Step (Grip T1) 5-36

5-40 Eight-Layer Zylon—Plot of In-Plane Strain ε_1 Superimposed on Deformation at the End of the Last Load Step (Grip T2) 5-37

5-41 Eight-Layer Zylon—Plot of In-Plane Strain ε_2 Superimposed on Deformation at the End of the Last Load Step (Grip T2) 5-37

5-42 Comparison of the Load-Displacement Graphs for a 24-Layer Zylon Test 5-38

5-43 Twenty-Four-Layer-Zylon—Plot of In-Plane Strain ε_1 Superimposed on Deformation at the End of the Last Load Step (Grip T1) 5-39

5-44 Twenty-Four-Layer-Zylon—Plot of In-Plane Strain ε_2 Superimposed on Deformation at the End of the Last Load Step (Grip T1) 5-39

5-45 Twenty-Four-Layer Zylon—Plot of In-Plane Strain ε_1 Superimposed on Deformation at the End of the Last Load Step (Grip T2) 5-40

5-46 Twenty-Four-Layer Zylon—Plot of In-Plane Strain ε_2 Superimposed on Deformation at the End of the Last Load Step (Grip T2) 5-40

5-47 Energy-Absorbed/Areal Density Graphs for 1-, 2-, 4-, 8-, and 24-Layer Kevlar Samples 5-43

5-48 Energy-Absorbed/Areal Density Graphs of 1-, 2-, 4-, 8-, and 24-Layer Kevlar Normalized by the Number of Layers 5-44

5-49 Energy-Absorbed/Areal Density Graphs for 1-, 2-, 4-, 8-, and 24-Layer Zylon Samples 5-44

5-50 Energy-Absorbed/Areal Density Graphs of 1-, 2-, 4-, 8-, and 24-Layer Zylon Normalized by the Number of Layers 5-45

5-51 Energy-Absorbed/Areal Density Graphs for all Kevlar and Zylon Samples 5-45

5-52 Energy-Absorbed/Areal Density Graphs for all Kevlar and Zylon Samples Normalized by the Number of Layers 5-46

LIST OF TABLES

Table		Page
2-1	Basic Material Properties	2-1
2-2	Summary of Test Results	2-13
3-1	Kevlar Test Specimen Details	3-2
3-2	Splice Test Results	3-2
4-1	Summary of Static Test Conditions and Results	4-5
5-1	Piecewise Linear Kevlar Stress-Strain Data	5-3
5-2a	Piecewise Linear Zylon Stress-Strain Data (T1)	5-4
5-2b	Piecewise Linear Zylon Stress-Strain Data (T2)	5-5
5-3	Static Test—FEA Comparison for a One-Layer Kevlar Test	5-10
5-4	Static Test—FEA Comparison for a Two-Layer Kevlar Test	5-12
5-5	Static Test—FEA Comparison for a Four-Layer Kevlar Test	5-15
5-6	Static Test—FEA Comparison for an Eight-Layer Kevlar Test	5-17
5-7	Static Test—FEA Comparison for a 24-Layer Kevlar Test	5-20
5-8	Static Test—FEA Comparison for a One-Layer Zylon Test	5-22
5-9	Static Test—FEA Comparison for a Two-Layer Zylon Test	5-26
5-10	Static Test—FEA Comparison for a Four-Layer Zylon Test	5-30
5-11	Static Test—FEA Comparison for an Eight-Layer Zylon Test	5-34
5-12	Static Test—FEA Comparison for a 24-Layer Zylon Test	5-38
5-13	Summary of Energy Absorption Data (Prepeak) for Static Test and FE Simulations	5-43

LIST OF ACRONYMS

AACE	Airworthiness Assurance Center of Excellence
ASU	Arizona State University
c/s	Cross-section
FAA	Federal Aviation Administration
FE	Finite element
FEA	Finite element analysis
GRC	Glen Research Center
Honeywell	Honeywell Engines, Systems & Services
ID	Internal diameter
NASA	National Aeronautics and Space Administration
OD	Outer diameter
SRI	SRI International

EXECUTIVE SUMMARY

Modeling a multilayer fabric composite for engine containment systems during a fan blade-out event has been a challenging task. Nonlinear transient (explicit) finite element analysis (FEA) has the greatest potential of any numerical approach available to industry for analysis of these events. Significant research is still required to overcome difficulties with numerical stability, material modeling (pre- and postfailure), and standardizing modeling methods to achieve accurate simulation of the complex interactions between individual components during these high-speed events. The primary focus of this research was to develop the methodology for testing, modeling, and analyzing a typical fan blade-out event in a multilayer fiber fabric composite containment system. ABAQUS finite element code was used to verify the basic material model (prefailure state) developed through laboratory testing. LS-DYNA was the primary modeling tool used in the explicit FEA of ballistic events.

During the Fourth Federal Aviation Administration (FAA) Uncontained Engine Debris Characterization Modeling and Mitigation Workshop (held in May 2000 at SRI International, Menlo Park, CA), a representative of Honeywell Engines, Systems & Services presented the capability of modeling complicated engine hub-burst and fan blade-out events, predicting most of the event with high confidence was shown. At the same time, SRI presented their efforts on modeling the material characteristics within LS-DYNA and developing a new composite fiber material called Zylon® that appeared to be stronger, lighter, and more temperature-resistant than Kevlar®. Both parties showed interest in each other's work, and both agreed they could benefit from each other if collaborative mechanisms could be arranged. After the workshop, Honeywell and SRI contacted each other and began talks of a joint project. The FAA, National Aeronautics and Space Administration (NASA) Glenn Research Center (GRC), and Arizona State University (ASU) were later invited into the discussion, resulting in this FAA-funded research under the Aircraft Catastrophic Prevention Program and the Airworthiness Assurance Center of Excellence Program.

The goal of this research was to use the technical strengths of Honeywell, SRI, and the ASU for developing a robust explicit finite element analysis modeling methodology for the purposes mentioned above. Since the development of an experimental set of data to support the calibration of the finite element models was essential, various experimental methods to measure material and structural response of the fabrics were conducted. NASA GRC, under the NASA Aviation Safety Program, conducted a series of engine containment ring tests that were used for modeling in this program.

Each member of the team took a leadership role and developed a comprehensive report describing the details of the research task and the findings. The complete FAA report is comprised of the following four separate reports (parts 1 through 4).

- Part 1: Static Tests and Modeling by Arizona State University Department of Civil Engineering
- Part 2: Ballistic Testing by NASA Glenn Research Center
- Part 3: Material Model Development and Simulation of Experiments by SRI International

- Part 4: Model Simulation for Ballistic Tests, Engine Fan Blade-Out, and Generic Engine by Honeywell Engines, Systems & Services

This report contains the details of the static tests and their finite element simulations carried out by ASU.

1. INTRODUCTION.

1.1 PURPOSE.

This research effort was undertaken as a direct result of discussions from the Fourth Federal Aviation Administration (FAA) Uncontained Debris Characterization Modeling and Mitigation Workshop (held in May 2000 at SRI International). A teaming effort between academia, and industry was seen as an excellent opportunity to transition fabric modeling and testing research that was being sponsored by the FAA Aircraft Catastrophic Failure Prevention Program.

1.2 BACKGROUND.

During the Fourth FAA Uncontained Engine Debris Characterization Modeling and Mitigation Workshop, a representative of Honeywell Engines, Systems & Services presented the capability of modeling complicated engine hub-burst and fan blade-out events. Predicting most of the event with high confidence was shown. At the same time, SRI International presented their efforts on modeling the material characteristics within LS-DYNA and developing a new composite fiber material called Zylon®. Both parties showed interest in each other's work, and both agreed they could benefit from each other if collaborative mechanisms could be arranged. It was especially attractive that Zylon seemed to be stronger, lighter, and had better endurance under high temperature compared to Kevlar®. After the workshop, Honeywell and SRI contacted each other and began talks of a joint project. The FAA, National Aeronautics and Space Administration (NASA) Glenn Research Center (GRC), and Arizona State University (ASU) were later invited into the discussion, resulting in this FAA-funded research.

The goal of this research was to use the technical strengths of Honeywell, SRI, NASA GRC, and ASU for developing a robust explicit finite element analysis modeling methodology for the purposes mentioned above. Since the development of an experimental set of data to support the calibration of the finite element models is essential, various experimental methods to measure material and structural response of the fabrics were conducted. Some of the specific program objectives were as follows.

1. Couple LS-DYNA modeling and the engine expertise of Honeywell with the material modeling capability of SRI, the ballistic test capability of NASA GRC and the experimental facilities and finite element analysis/modeling capabilities of ASU.

2. Incorporate the material model developed by SRI into the LS-DYNA modeling methodology developed by Honeywell for controlled laboratory hardware test, developing new methodologies if necessary.

3. Develop methodologies for numerical simulation of engine fan blade-out events with composite fiber fabric wraps using SRI's material model and Honeywell's LS-DYNA modeling methodology. Calibrate the methodologies to the existing engine test results from Honeywell.

4. Compare the efficiency of Kevlar and Zylon wraps by laboratory hardware test and LS-DYNA for the test coupons.

5. Explore the potential of Zylon for future engine containment systems.

The reasons for including both Kevlar and Zylon in the project are as follows.

- Quantify back-to-back comparison of the two materials.

- Currently, there are no engine containment systems made of Zylon. However, Kevlar data are available from the existing hardware tests at Honeywell. For calibrating the analysis model for Kevlar, basic modeling techniques for Kevlar will need to be investigated.

- Having both Kevlar and Zylon analyzed for engine containment systems will provide a better understanding of the strength and weakness of both fabrics.

The research was divided into four tasks:

- Task 1: Static Tests and their FE modeling and simulation.
- Task 2: Ballistic Tests.
- Task 3: Finite element (FE) modeling and simulation of the Ballistic Tests.
- Task 4: FE modeling and simulation of a fan blade out condition for a generic engine.

This report deals with the details of the static tests. This entire report deals specifically with Kevlar 49® 17x17 fabric and Zylon AS® 35x35 fabric. Tension tests were conducted to develop the basic material properties, which are discussed in section 2. Section 3 presents the results from splice tests used in investigating the bond properties of the fabrics using different epoxies. The static tests of multiple-layer specimens wrapped around a ring and subjected to static load due to penetration of a blunt penetrator are discussed in section 4. This is followed by the finite element modeling and simulation of the static tests in section 5. A summary and suggestions for improvements are made in section 6. Additional photographs and load-deflection plots for the static tests are contained in appendix A.

2. TENSION TESTS.

Tension tests are used in creating the stress-strain curve for a material. These curves can then be used as a basis of a material model suitable for use in a finite element analysis.

2.1 OBJECTIVES.

The primary objective of these simple tension tests was to construct the engineering stress-strain diagram up to ultimate failure in the principal material direction for Kevlar 49 and Zylon AS fabrics.

2.2 SPECIMEN PREPARATION PROCEDURE.

The specimens were custom-made with their sides stitched (Lincoln Fabrics LTD, Canada). The dimensions and other properties of the specimens are provided in table 2-1.

TABLE 2-1. BASIC MATERIAL PROPERTIES

Material	Yarn Count	Bulk Density (lb/in^3)	Linear Density (lb/in.)	c/s Area per Yarn (in^2)	Specimen Size (in.)
Kevlar 49	17 x 17	0.00530516	$9.457(10^{-7})$	$1.78(10^{-4})$	2.5 x 12
Zylon AS	35 x 35	0.00567358	$3.175(10^{-7})$	$5.59(10^{-5})$	2.5 x 12

2.2.1 Area Properties.

The cross-section (c/s) area of each yarn was calculated by taking into account the linear density of the yarn material and dividing it by its bulk density. The total c/s area of the specimen was defined as the cross-sectional area per yarn multiplied by the number of yarns per inch of fabric times the total width of the fabric. The calculated c/s area values are shown in table 2-1.

2.2.2 End Tabs.

Initially, two Zylon specimens and two Kevlar specimens were tested. Flat, perforated, aluminum pieces, 2.5″ long by 2.5″ wide by 0.025″ thick, were used as end tabs. These tabs were attached to both the ends of the specimen using epoxy to ensure a firm grip in the testing machine. The arrangement is shown in figures 2-1 and 2-2. In the testing machine, these tabs were held in place under hydraulic pressure, as shown in figure 2-3. An alignment setup was prepared and used to ensure that the end pieces were aligned (parallel) and resulted in the same thickness, avoiding any eccentricity. Commercial-grade 5-minute epoxy consisting of a two-component resin and hardener was mixed in equal proportion by volume and used to glue the end tabs. The specimen was left for 24 hours at room temperature to cure. Tests conducted with this end tab arrangement are denoted in this report as Grip T1.

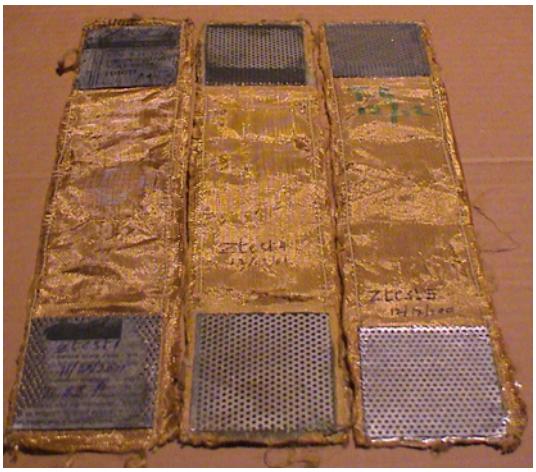

FIGURE 2-1. ZYLON SPECIMENS (T1)

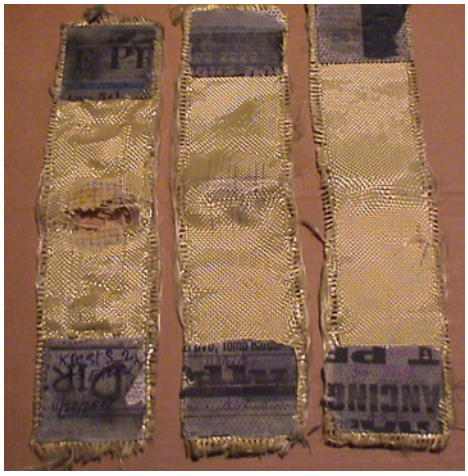

FIGURE 2-2. KEVLAR SPECIMENS (T1)

FIGURE 2-3. TEST SETUP WITH SPECIMEN

2.2.3 End Plates.

To ensure that slipping of the specimens (from the grips) did not influence the deflection values, a different gripping fixture was used as shown in figures 2-4a through 2-4c. Flat steel plates, 2.5″ wide, 2″ long, 0.25″ thick, are used to grip the specimen at both ends. At each end, one of the two pieces has a curved groove at the center of the plate throughout its width, which is half the thickness of the plate. The other plate has a V-notch cut in the same position about half the thickness of the plate. A round aluminum rod is cut along the length to the shape of the groove to match the existing grooves in the steel plate. Two shoulder pins are assembled at the top of the plates to keep the assembly intact and prevent any wobble of the plates, with respect to each

other about the aluminum piece. The fabric was held between the V-notch and the aluminum piece so that the notch pinches against the fabric and prevents it from slipping, with respect to the end plates. The two plates were pressed with hydraulic grips, thereby ensuring uniform pressure application to minimize, if not prevent, any fabric slippage. The revised grip assembly is denoted as Grip T2. Two specimens of each fabric type were tested with the T2 gripping fixture.

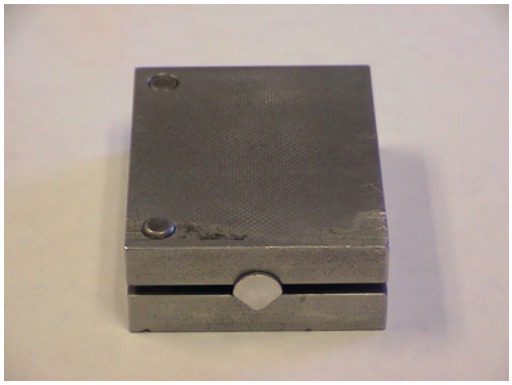

FIGURE 2-4a. END PLATES FOR GRIPPING (T2)

FIGURE 2-4b. SIDE VIEW (T2)

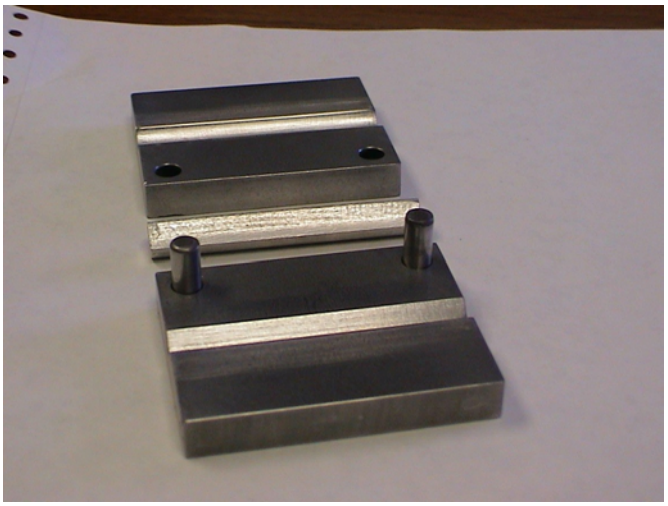

FIGURE 2-4c. INNER VIEW OF THE GRIP ASSEMBLY (T2)

2.3 TEST PROCEDURE AND RESULTS.

The tests were performed according to the Standard ASTM procedure, Tensile Testing of Polymer Matrix Composites—ASTM D 3039 "Standard Test Method for Tensile Properties of Fiber-Resin Composites."

Tests were conducted in a 55-kips servo-hydraulic test frame operated under closed-loop control. The test procedure was a displacement control test with the rate of displacement of actuator (stroke) set at 0.1″/min. A digital data acquisition was used to collect data at every 0.5 second.

The test was continued until complete failure of the specimen was achieved. The load-deformation results were used to calculate the stress-strain response. The overall deformation of the specimen was measured by the stroke movement of the actuator.

The various load-deflection and stress-strain graphs are presented in figures 2-5a through 2-12b. In the figures, K refers to the Kevlar specimens and Z refers to the Zylon specimens.

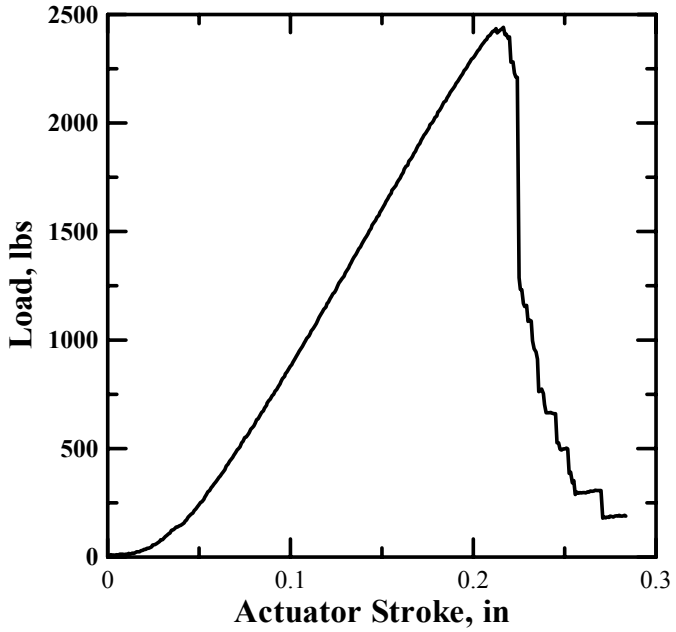

FIGURE 2-5a. LOAD VS ACTUATOR STROKE (KTest1) (GRIP T1)

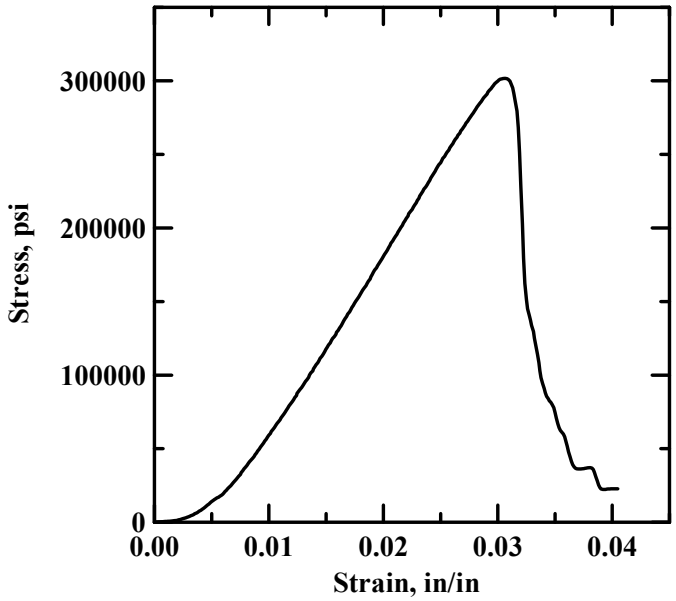

FIGURE 2-5b. STRESS VS STRAIN DIAGRAM (KTest1) (GRIP T1)

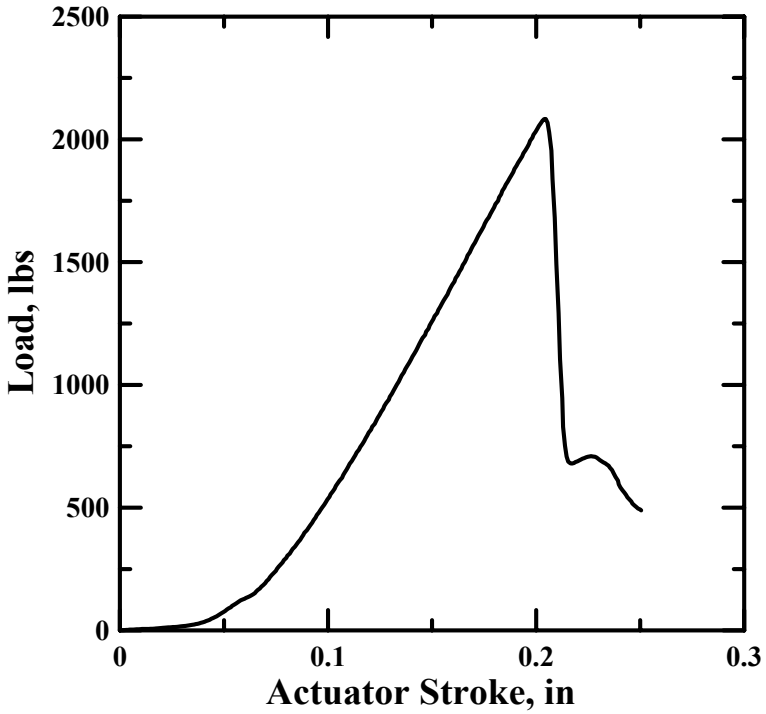

FIGURE 2-6a. LOAD VS ACTUATOR STROKE (KTest2) (GRIP T1)

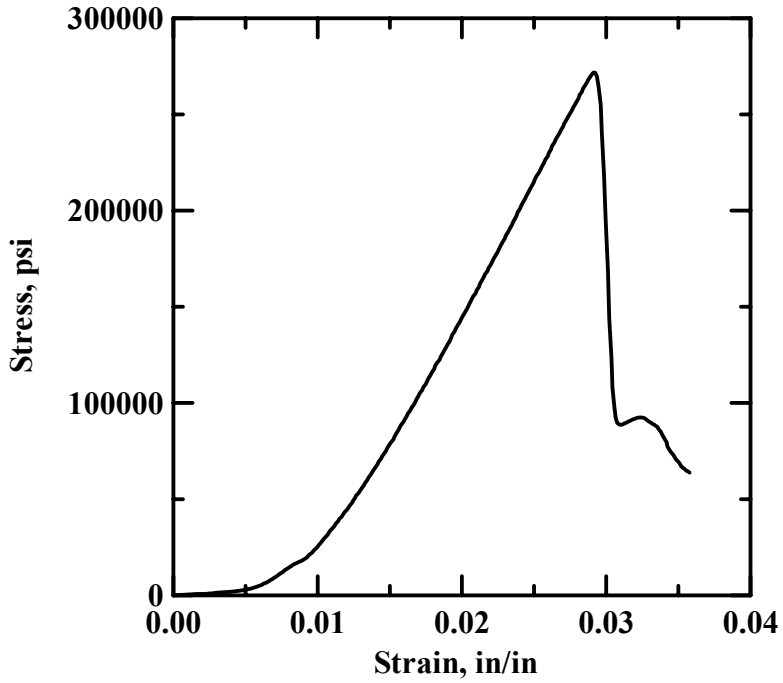

FIGURE 2-6b. STRESS VS STRAIN DIAGRAM (KTest2) (GRIP T1)

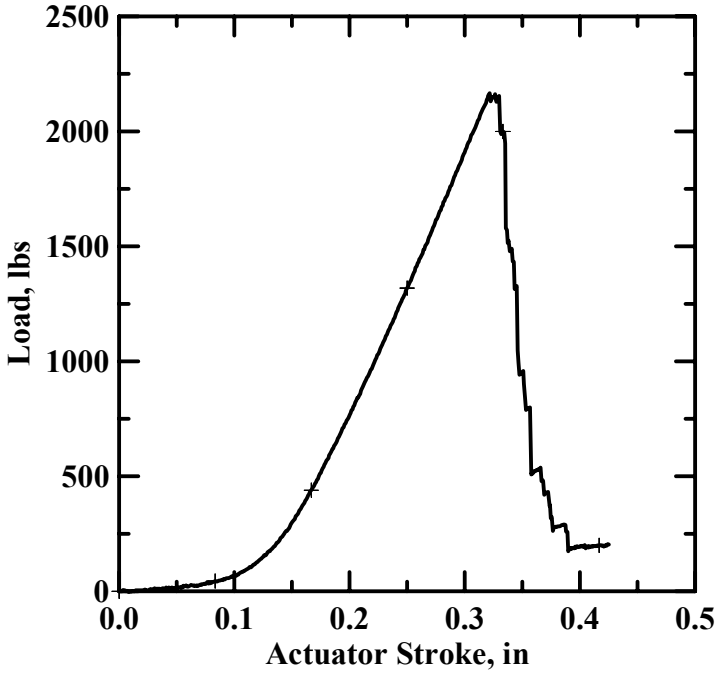

FIGURE 2-7a. LOAD VS ACTUATOR STROKE (KSwath1) (GRIP T2)

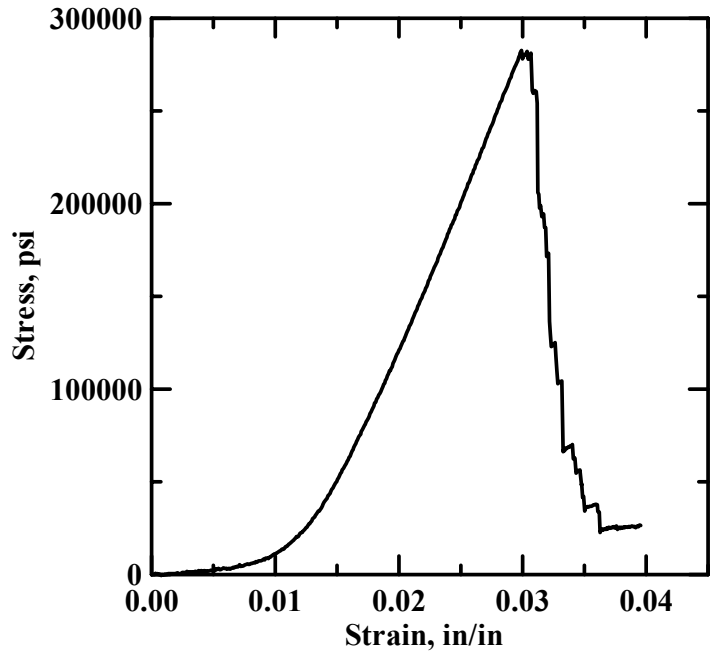

FIGURE 2-7b. STRESS VS STRAIN DIAGRAM (KSwath1) (GRIP T2)

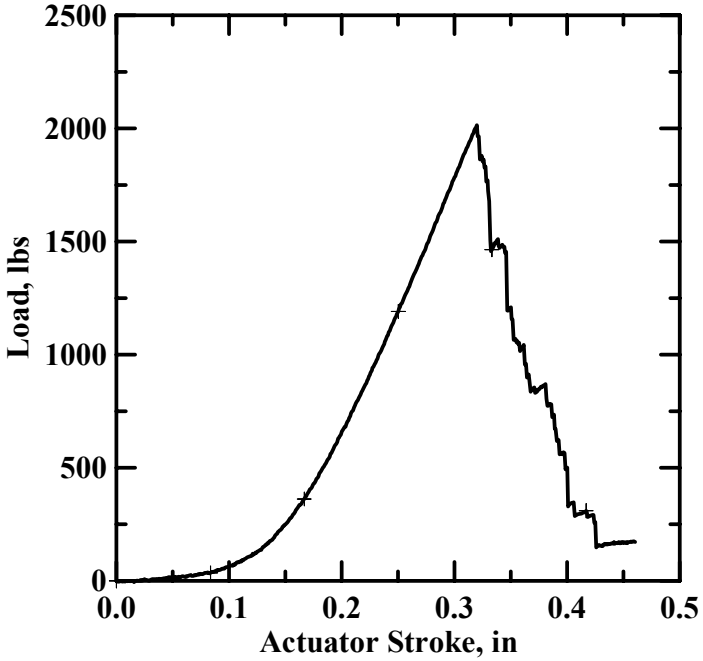

FIGURE 2-8a. LOAD VS ACTUATOR STROKE (KSwath2) (GRIP T2)

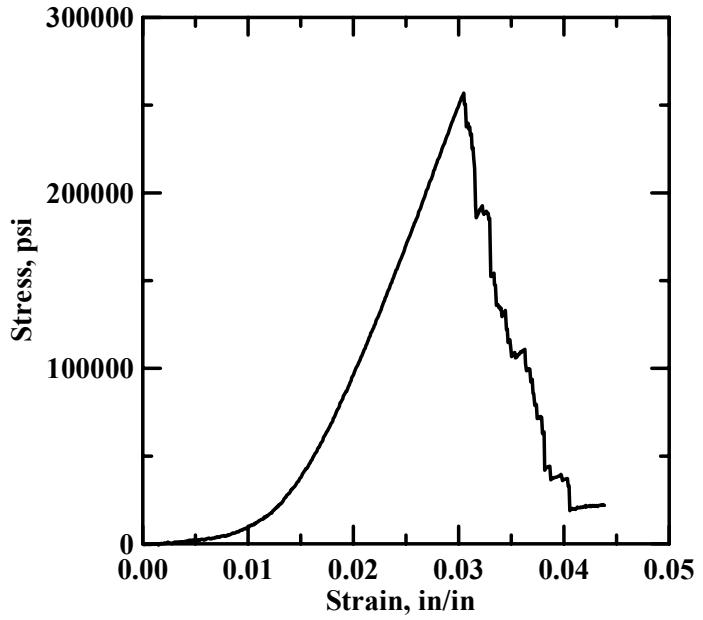

FIGURE 2-8b. STRESS VS STRAIN DIAGRAM (KSwath2) (GRIP T2)

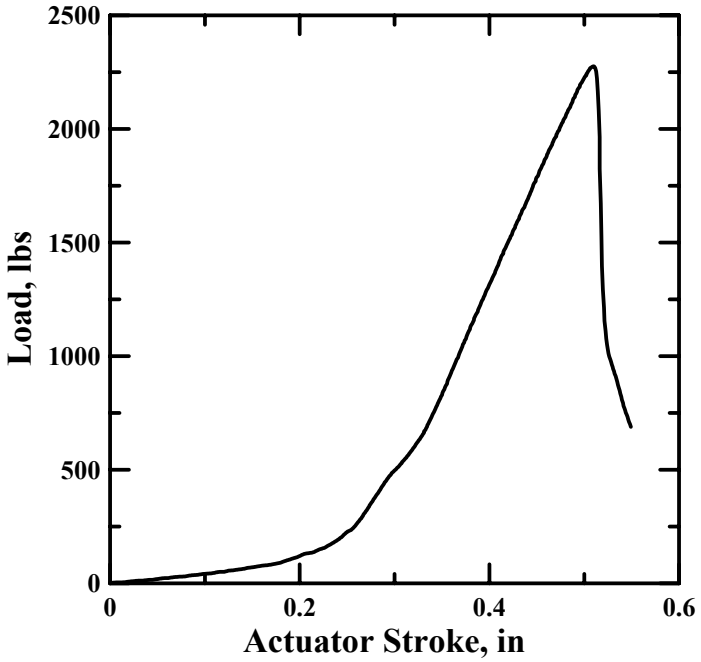

FIGURE 2-9a. LOAD VS ACTUATOR STROKE (ZTest1) (GRIP T1)

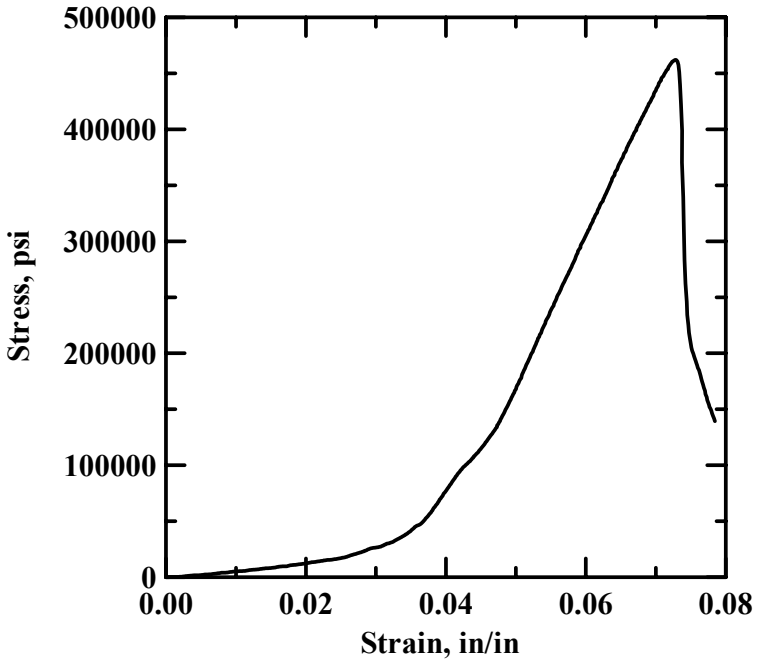

FIGURE 2-9b. STRESS VS STRAIN DIAGRAM (ZTest1) (GRIP T1)

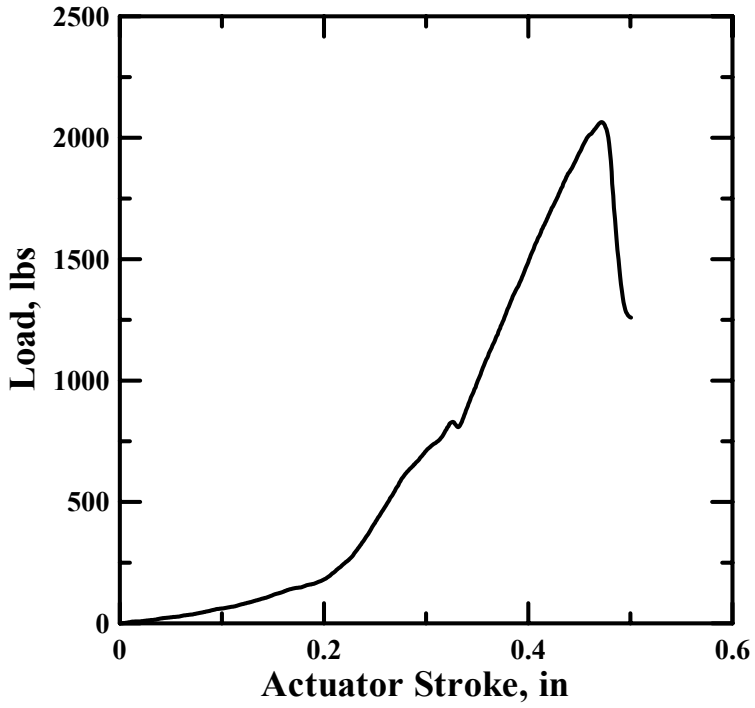

FIGURE 2-10a. LOAD VS ACTUATOR STROKE (ZTest2) (GRIP T1)

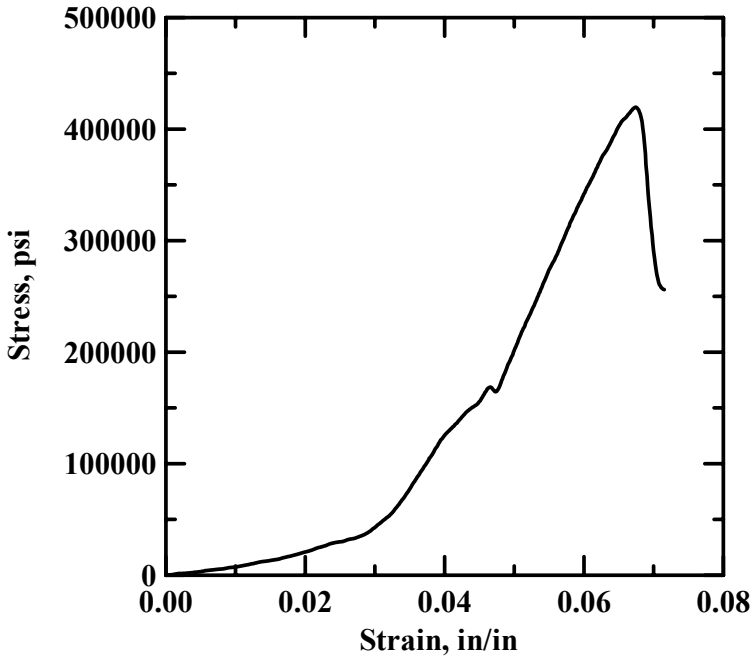

FIGURE 2-10b. STRESS VS STRAIN DIAGRAM (ZTest2) (GRIP T1)

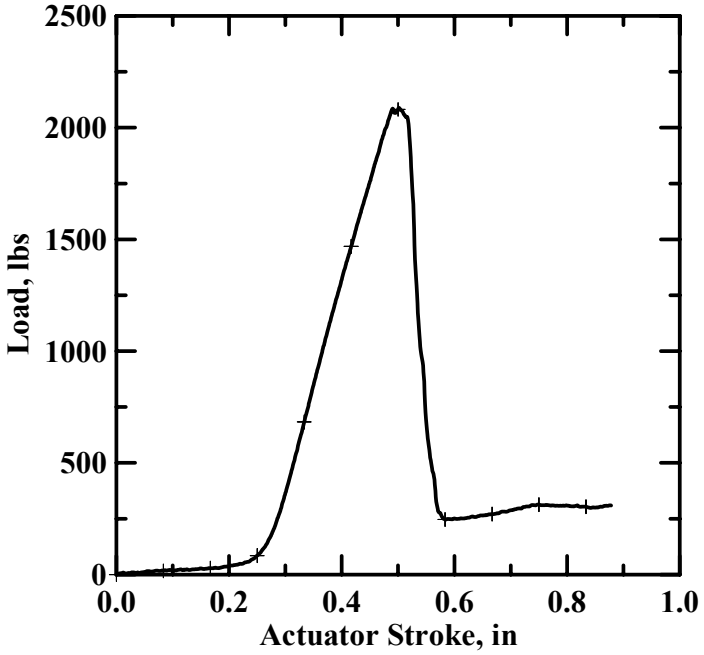

FIGURE 2-11a. LOAD VS ACTUATOR STROKE (ZSwath1) (GRIP T2)

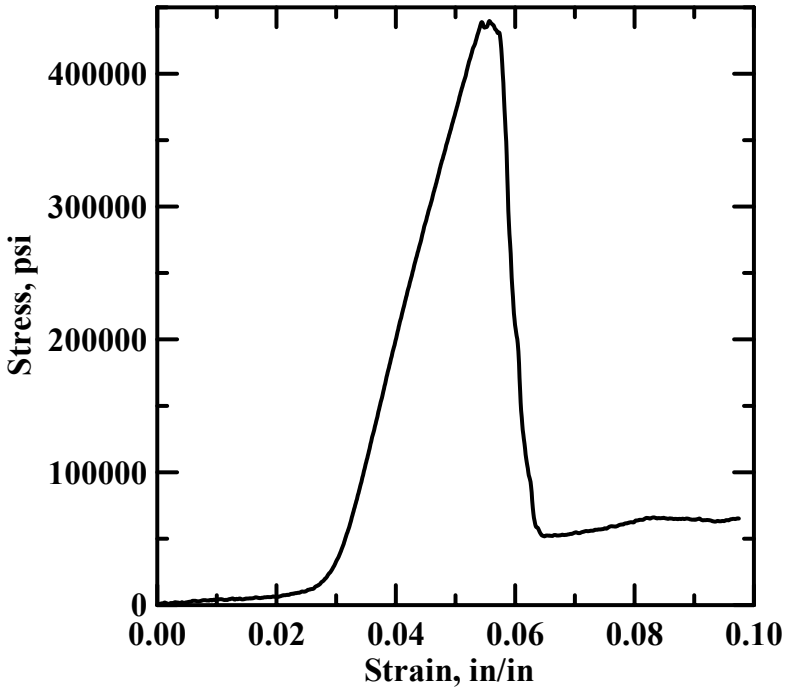

FIGURE 2-11b. STRESS VS STRAIN DIAGRAM (ZSwath1) (GRIP T2)

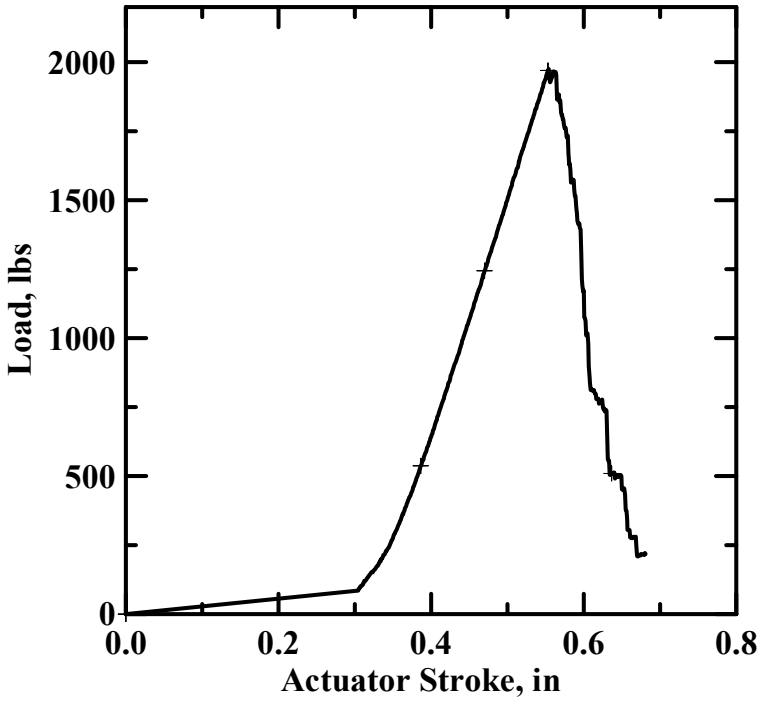

FIGURE 2-12a. LOAD VS ACTUATOR STROKE (ZSwath2) (GRIP T2)

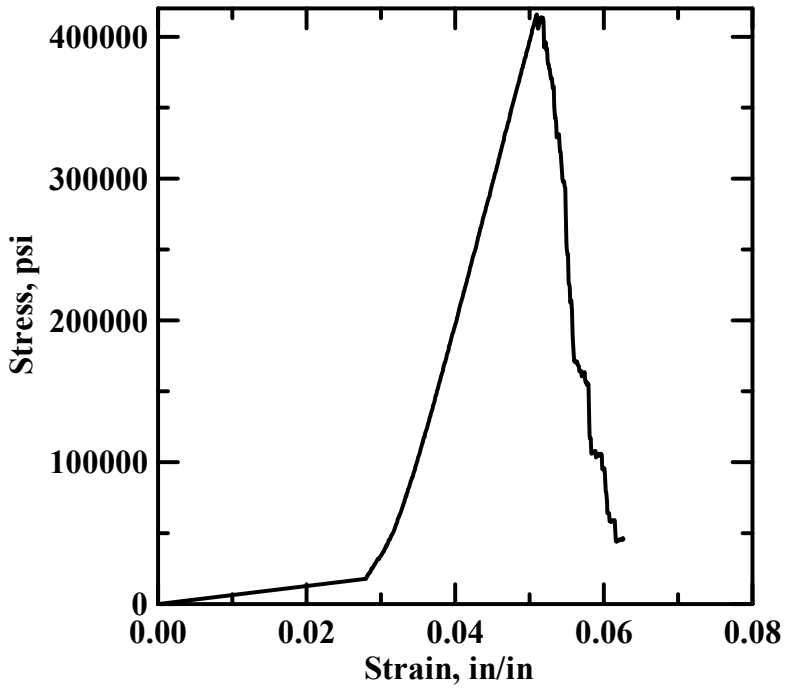

FIGURE 2-12b. STRESS VS STRAIN DIAGRAM (ZSwath2) (GRIP T2)

The stress-strain curves are summarized for all the Kevlar specimens in figure 2-13 and for the Zylon specimens in figure 2-14. The results are summarized in table 2-2.

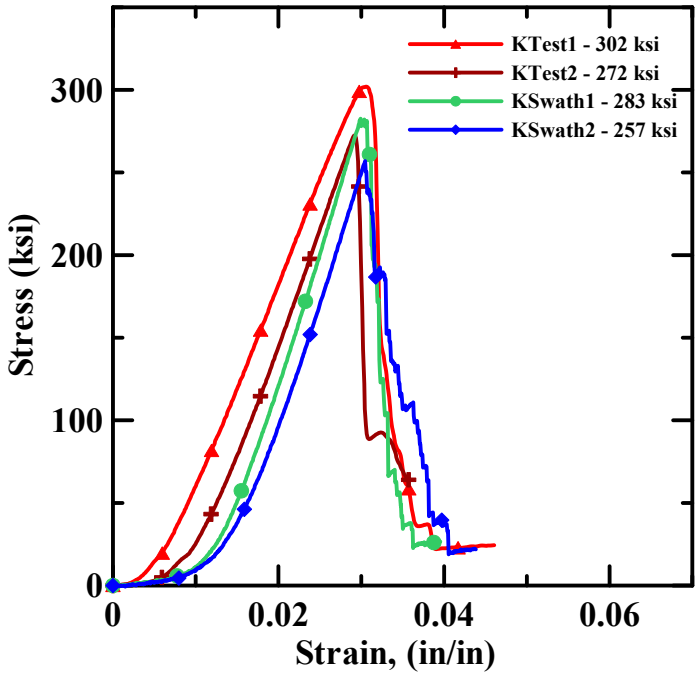

FIGURE 2-13. STRESS VS STRAIN DIAGRAMS FOR ALL KEVLAR SPECIMENS

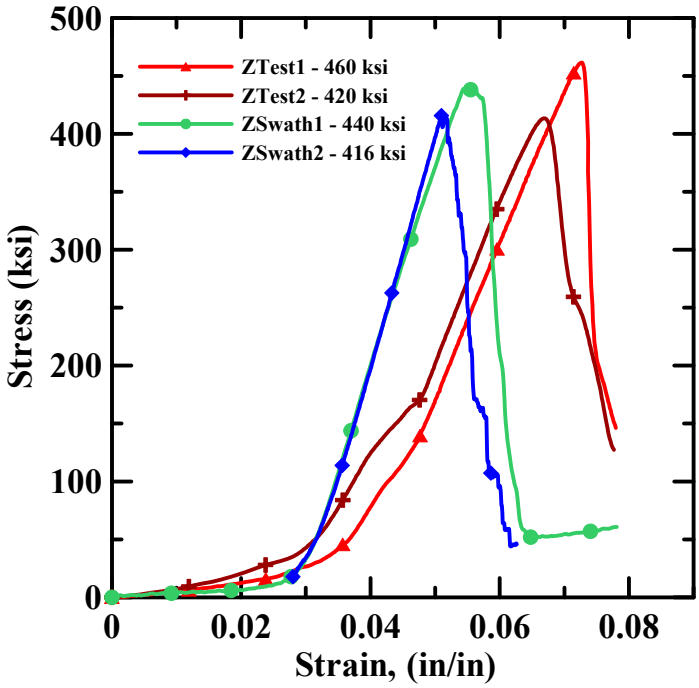

FIGURE 2-14. STRESS VS STRAIN DIAGRAMS FOR ALL ZYLON SPECIMENS

TABLE 2-2. SUMMARY OF TEST RESULTS

Test ID	Peak Load (lb)	Elongation (in.)	Tensile Strength (psi)[(a)]	Ultimate Tensile Strain (%)[(b)]	Modulus of Elasticity (ksi)[(c)]	Energy Absorbed per Unit Volume (lb-in/in^3)	
						En1*[(d)]	En2*[(e)]
Kevlar Specimens							
KTest1 (T1)	2419	0.214	301950	3.06	17115	3650	3590
KTest2 (T1)	2085	0.204	272453	2.92	18590	2584	2519
KSwath1 (T2)	2166	0.322	282644	2.99	16345	3472	3340
KSwath2 (T2)	2014	0.320	256911	3.05	15321	3539	3387
Average	2171	0.265	278490	3.01	16843	3311	3209
Std. Dev.	177	0.065	18883	0.065	1377	490	473
Zylon Specimens							
ZTest1 (T1)	2276	0.510	461550	7.27	18242	7923	6875
ZTest2 (T1)	2064	0.472	419554	6.75	18960	7217	6188
ZSwath1 (T2)	2088	0.501	439618	5.56	17166	10597	10366
ZSwath2 (T2)	1975	0.554	415788	5.10	19868	6842	6735
Average	2101	0.509	434128	6.17	18559	8145	7541
Std. Dev.	127	0.0340	21062	1.011	1142	1695	1907

Notes:
(a) Stress is obtained by dividing the peak load by the cross-section area as tabulated in table 2-1.
(b) Ultimate tensile strain is obtained by dividing the elongation at peak load by the specimen gage length.
(c) Modulus of elasticity is taken as the maximum (linear) slope from the prepeak region of the stress-strain graph.
(d) En1* - Energy absorbed by the fabric as calculated by total area under the stress-strain curve.
(e) En2* - Energy absorbed by the fabric as calculated by linear approximation of the area under the stress-strain curve extended from the modulus of elasticity slope.

The initial portion of the load-deflection graph shows a large increase in displacement (actuator stroke) for a very small increase in load. In this portion, the load essentially straightens the yarns by removing the crimp. Woven fabrics inherently have crimp (or waviness). As the load increases, the yarns stiffen, as shown by the increase of the slope of the load-deflection graph. The graph of one specimen (figure 2-10a) exhibits a small nonsmooth behavior (or waviness) in the prepeak region. This is perhaps due to total or partial failure of yarn(s) in the specimen. This behavior is much more pronounced in the postpeak region of Kevlar specimens (figures 2-5a, 2-7a, 2-8a) and one Zylon specimen (Figure 2-12a). The failure of all the specimens is sudden (brittle behavior).

Examination of the results showed that the scatter for the Kevlar tests was much smaller compared to the Zylon tests. The standard deviation for the (Kevlar) peak strain values of four tests is 0.065%. In the case of Zylon, the peak strain values obtained using Grip T2 are less than those obtained from Grip T1. This is probably due to less slippage occurring at the grips with

Grip T2. The standard deviation of the peak strain for the four tests was 1.011%. The ultimate tensile strain was obtained by dividing the elongation at peak load by the specimen gage length. The gage length used for Grip T1 was determined based on the average distance of grip face to grip face. The gage length used for Grip T2 was determined based on the average distance of groove edge to groove edge. The modulus of elasticity was measured as the maximum slope within the linear range of the ascending portion of the stress strain curve. In addition, the curves were converted to piecewise linear responses, which were used in the finite element modeling. The average Young's Modulus of Kevlar fabrics was measured as 16,843 ksi, and the average modulus for the Zylon fabrics was measured as 18,559 ksi. In addition, two different means of measuring the energy absorbed were investigated. In the first method, the energy absorbed by the fabric was calculated from the total area under the stress-strain curve. This included the initial nonlinear ascending portion of the curve. In the second method, the energy absorbed by the fabric was calculated by linear approximation of the area under the stress-strain curve extended from the modulus of elasticity slope. This in effect resulted in assuming that the response of the material was a linear elastic behavior. The differences between these two methods are insignificant as the energy absorbed for Kevlar measured 3311 lb-in. for the exact integration versus 3209 psi for the linearized case. For the Zylon material exact integration yields energy of 8145 lb-in. versus 7541 psi for the linearized case. This represents that the modeling of the material by means of elastic or quasi elastic response results in 3.0% and 7.4% underestimation of the energy absorbed for Kevlar and Zylon respectively.

Some of the failure modes using Grip T2 are shown in figures 2-15 through 2-18. The failure (broken yarns) occurs at the middle of the specimen for the Kevlar specimen, while the failure occurred near the grips for the Zylon specimen.

FIGURE 2-15. KEVLAR SPECIMEN (T2)

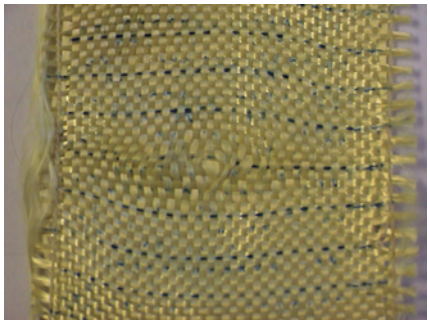

FIGURE 2-16. FAILURE AT CENTER (T2)

FIGURE 2-17. ZYLON SPECIMEN (T2)

FIGURE 2-18. FAILURE AT THE EDGE (T2)

3. SPLICE TESTS.

To conduct a valid single or multilayer static test, the Kevlar and Zylon fabrics must be wrapped around a steel cylinder. The implication is that the two ends of the continuous fabric wraps need to be anchored so that the fabrics would not unwrap when they are subjected to an external load. It was, therefore, decided to investigate how two different epoxies could provide the anchor by preparing and testing splice joints made of these epoxies and fabrics.

3.1 OBJECTIVES.

The primary objective of the splice tests was to determine the bond strength of the epoxy and the suitability of using these epoxies in preparing the specimens for the static tests.

3.2 SPECIMEN PREPARATION PROCEDURE.

Three Kevlar specimens and one Zylon specimen were tested. Two overlap lengths of 4″ and 6″ were investigated. The specimen sizes (lengths) were chosen in such a way that the final length after overlap was 12″. The specimens were prepared as follows.

- Epoxy was applied evenly on the overlap areas of the two fabrics. Heavy flat plates were placed on top of this area to apply an even pressure and facilitate the bonding process. The overlap was left 24 hours at room temperature for curing.

- Aluminum tabs were attached to the two ends of the test specimen, similar to the procedure used with the simple tension tests. This was done after ensuring that the total specimen length was exactly 12″.

The specimens were gripped (in the test fixture) using Grip T1, as described in section 2.

Two different epoxies were used in the tests. They are identified as Epoxy A (5-minute® epoxy) and Epoxy B (Hardman® extra fast setting epoxy). The epoxies consisted of two parts (resin and hardener) to be mixed in equal proportions by volume.

3.3 TEST PROCEDURE.

The tests were performed according to the Standard ASTM procedure—ASTM D 3039 "Standard Test Method for Tensile Properties of Fiber-Resin Composites." A 55-kips servo-hydraulic test frame, operated under closed-loop control, was used. The test procedure was a displacement control test with the rate of displacement of actuator (stroke) set at 0.1 in./min. Digital data acquisition was used to collect data at every 0.5 second. The test was continued until complete failure of the specimen was achieved. The load-deformation results were used to calculate the stress-strain graph. The overall deformation of the specimen was measured by the stroke movement of the actuator.

3.4 TEST RESULTS.

The details of the Kevlar test specimens are shown in table 3-1.

TABLE 3-1. KEVLAR TEST SPECIMEN DETAILS

Specimen ID	Epoxy Type	Overlap Length (in.)
GTestk4_ne	B	4
GTestk4_oe	A	4
GTest6_ne	B	6

In all three tests, failure occurs at the edge of the overlap region. The failure was sudden.

One Zylon specimen was tested with a 4″ overlap using 5-minute® epoxy. The load level reached was low, and the two Zylon layers peeled off. Zylon surface adhesion property is even lower than a carbon surface. The test results are summarized in table 3-2.

TABLE 3-2. SPLICE TEST RESULTS

	Kevlar			Zylon
Test ID	GTest4_oe	GTestk4_ne	GTestk6_ne	GTestz4_oe
Deflection at ultimate load (in.)	0.029	0.066	-	0.082
Ultimate load (lb)	1998	1491	1650	627
Ultimate load per yarn (lb)	51	48	43	7.7
Ultimate strain	0.0077	0.0177	-	0.0218
Ultimate stress per yarn (psi)	287,848	270,278	-	136,774

The test results showed that the bond strength of the 5-minute epoxy, even for a 4″ overlap, was more when compared to the 6″ overlap strength provided by the fast-setting epoxy.

The load-deflection and stress-strain graphs are shown in figures 3-1a through 3-4b.

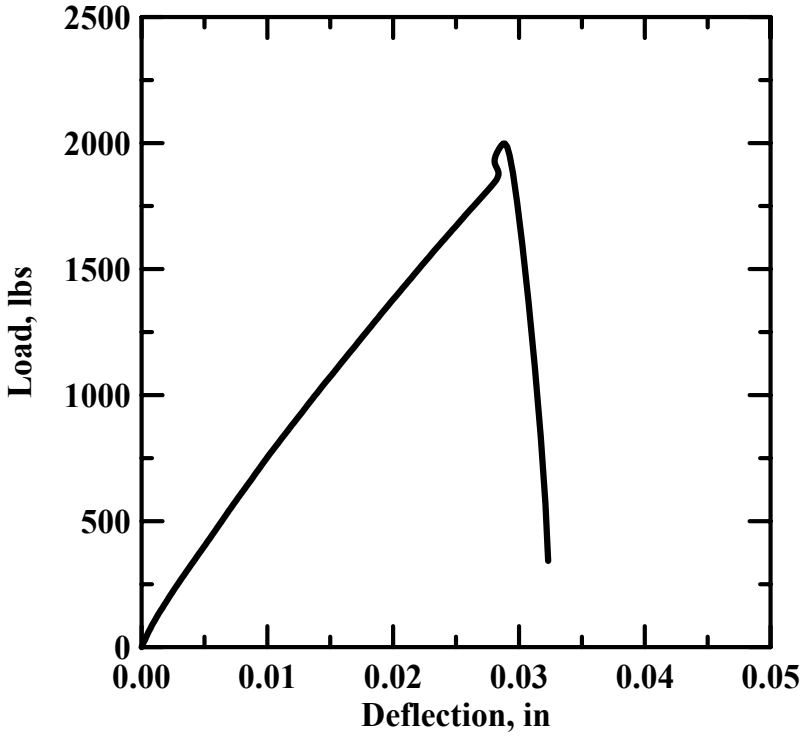

FIGURE 3-1a. LOAD VS DEFLECTION (GTestk4_oe) (LVDT)

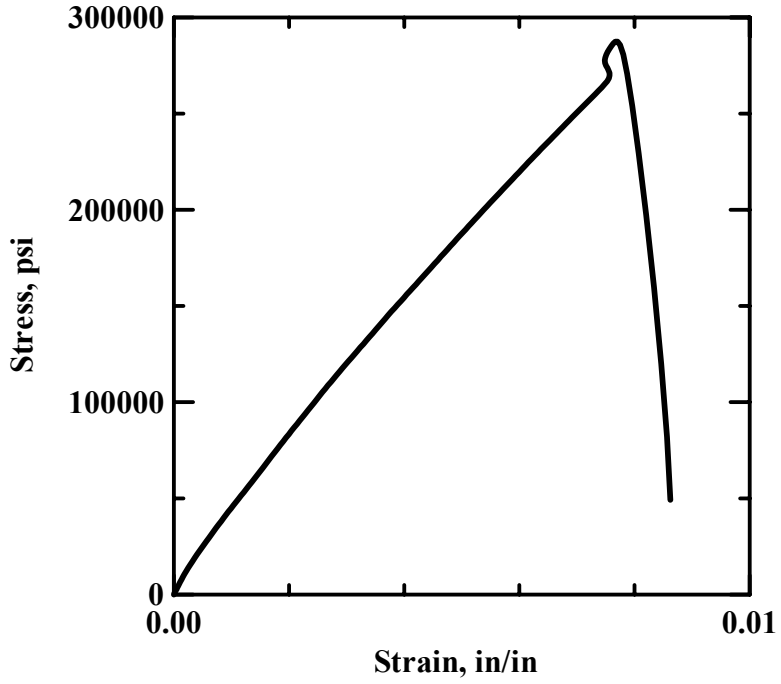

FIGURE 3-1b. STRESS VS STRAIN DIAGRAM (GTestk4_oe) (LVDT)

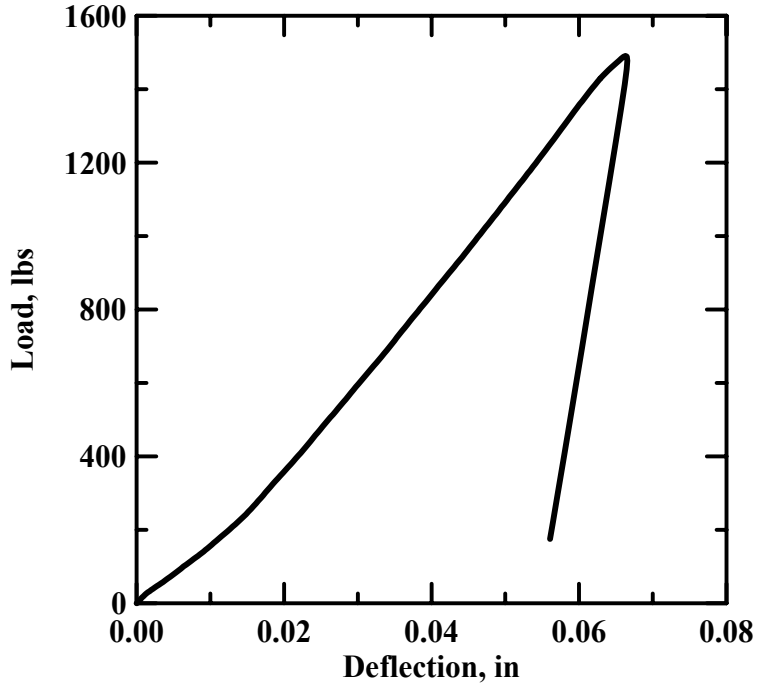

FIGURE 3-2a. LOAD VS DEFLECTION (GTestk4_ne) (LVDT)

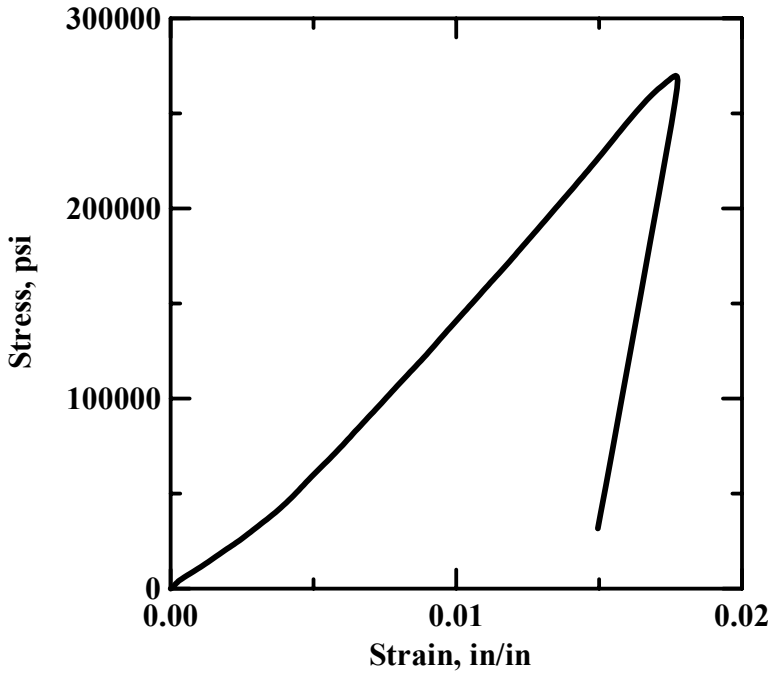

FIGURE 3-2b. STRESS VS STRAIN DIAGRAM (GTestk4_ne) (LVDT)

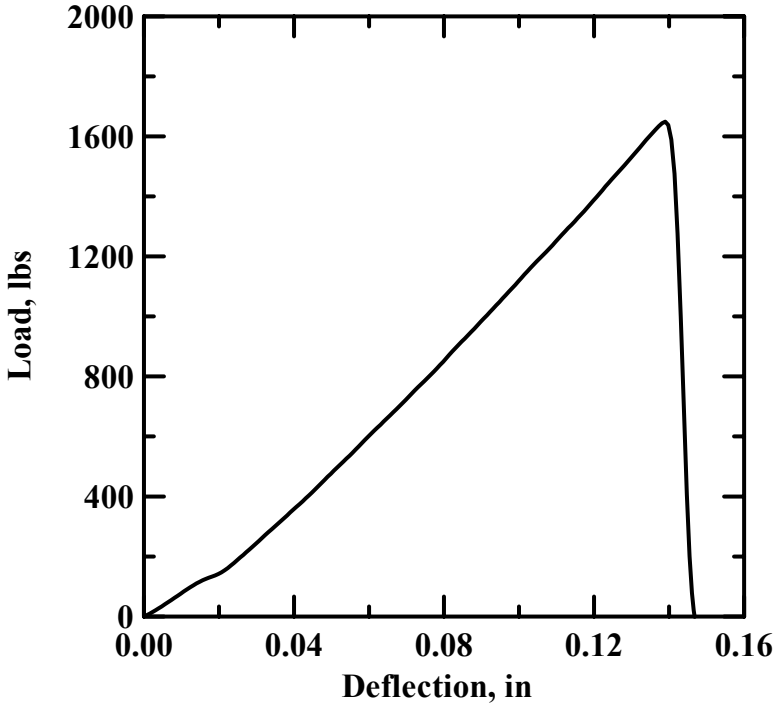

FIGURE 3-3. LOAD VS ACTUATOR STROKE (GTestk6_ne) (ACTUATOR)

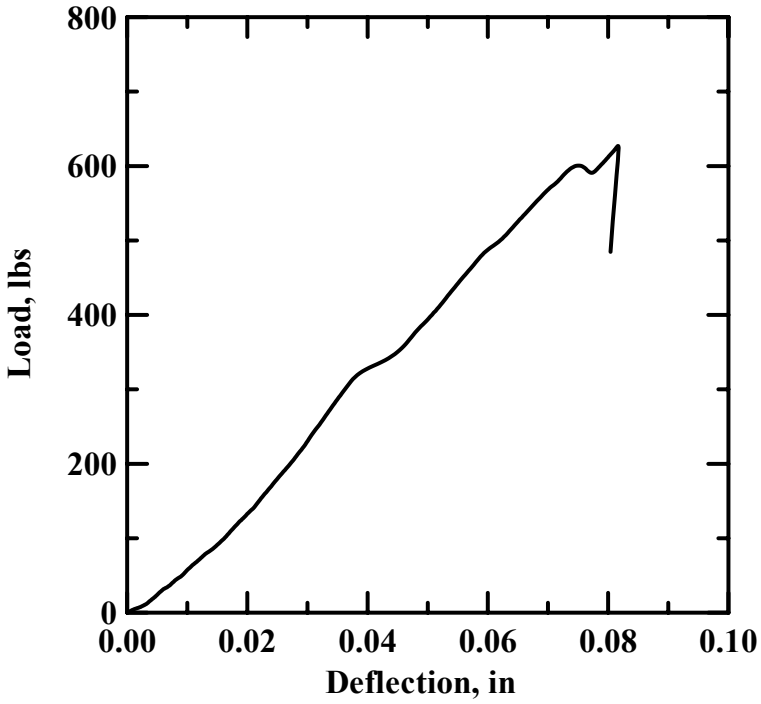

FIGURE 3-4a. LOAD VS DEFLECTION (GTestz4_oe) (LVDT)

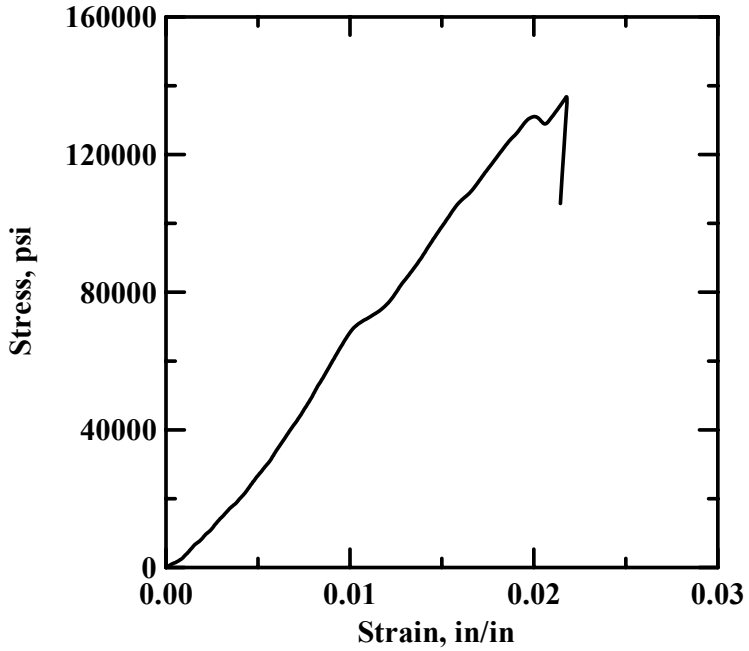

FIGURE 3-4b. STRESS VS STRAIN DIAGRAM (GTestz4_oe) (LVDT)

The test results showed that while it is possible to generate a Kevlar splice joint with some strength, the Zylon splice joints have little or no bond strength. Based on this observation, it was decided to clamp the Kevlar and the Zylon specimens to the steel ring at distances sufficiently far away from the point of application of the load. Details of this setup are discussed in section 4.

4. STATIC TESTS.

4.1 OBJECTIVES.

The primary objective of static tests is to simulate the penetration of the blunt object through the engine containment system assembly. A steel cylinder is used to simulate the engine housing, and the composite fabric is wrapped around this cylinder. The tests were conducted by applying the load in a quasi-static manner until failure, defined as full penetration of the blunt nose through the single or multilayer fabric. The load and deformation history were collected throughout the test, and the energy absorption capacity of the structure was calculated from this response. This test may ultimately be used as one of the key parameters in the determination of properties and design of the containment chamber. In this section the details of the static tests are presented. Relevant pictures and graphs are also presented to facilitate the understanding of the test procedures and results. Additional information in the form of pictures and graphs can be found in appendix A. (A detailed data disk including the ABAQUS model, is available upon request from the FAA William J. Hughes Technical Center.

4.2 SPECIMEN PREPARATION PROCEDURE.

The proposed plan for testing required determination of the load-deformation response of single and multilayer specimens for both Kevlar and Zylon wraps. The specimens were subjected to outward penetration motion of a blunt nose assembly that was initially set up inside the steel ring. The specimen dimensions were 32″ in diameter, 4″ wide, and consisted of 1, 2, 4, 8, and 24 layers wrapped around the outside of the steel cylinder, see figure 4-1. A small window was machined in the ring, allowing the penetration of the blunt nose assembly.

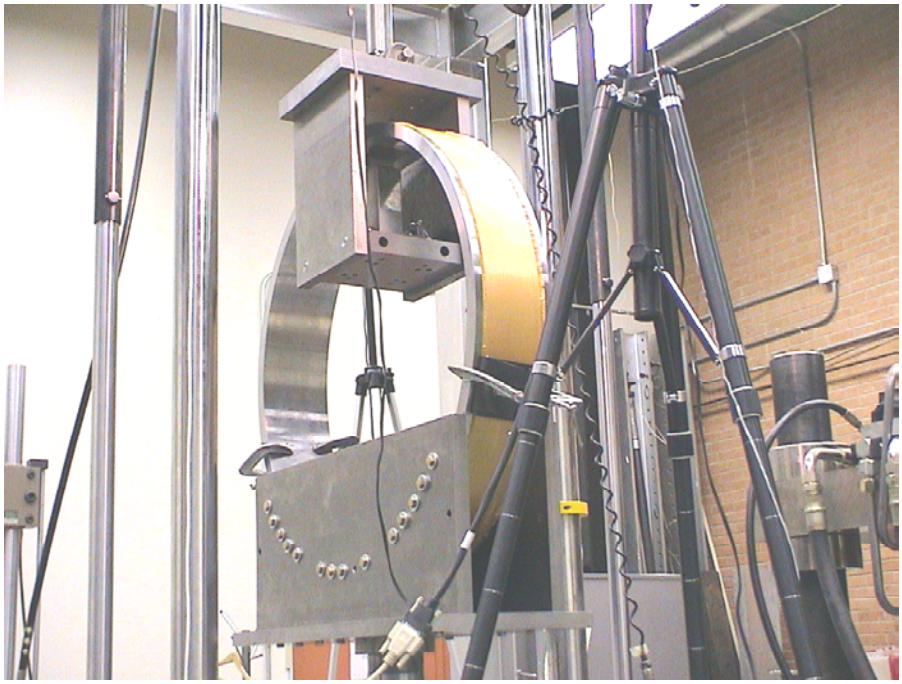

FIGURE 4-1. TEST SETUP

For the single-layer specimens, a 6″ length of fabric overlap was used to glue the fabric onto itself. For multilayer specimens, the fabric was wrapped around the outside diameter of a custom-designed mandrel (figure 4-2a). The first layer was held on the mandrel by temporary glue. The last layer was glued to the previous layer using 5-minute® epoxy. Overlap length for all specimens was 6″. The specimen was cured for 24 hours before testing. To ensure proper alignment of the layers and cause minimal disturbance during the assembly process, a 32″ diameter transfer ring (figure 4-2b) was manufactured. The rolled sample was slipped from the mandrel onto a transfer ring in order to transport it to the test fixture. The specimens were covered with opaque plastic sheeting to minimize the degrading effects of moisture and ultraviolet light.

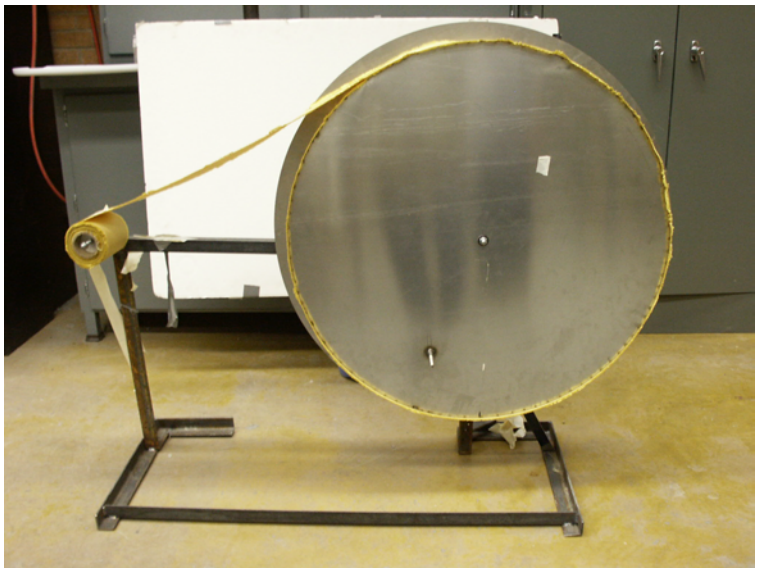

FIGURE 4-2a. MANDREL FOR SPECIMEN PREPARATION

FIGURE 4-2b. SPECIMEN TRANSFER RING

4.3 TEST SETUP.

A test fixture was manufactured by rolling a section of A36 mild steel to the inner diameter dimensions of the test setup. The ring dimensions are as follows:

- Outer diameter (OD) 32″
- Internal diameter (ID) 30″
- Width 6″
- 1″ thick

This ring was the main component of the loading fixture and was fabricated at Karlson Machinery, Phoenix, AZ. The complete loading fixture consisted of four major parts. The ring was assembled in two parts—as a large and a small arc at bottom to allow for installation of the fabric ring. The other components include the two side support plates and end plate to connect the two ring components. A detailed view of the cylinder with side plates is shown in figure 4-1. The small arc that was cut out from the ring was connected at the bottom of the ring assembly and did not alter the geometry of the test setup. The size of the small arc corresponds to a 38° angle. Using of the ring as two parts allowed easy installation of the specimen in the loading fixture. The specimens were first wrapped on an aluminum mandrel. Removal of the small arc during the sample mounting stage facilitated the transfer of the test specimen from the transfer ring. The cylinder was attached to two side plates using 15-3/4″ diameter, high-strength bolts connected along the ring's perimeter. These side plates were connected to the base plate; hence, the ring had a clearance of 3″ from the base plate.

A blunt nose assembly (see figure 4-3) was used as the penetrator for all the tests in this program. The steel nose was 2″ wide by 5/16″ thick. The top nose surface that was in contact with the fabric layer had a radius of 5/32″ in the major direction and the corners. The cross-section of the base of the blunt nose was 2″ by 2″.

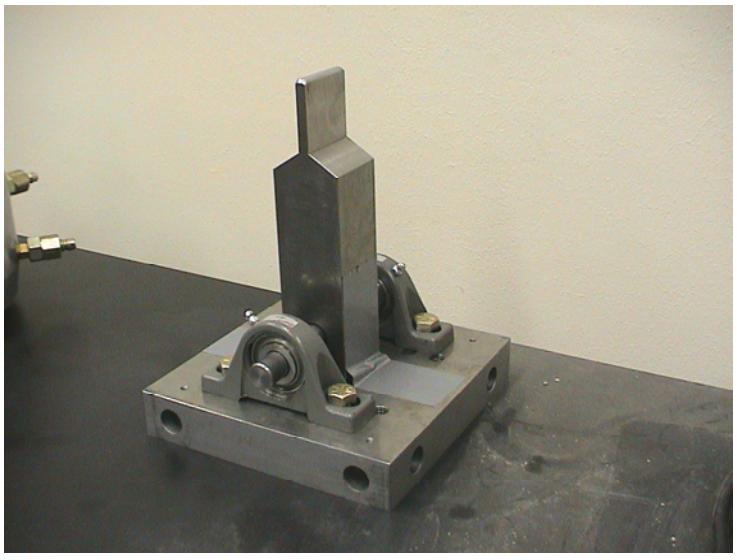

FIGURE 4-3. BLUNT NOSE WITH BEARINGS

The amount of load transferred through the lap (splice) joint and its potential failure were a major concern, especially in the one-layer tests. The tests conducted with the bond strength of Zylon indicated the difficulty in gluing the material and potential problems with interface failures. To avoid transferring the entire load to the end joint, it was decided to use clamps at points remote from the blunt head contact. The effect of clamping the specimen to the ring on the integrity of the test results was studied using one-layer specimens. Specimens with and without clamps were tested, and the results are discussed in the following sections. For the multilayer Kevlar specimens and all the Zylon specimens, the tests were conducted with the clamps in place. Figure 4-4 shows the clamps placed on the side of the specimen. The clamps were placed at the same height on both sides of the ring to maintain symmetry and uniformity. The clamps are placed at 13.75″ from the top of the base plate or at 10.75″ from the bottom of the cylinder OD.

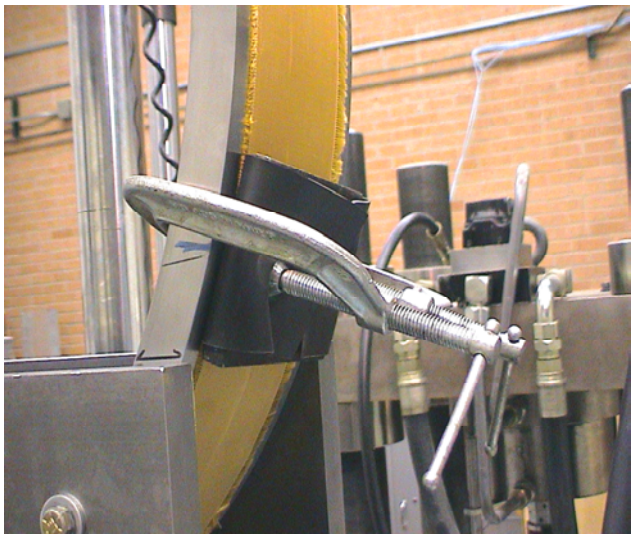

FIGURE 4-4. ATTACHMENT OF C-CLAMPS TO THE SPECIMEN

Another important parameter was the effect of fixing the blunt nose loading mechanism with respect to the specimen, especially with large displacements expected throughout the test. It was expected that if the side loads were not removed through the use of hinges, a stiff system would be created, which would result in side loads. Alternatively, any rotation of the test assembly could result in loss of contact of the full length of the blunt nose with the fabric, thus increasing the contact pressure and premature failure of the specimen. Measurement of such second-order effects would be difficult, if not impossible. To make sure that the load applied is purely uniaxial, one has to allow for at least two hinges to remove forces in the two minor directions. Based on the above, samples were tested with bearings placed at the nose and load cell. Both cases of parallel and orthogonal hinges were studied. However, the hinge-to-hinge conditions were found to be unstable due to eccentricities in the test assembly. It was found necessary to fix the end conditions at the top of the blunt nose housing by fixing the load cell bearings that were placed orthogonal to the nose bearings, as shown in figure 4-5. It should be noted that the aluminum plates placed between the vertical shaft that is connected to the test machine crosshead and the top plate of the blunt nose housing, restrict the ability of the housing to rotate under eccentric loads. This setup corresponds to the fixed-hinge end conditions shown in table 4-1.

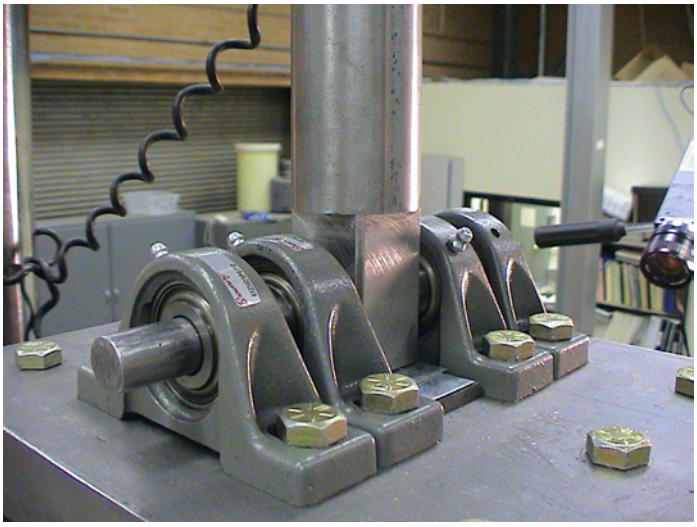

FIGURE 4-5. TOP PLATE WITH BEARINGS ORTHOGONAL TO NOSE BEARINGS (FIXED-END CONDITION AT TOP)

TABLE 4-1. SUMMARY OF STATIC TEST CONDITIONS AND RESULTS

Test ID	No. of Layers	Special Provisions	Peak Load (lb)	Peak Stroke (in.)	Stiffness (lb/in.)	Area Under the Curve (lb-in.)	
						Prepeak	Postpeak
Kevlar Specimens							
Kring1_2	1	Fixed-hinge, no clamps	1685	3.17	1503	1157	78
Kring1_3	1	Fixed-hinge, no clamps	1486	2.69	1115	993	507
Kring1_4	1	Fixed-hinge, no clamps	1522	2.39	1052	1062	721
Kring1_5	1		1571	3.10	1161	1260	203
Kring2_1	2		3429	3.30	2694	2371	590
Kring4_1	4	Preload: 250 lb	6625	3.23	4942	4503	889
Kring8_1	8	Preload: 250 lb	13231	3.62	9463	9907	1036
Kring24_2	24	Preload: 2000 lb	31131	3.35	16314	37434	5629
Zylon Specimens							
Zing1_2	1		1730	4.69	1481	1323	162
Zring2_1	2		3408	4.47	2635	2906	143
Zring4_2	4		7363	4.39	5463	6105	56
Zring8_3	8	Preload: 1000 lb	12640	4.74	10006	9499	410
Zring24_1	24	Preload: 2000 lb	34148	4.84	22704	32526	61

Note: Unless otherwise mentioned under special provisions, the specimens were not preloaded, the blunt nose end conditions were fixed-fixed and clamps were used.

It was furthermore observed through the preliminary tests that significant slack existed for the multilayer Zylon samples. This can be verified through the analysis of the raw test data, which indicated up to 2″ of stroke travel under an insignificant amount of load (e.g., up to 250 lb). To relieve the slack, the specimens were pretensioned using an outward pressure applied at the bottom portion of the ring. The pressure was applied by placing two steel spacer blocks between the small arc of the ring and the spacer plate, and pushing the spacer plate outward by tightening the screws. Schematic diagrams of this setup are shown in figures 4-6a and 4-6b. This ensured some of the slack recovery.

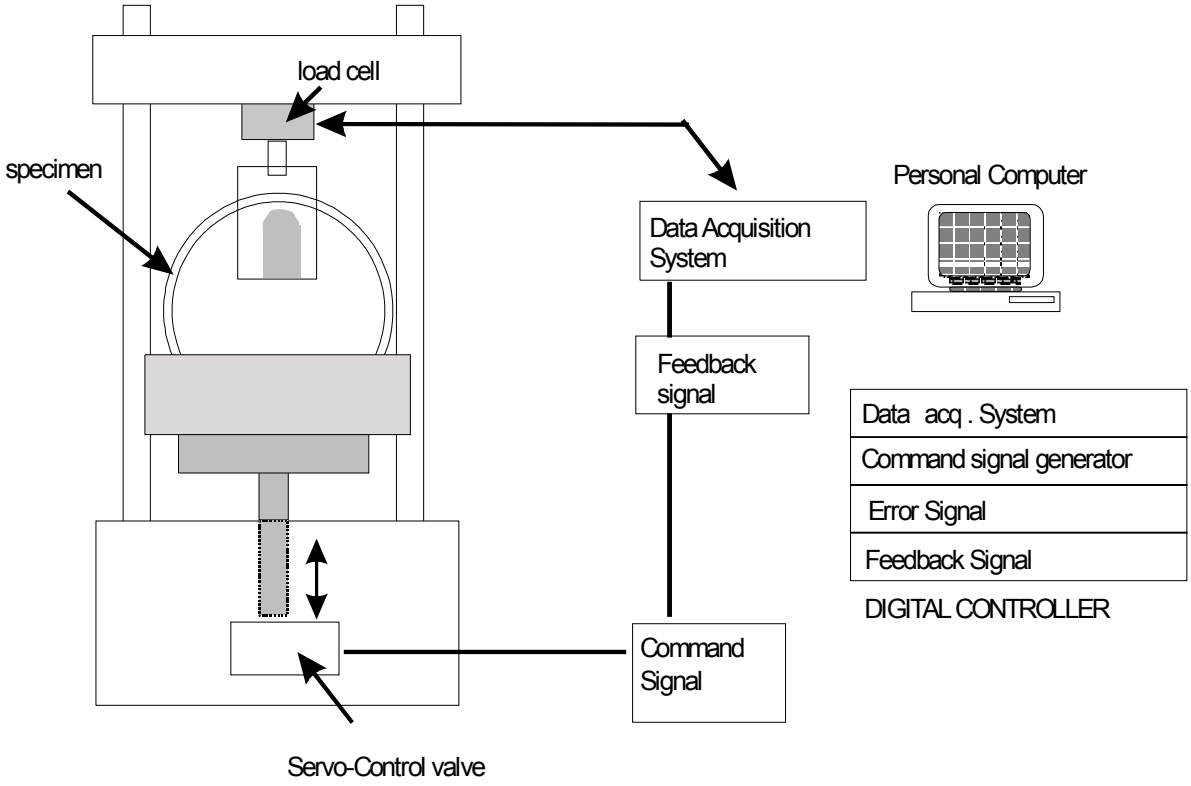

FIGURE 4-6a. SCHEMATIC DIAGRAM OF THE TEST SETUP

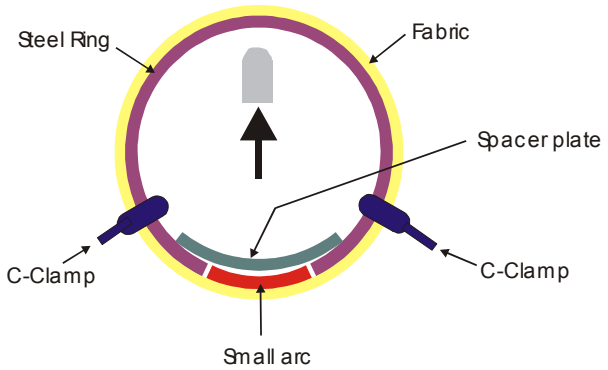

FIGURE 4-6b. SCHEMATIC OF TEST SETUP WITH CLAMPS AND HINGES TO REMOVE SPURIOUS LOADS

Even with the best-case efforts in ensuring that the test setup was exactly as discussed above, side loads were generated during the testing. The blunt nose assembly would start to tilt due to the hinge condition at the bottom of the blunt nose housing. To overcome this problem, a revised housing (and blunt nose) was designed, as shown in figure 4-6c. This corresponds to the fixed-fixed end conditions shown in table 4-1. Additionally, a threaded rod was used in between the blunt nose and the support plate to increase the length of the nose.

FIGURE 4-6c. REVISED BLUNT NOSE HOUSING DESIGN
(FIXED-FIXED CONDITIONS)

4.4 TEST PROCEDURE.

Each sample was transferred from the wrapping mandrel to the test rig, then the side plates were attached. An MTS servo-hydraulic test machine with Digital Teststar2 controller software was used for all the specimens. All the tests were conducted under actuator control using a constant rate of travel of 0.4 in./min. The test was conducted in a manner such that the load cell housing the blunt nose remained stationary throughout the test, while the actuator and, hence, the ring moved downward, thus loading the fabric against a stationary blunt nose. The data were collected using an automatic digital data acquisition system at a rate of 2 Hz.

For certain specimens, the test was run in a single step and continued until failure occurred. For multilayer specimens (4-, 8-, 24-layer Kevlar and all Zylon), tests were performed in two steps. Since the maximum actuator travel length was limited to 4 inches, a readjustment of the position of the sample was necessary to extend the total displacement beyond the 4″ expected in the multilayer and Zylon tests. During the first stage, the sample was loaded to 250 lb (see exceptions in table 4-1), and the test was placed on hold. At this point, the actuator was brought

back to the zero position, while the crosshead was moved up to maintain the preload of the sample at 250 lb. At this point, the test was resumed and displacement was imposed until failure of the specimen. The adjustment of the crosshead was necessary to ensure enough travel was available for the sample to fail without causing any impact on the quality of the data obtained.

4.5 TEST RESULTS.

The data collected by the test generated the load-deflection curve for each test. The various load-deflection results are presented in table 4-1.

Figure 4-7 shows the response of single-layer Kevlar specimens tested without clamps. Note that the initial region of the response curve indicates a gradual increase in the load-carrying capacity. This is considered to be the region dominated by slack recovery (there is some deformation because of the straightening of the yarns) and gradual loading of the specimen to reach the stiffness of the fabric being loaded in tension. Finally, the ultimate load was reached in these samples in an abrupt manner after several yarns fracture. The fracture of some yarns before the peak load was observed as the sudden jump in the load response. The load carried by the fractured yarns was being transferred to unbroken yarns. It was expected that the load redistribution after the fracture of a few yarns results in an excess load on the surviving yarns. This excess load was sufficient to push the average stress on the yarns beyond the average ultimate tensile strength. There was an insignificant amount of postpeak response observed in these samples. This was partly due to the fact that once the failure takes place, the frictional pullout force of the yarns was insignificant compared to the overall load-carrying capacity of the member. For example, a maximum level of 26% postpeak strength was observed in sample Kring1_4. A limiting deformation value of 4″ was used in all one-layer tests.

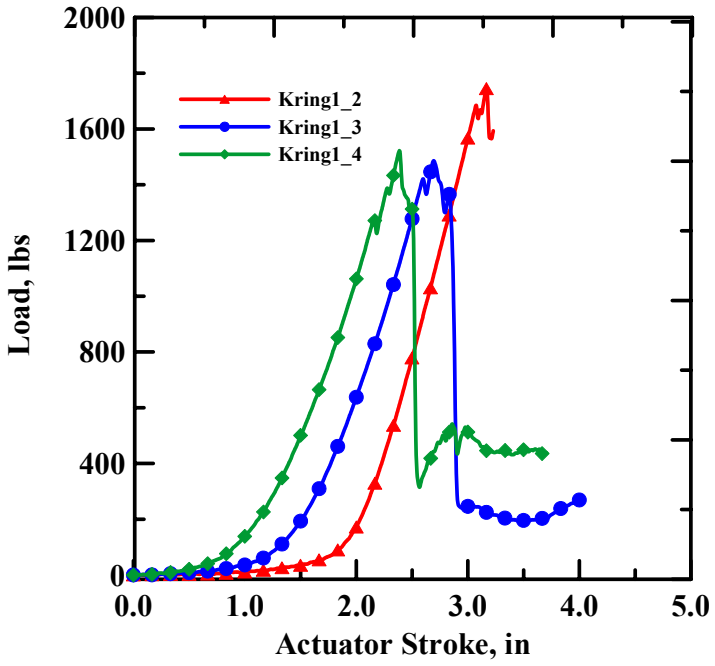

FIGURE 4-7. LOAD-DEFORMATION RESPONSE OF SINGLE-LAYER KEVLAR SPECIMENS PRIOR TO SLACK ADJUSTMENT

Figure 4-8 shows the load versus actuator stroke response of all one-layer Kevlar specimens after slack adjustment. For the unclamped specimens, this was achieved by shifting the raw load-deformation curves along the x axis so that the stiffnesses of the curves were coincident at the 250-lb load level. For the clamped specimen (Kring1_5), the shift was such that the maximum stiffness of the specimen was coincident with the unclamped specimens. Examination of figure 4-8 indicates that the stiffnesses of the samples are quite comparable. The average value of the stiffness for the single-layer specimens is 1108 lb/in., with a standard deviation of 50 lb/in. The ultimate loads for the hinged specimens, labeled Kring1_2, Kring1_3, and Kring1_4, are 1685, 1486, and 1522 lb respectively. This represents an average of 1564 lb and a standard deviation of 106 lb.

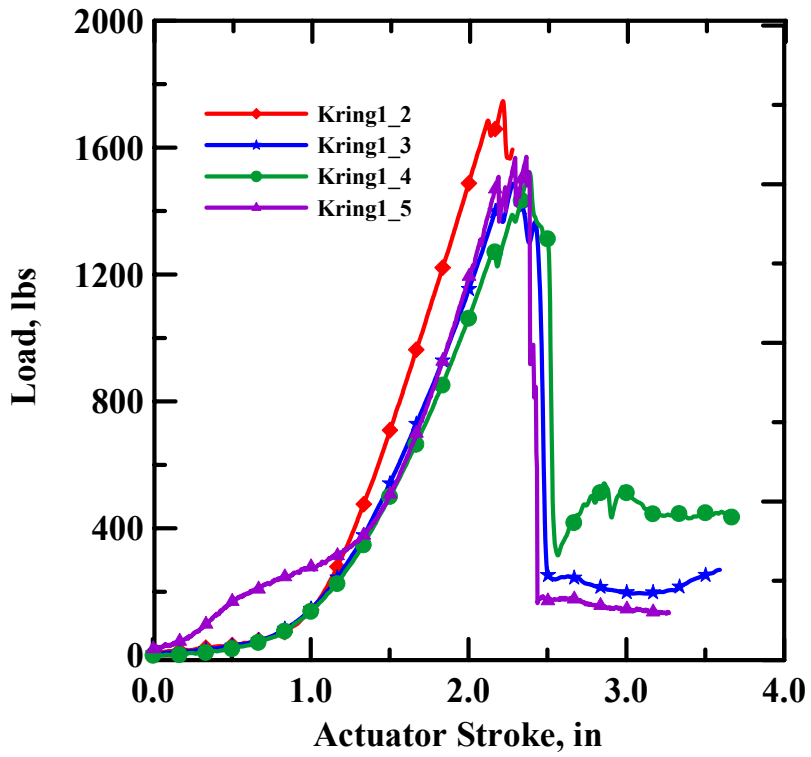

FIGURE 4-8. LOAD-DEFORMATION RESPONSE OF SINGLE-LAYER KEVLAR SAMPLES AFTER SLACK ADJUSTMENT

Note that after the slack adjustments (to equalize the zero to 1-inch actuator stroke), all the specimens follow the same slack recovery pattern. Specimen Kring1_5 represents the only specimen in this category that was clamped, and exhibits a knee in the early loading response. The clamped sample during the initial loading stages starts to pick up the load much earlier than the unclamped samples, indicating a reduced level of slack. This knee in the load-deformation response indicates the role of clamps. Between the 200- and 300-lb load, there are indications of sliding and loss of gripping at the clamps. This is shown by the increasing displacements at relatively the same level of load, which may indicate the slippage of the fabric at the grips. Beyond this level, the specimen behaved quite similar to the other unclamped specimens. Test results showed that the knee behavior is less noticeable with multilayer specimens.

Figure 4-9 shows a summary response plot for 1-, 2-, 4-, 8-, and 24-layer Kevlar specimens after slack adjustment (0.65, 1, 0.8, 1.1, and 0.3 in. in the 1-, 2-, 4-, 8-, and 24-layer specimens respectively). Although the peak load seems to scale proportional to the number of layers (up to eight layers), these responses may be viewed as highly nonlinear due to the progressive mechanism of failure that is operational in these specimens. It was observed that the two-layer specimen deviated from the one-layer curve at about 1000 lb, approximately 65% of the ultimate strength of a single layer. The four-layer specimen deviated from the two-layer specimen at about 1400 lb, and the eight-layer deviated from the four-layer specimen at about 2000 lb. This indicates that the contribution of outer layers to the stiffness of the overall assembly does not directly start at the beginning of the loading cycle. Significant displacement of the inner layers must take place before the outer layers are able to carry the load. This also indicated the importance of parameters such as the coefficient of friction between the layers, which is responsible for the mechanical interlock and, thus, the transfer of load from one layer to another.

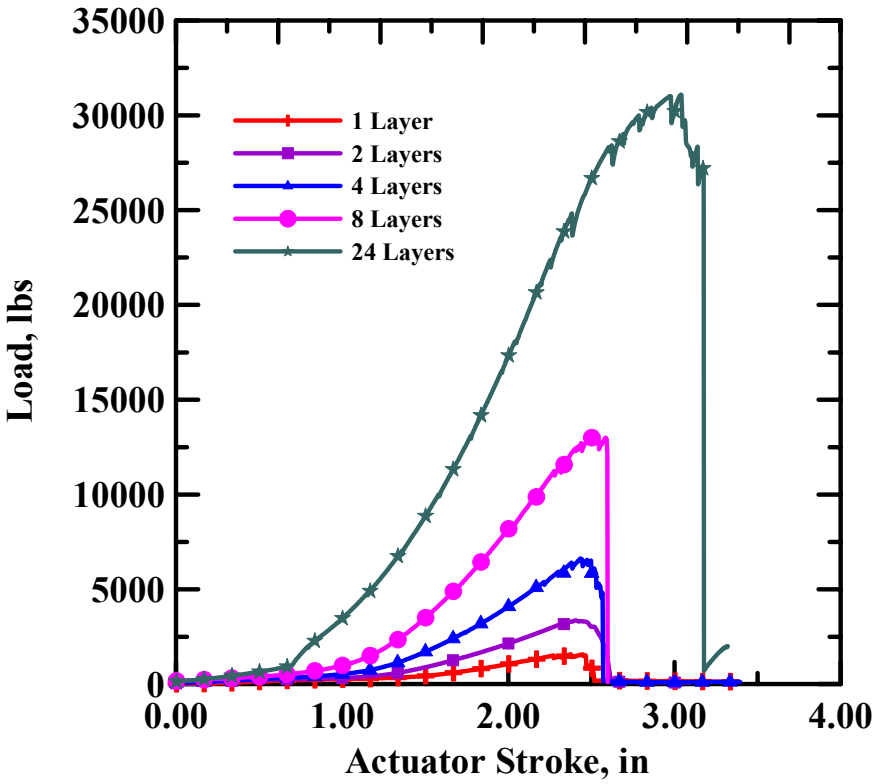

FIGURE 4-9. LOAD-DEFORMATION RESPONSE OF 1-, 2-, 4-, 8-, AND 24-LAYER KEVLAR SAMPLES

Figure 4-10 represents the response of 1-, 2-, 4-, 8-, and 24-layer Zylon samples after the slack adjustment (1, 0.47, 0.5, 0, and 0 in. in the 1-, 2-, 4-, 8-, and 24-layer specimens respectively). The amount of slack in these specimens was significant to the level of up to 3″ of travel distance. The use of clamps aided with the transfer of the load, as shown by the knee in the response; however, the stiffnesses of the material did not seem to be different during the early stages of loading. The one- and two-layer samples have almost the same stiffness up to the ultimate strength of the first layer. This indicates that the two-layer Zylon was not twice as stiff as the

single-layer specimens, and the sample had to be loaded to a significantly high level of its single load-carrying level for the second and subsequent layers to participate in load sharing.

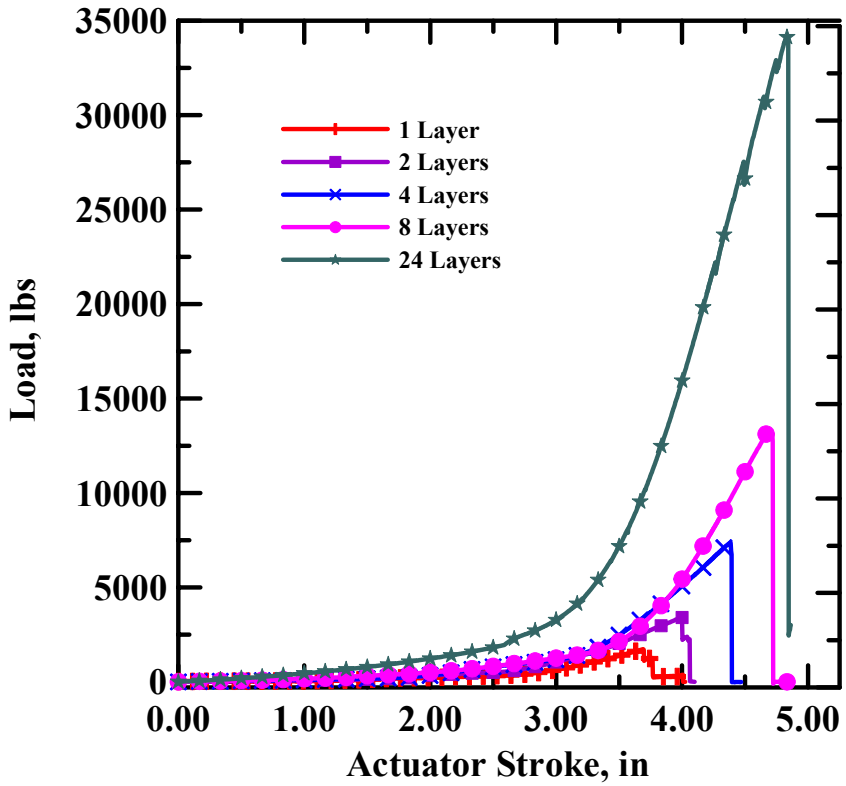

FIGURE 4-10. LOAD-DEFORMATION RESPONSE OF 1-, 2-, 4-, 8-, AND 24-LAYER ZYLON SAMPLES

Figures 4-11 and 4-12 show the energy absorbed/areal density and normalized energy absorbed/areal density graphs, respectively, for both the Kevlar and Zylon samples. The Zylon results showed more energy absorption capacity than the corresponding Kevlar specimens. The energy-absorbed graphs predict the fabric capacities as near linear in nature, but the normalized energy absorbed capacity show that there is no consistency in the energy absorption capacity of the fabrics. Figure 4-13 shows the peak load versus the number of layers for Kevlar and Zylon, and figure 4-14 shows the peak load normalized by areal density of both Kevlar and Zylon. Figure 4-15 shows the stiffness versus the number of layers as well as linearly extrapolated stiffness values for Kevlar and Zylon. Figure 4-16 shows the same with the peak load value normalized with the areal density of the respective material.

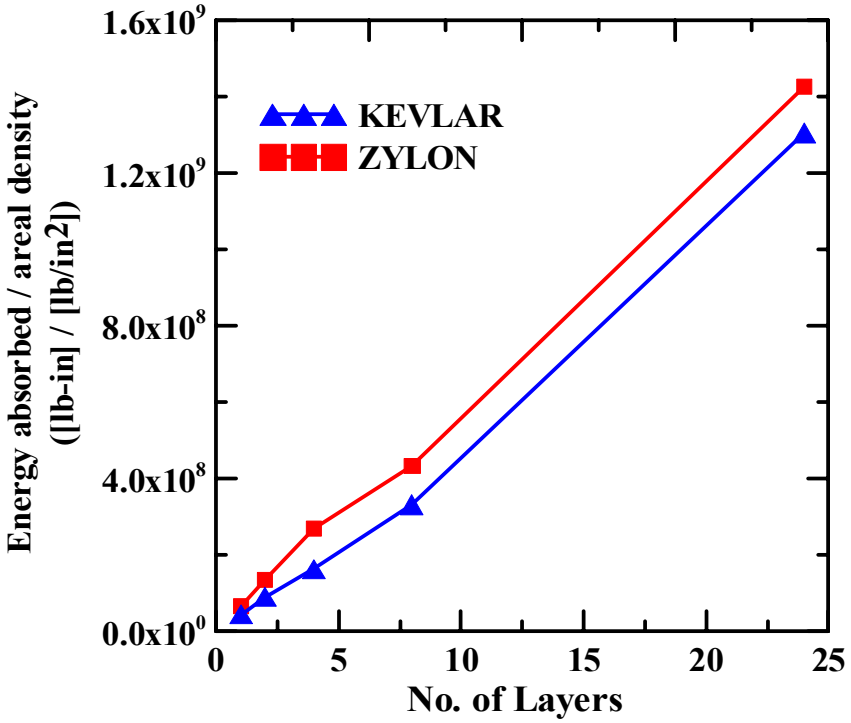

FIGURE 4-11. ENERGY-ABSORBED/AREAL DENSITY GRAPHS OF 1-, 2-, 4-, 8-, AND 24-LAYER KEVLAR AND ZYLON SAMPLES

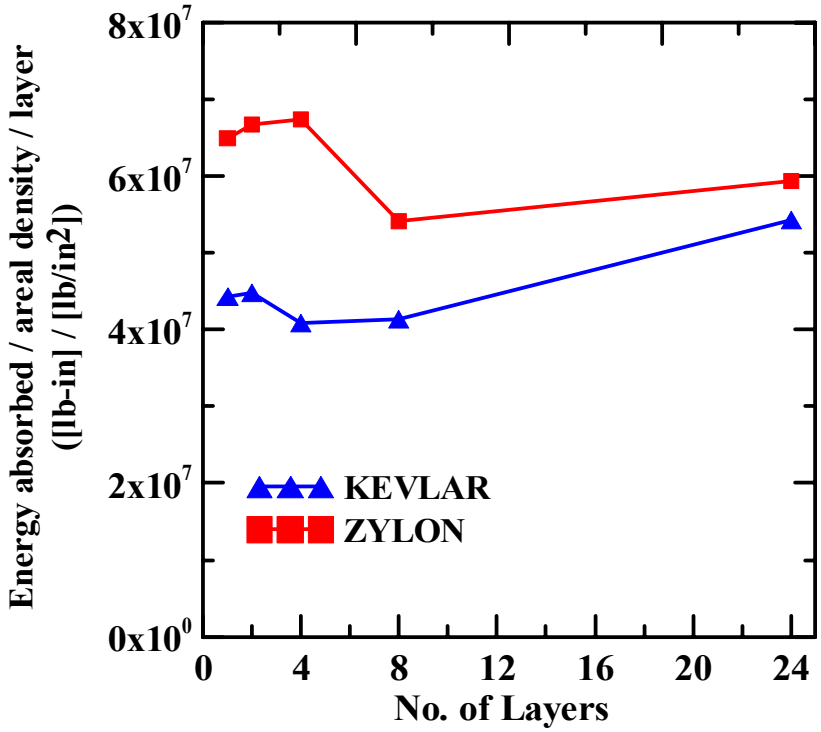

FIGURE 4-12. ENERGY-ABSORBED/AREAL DENSITY GRAPHS OF 1-, 2-, 4-, 8-, AND 24-LAYER KEVLAR AND ZYLON SAMPLES NORMALIZED BY NUMBER OF LAYERS

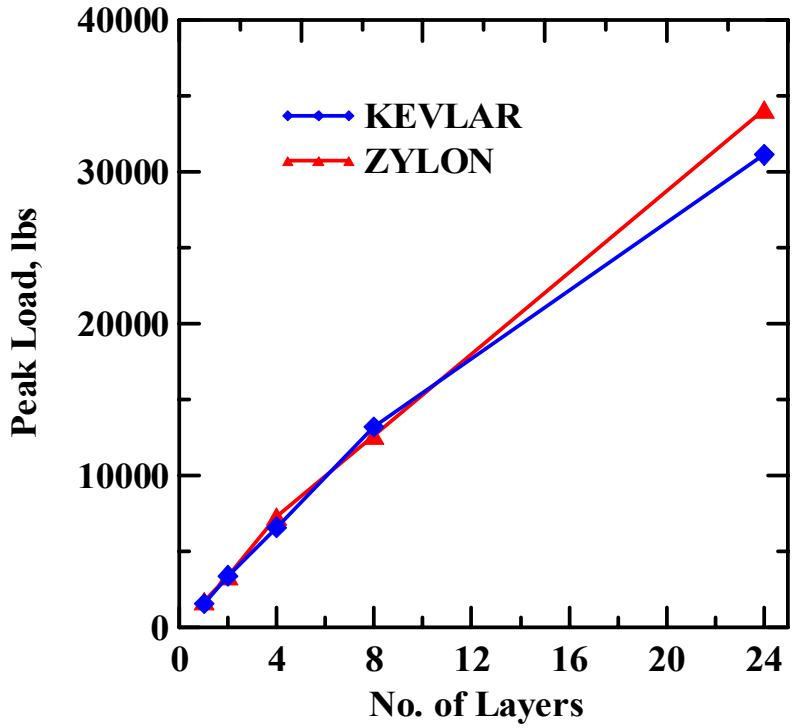

FIGURE 4-13. NUMBER OF LAYERS VS PEAK LOAD FOR ALL TESTS

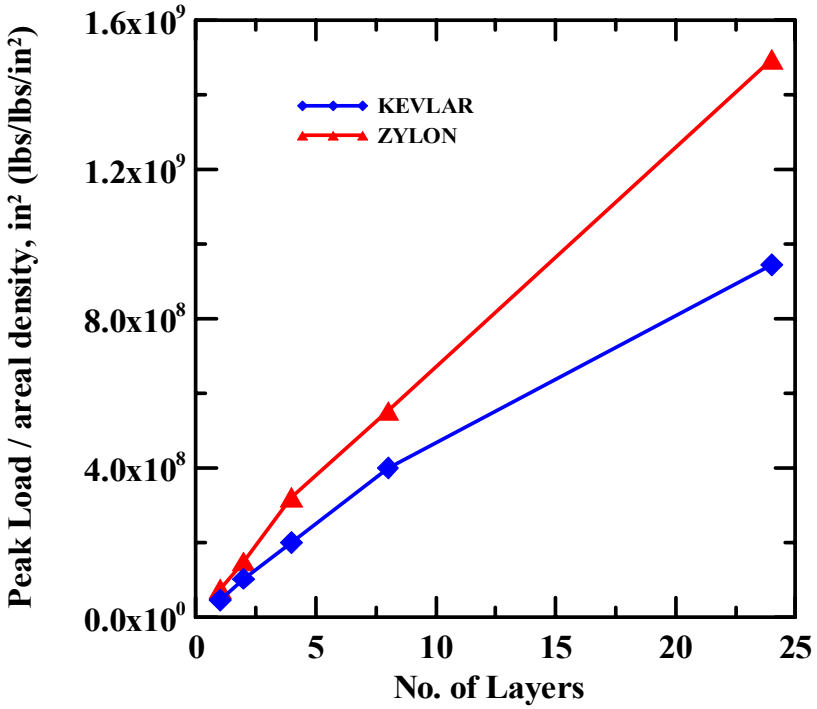

FIGURE 4-14. NUMBER OF LAYERS VS NORMALIZED PEAK LOAD FOR ALL TESTS

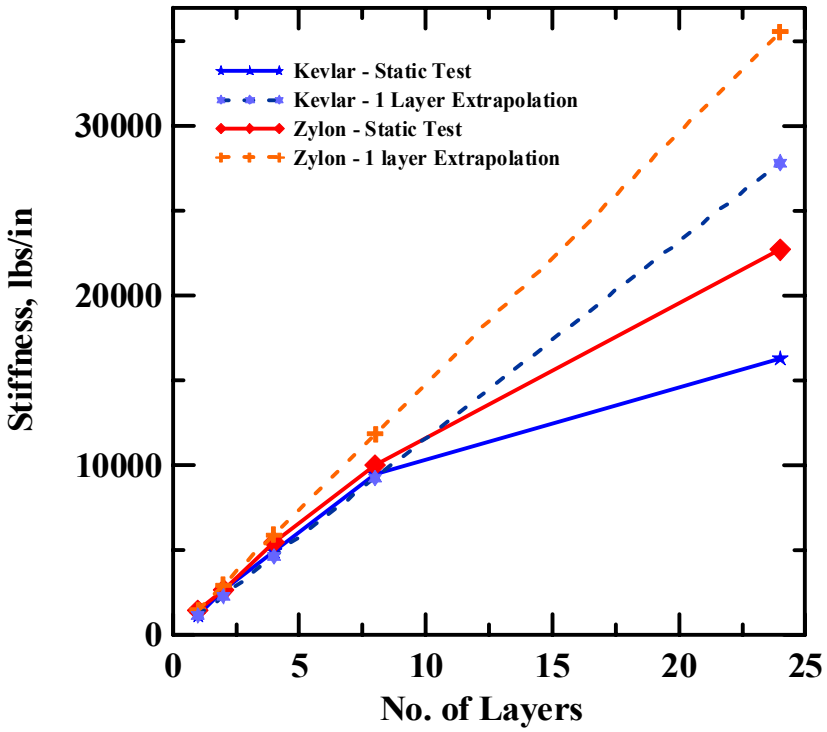

FIGURE 4-15. NUMBER OF LAYERS VS STIFFNESS FOR ALL TESTS (ACTUAL AND LINEARLY EXTRAPOLATED)

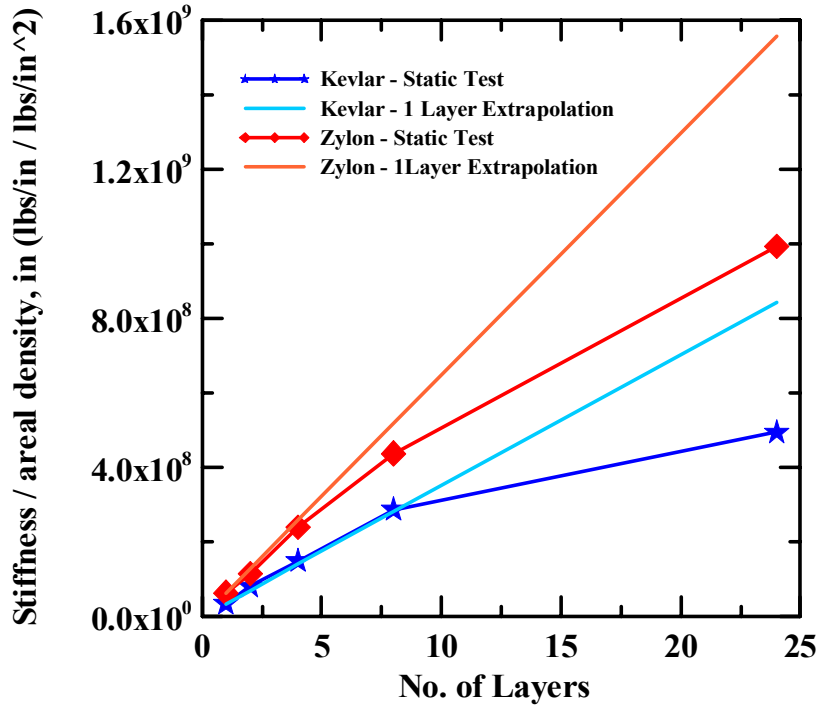

FIGURE 4-16. NUMBER OF LAYERS VS NORMALIZED STIFFNESS FOR ALL TESTS (ACTUAL AND LINEARLY EXTRAPOLATED)

5. FINITE ELEMENT MODELING.

To develop and validate a numerical model of the two fabrics used in this research project, the FE method is used. The FE modeling of the fabrics and the static tests is discussed in this section along with the comparison of the FE response with those obtained experimentally, as discussed in section 4.

5.1 OBJECTIVES.

There are two major objectives.

1. To develop a material model for Kevlar and Zylon fabrics using results from the simple tension tests, for use with FE analysis.

2. To use the material model from objective 1. in the FE models of the static tests, and compare the FE results with the experimentally obtained values. The focus is on capturing the behavior of the fabrics up until the peak response.

One can look at the Kevlar and Zylon fabrics as exhibiting orthotropic material behavior. The material modeling starts with the strain-stress relationship expressed as

$$\varepsilon = \mathrm{S}\sigma \tag{5-1}$$

where $\varepsilon_{6\times1}$ is the vector of strains and $\sigma_{6\times1}$ is the vector of stress and the two areas related to each other via the following material matrix

$$\mathrm{S}_{6\times6} = \begin{bmatrix} \frac{1}{E_1} & -\frac{\nu_{21}}{E_2} & -\frac{\nu_{31}}{E_3} & 0 & 0 & 0 \\ -\frac{\nu_{12}}{E_1} & \frac{1}{E_2} & -\frac{\nu_{32}}{E_3} & 0 & 0 & 0 \\ -\frac{\nu_{13}}{E_1} & -\frac{\nu_{23}}{E_2} & \frac{1}{E_3} & 0 & 0 & 0 \\ 0 & 0 & 0 & \frac{1}{G_{12}} & 0 & 0 \\ 0 & 0 & 0 & 0 & \frac{1}{G_{23}} & 0 \\ 0 & 0 & 0 & 0 & 0 & \frac{1}{G_{13}} \end{bmatrix} \tag{5-2}$$

The modulus of elasticity, E, Poisson's Ratio, ν, and shear modulus, G, are directional-dependent. Because of symmetry, there are a total of nine independent material constants: $E_1, E_2, E_3, G_{12}, G_{23}, G_{13}, \nu_{12}, \nu_{23}$, and ν_{13}. It should be noted that the material compliance matrix, *S*, is inverse of the material stiffness matrix, *E*.

In the current study, a simplified approximation is made. The results from the simple tension tests are used to obtain the major modulus of elasticity value, E_1, and the rest of the material constants are suitably adjusted as explained later in this section. When the material behavior of orthotropic material is extended beyond the elastic regime, one needs to define the appropriate failure criterion. In the current study, (principal) strain is used to determine when the initial material failure takes place. The limiting value is obtained from the simple tension tests that were discussed in section 2.

In the following sections, the FE models that are used to generate the various models have the following characteristics.

1. The ABAQUS/Standard FE program [1] is used.

2. The FE analysis involves static loads (load control), nonlinear stress-strain material behavior with smooth, finite sliding between the various contact surfaces, and uses large displacement theory.

3. Linear solid elements (eight-noded hexahedral and four-noded tetrahedral elements) are used throughout the model. The use of ABAQUS/Standard [1] precludes the use of shell elements to model the fabrics. Contact definition between shell and solid elements is difficult to capture in ABAQUS/Standard. The use of higher-order elements (20-noded hexahedral and 10-noded tetrahedral elements) is also not encouraged due to the underlying contact problem. Convergence studies using the developed model show that the linear elements are adequate in providing the required results.

The following section explains how the user-defined material model is developed. The static test FE models are discussed in section 5.3.

5.2 TENSION TEST MODELS.

A nonlinear stress-strain material behavior in the context of an FE analysis using ABAQUS requires a user-defined subroutine. The UMAT (user subroutine to define a material's mechanical behavior) feature is used. The major features of this user subroutine [2] are as follows:

1. It can be used to define the mechanical-constitutive behavior of a material.

2. It can be used with any procedure that includes mechanical behavior.

3. Solution-dependent state variables can be used.

4. The subroutine must update the stresses and solution-dependent state variables to their values at the end of the increment for which it is called.

5. The subroutine must provide the material Jacobian matrix, $\partial\Delta\sigma/\partial\Delta\varepsilon$, for the mechanical-constitutive model.

A piecewise linear approximation to the nonlinear stress-strain relationship obtained from the simple tension tests for Kevlar is shown in figure 5-1. The experimentally obtained curve (KTest1) is approximated by nine linear segments. Table 5-1 shows the limiting strain value in each segment and the corresponding modulus of elasticity. In the FE simulations, the strain-softening zone is not implemented. The steep negative slope leads to convergence problems. Beyond the peak, the slope of the stress-strain curve is taken as $1/10^{th}$ of the largest slope. The slope of the compressive stress-strain curve is also assumed to be the same as the postpeak tensile stress-strain curve.

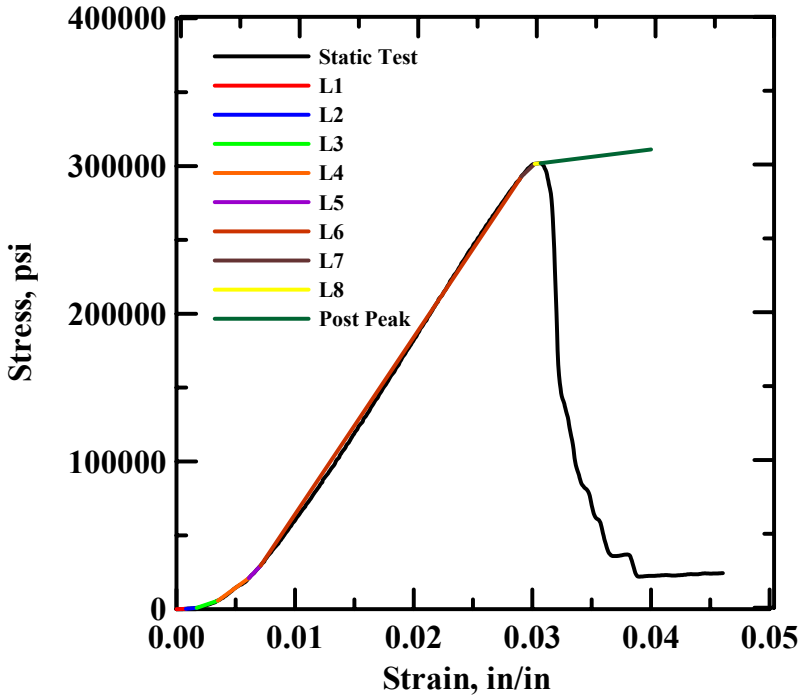

FIGURE 5-1. USER-SUPPLIED PIECEWISE LINEAR STRESS-STRAIN CURVE FOR KEVLAR (KTest1)

TABLE 5-1. PIECEWISE LINEAR KEVLAR STRESS-STRAIN DATA

Identification	Limiting Strain Value	Slope, E (psi)
L1	0.0008	$0.5354(10^6)$
L2	0.0017	$0.6637(10^6)$
L3	0.0035	$3.0000(10^6)$
L4	0.0061	$6.0000(10^6)$
L5	0.0071	$9.0000(10^6)$
L6	0.0291	$1.0000(10^7)$
L7	0.0302	$8.0000(10^6)$
L8	0.0307	$1.0000(10^6)$
Postpeak	> 0.0307	$1.0000(10^6)$

Two piecewise linear approximations to the nonlinear stress-strain relationship obtained from the simple tension tests for Zylon are shown in figures 5-2a and 5-2b. The graphs represent results obtained from the two sets of grips (ZTest1:T1 and ZSwath1:T2). The experimentally obtained curves are approximated by five linear segments. Tables 5-2a and 5-2b show the limiting strain value in each segment and the corresponding modulus of elasticity that is the slope of the segment.

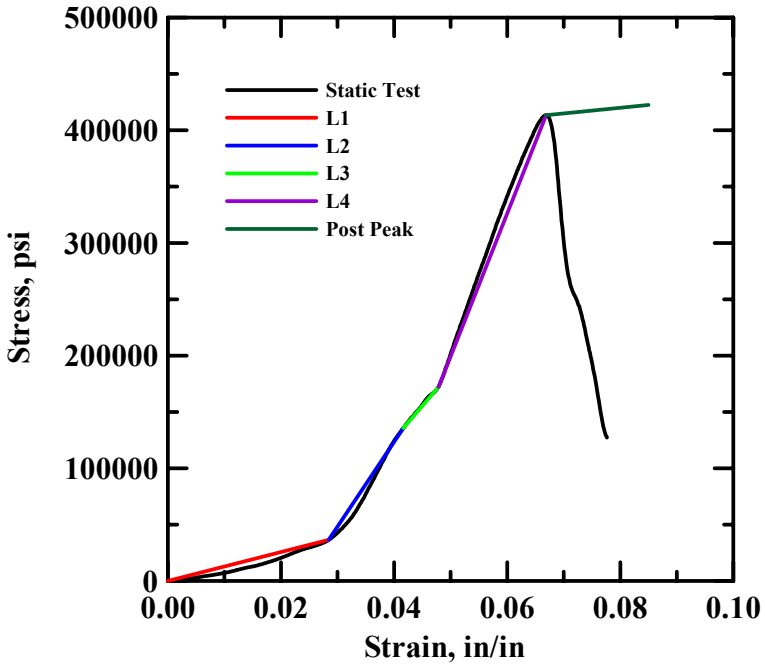

FIGURE 5-2a. PIECEWISE LINEAR STRESS-STRAIN CURVE FOR ZYLON (ZTest1, GRIP T1)

TABLE 5-2a. PIECEWISE LINEAR ZYLON STRESS-STRAIN DATA (T1)

Identification	Limiting Strain Value	Slope, *E* (psi)
L1	0.0282	$1.2814(10^6)$
L2	0.0403	$8.164686(10^6)$
L3	0.0480	$5.841931(10^6)$
L4	0.0671	$1.3277577(10^7)$
Post Peak	> 0.0671	$5.00000(10^5)$

In the FE simulations, the strain-softening zone is not implemented. The steep negative slope leads to convergence problems. Beyond the peak, the slope of the stress-strain curve is taken as a small fraction of the previous slope value. The slope of the compressive stress-strain curve is also assumed to be the same as the postpeak tensile stress-strain curve.

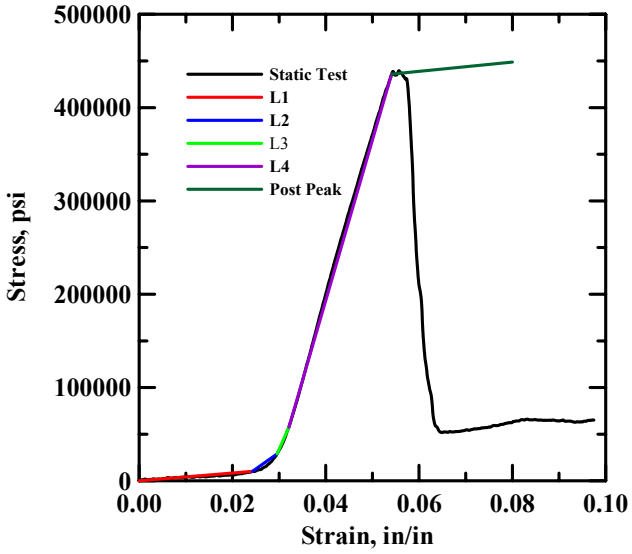

FIGURE 5-2b. PIECEWISE LINEAR STRESS-STRAIN CURVE FOR ZYLON (ZSwath1, GRIP T2)

TABLE 5-2b. PIECEWISE LINEAR ZYLON STRESS-STRAIN DATA (T2)

Identification	Limiting Strain Value	Slope, E (psi)
L1	0.02429	3.11356 (10^5)
L2	0.02957	3.495549 (10^6)
L3	0.03208	1.159249 (10^7)
L4	0.05413	1.743572 (10^7)
Postpeak	> 0.05413	5.00000 (10^5)

To verify the user-developed material modeling subroutine for both Kevlar and Zylon, the displacement control approach was used in the FE analysis, and the results from the FE analysis matched the experimental values obtained from the simple tension tests up until the peak response.

In the absence of a more sophisticated procedure, the material values used in the material model are assumed as follows. The motivation was that the fabric in the static tests would primarily be loaded in the (warp) direction; the direction used in the simple tension tests to generate the stress-strain diagram for the two fabrics.

1. The in-plane tensile moduli are taken as $E_1 = E_2 = E$.

2. The out-of-plane tensile modulus is taken as $E_3 = 0.05E$.

3. The in-plane shear modulus is taken as $G_{12} = 0.2E$. Similarly, the rest of the shear moduli are also taken as $G_{13} = G_{23} = G_{12} = 0.2E$.

4. All the Poisson's ratios are considered to be negligible and are taken as 0.01 to avoid numerical problems.

5.3 FINITE ELEMENT ANALYSIS OF STATIC TEST MODELS.

Because of the inherent symmetry (figure 5-3) of the geometry and the loading, the analysis is performed on a quarter symmetry model. The static test FE model contains the following components:

1. The A-36 steel cylinder—outer diameter 32 in., width 6 in. (z direction), and thickness 1 in. The cylinder contains an opening or window that is in the circumferential direction.

2. A cold-rolled steel blunt nose (or penetrator) dimensions are 2 by 8.5 by 5/16 in. The nose is constrained to move in radial direction, passes through the window in the cylinder, and pushes the fabric, thereby loading it.

3. One concentric layer of finite elements representing the fabric (either Kevlar or Zylon) wrapped circumferentially around the cylinder. It should be noted that in the actual tests, the multilayer fabric assumes the shape of a spiral. The dimensions of the fabric specimen that is modeled as a cylinder are as follows:

    - Radius = 16 in.
    - Thickness of each layer (Kevlar) = 0.003024 in.
    - Thickness of each layer (Zylon) = 0.00194532 in.
    - Width = 4 in.

The steel cylinder and the blunt nose are modeled with elastic, isotropic material properties.

- Modulus of elasticity = 29(106) psi
- Poisson's Ratio = 0.3

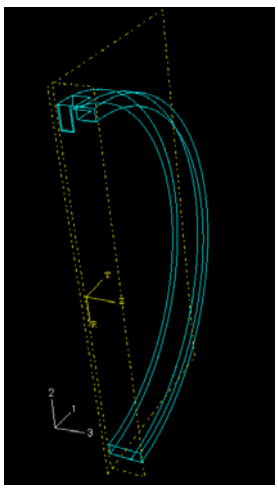

FIGURE 5-3. GEOMETRIC MODEL SHOWING QUARTER MODEL OF THE STATIC TEST SETUP

The fabric is modeled using the user-defined stress-strain relationship discussed in section 5-2. The FE mesh (figure 5-4) of the quarter symmetry model has 4909 nodes (14,727 degrees of freedom), and 2255 elements. Linear hexahedral (eight-noded, fully integrated) elements were used to mesh the cylinder, fabric strip, and the blunt nose. The region in the vicinity of the blunt nose tip and the window in the cylinder has a substantially higher grid density than the other regions (figure 5-5). Convergence studies showed that the displacements had converged with the mesh density shown in the figures.

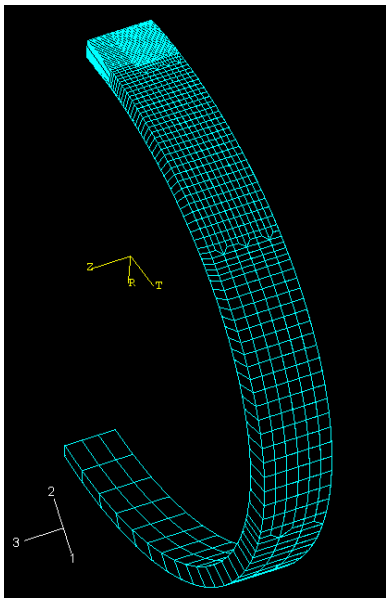

FIGURE 5-4. FINITE ELEMENT MESH

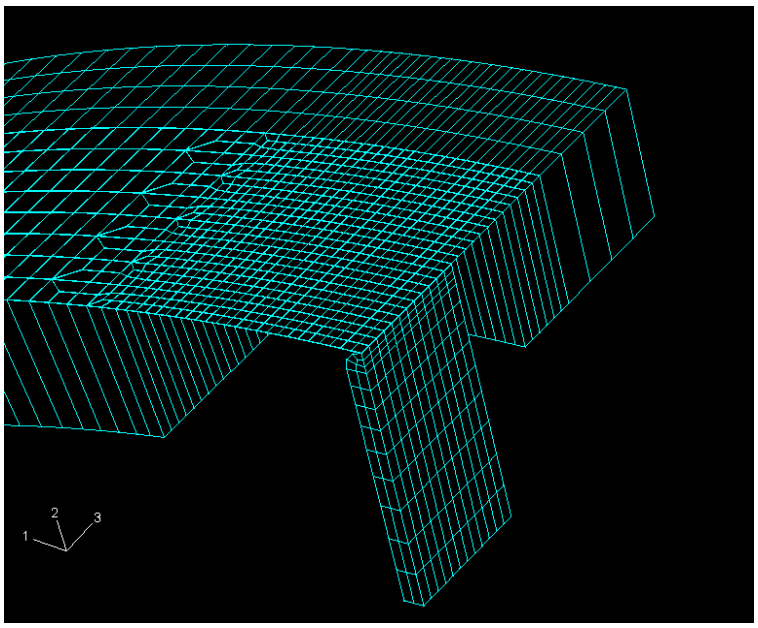

FIGURE 5-5. DETAILS OF THE FE MESH SHOWING THE BLUNT NOSE, STEEL CYLINDER, AND THE FABRIC

The loads and boundary conditions applied during the experiment are replicated on the FE model (figures. 5-6a and 5-6b)—the line of nodes corresponding to the location of the clamps were constrained from moving in all directions. In addition, the blunt nose is constrained to move in the radial (or 2) direction. The nodes at the bottom of the cylinder are also constrained from moving in all directions.

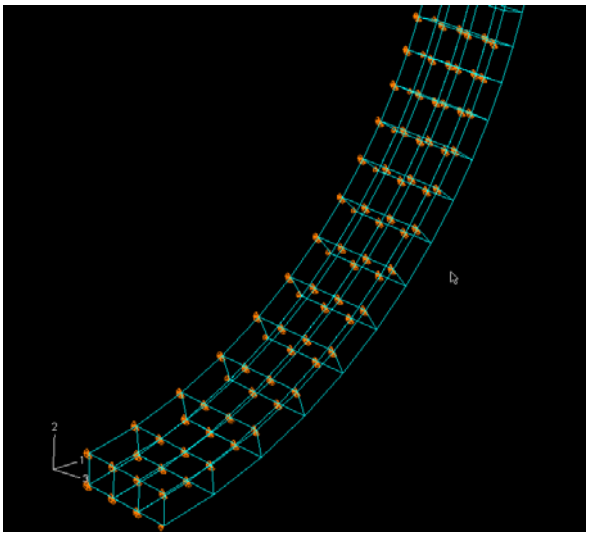

FIGURE 5-6a. BOUNDARY CONDITIONS IMPOSED ON THE BOTTOM OF THE STEEL CYLINDER AND AT THE POSITION OF THE CLAMPS

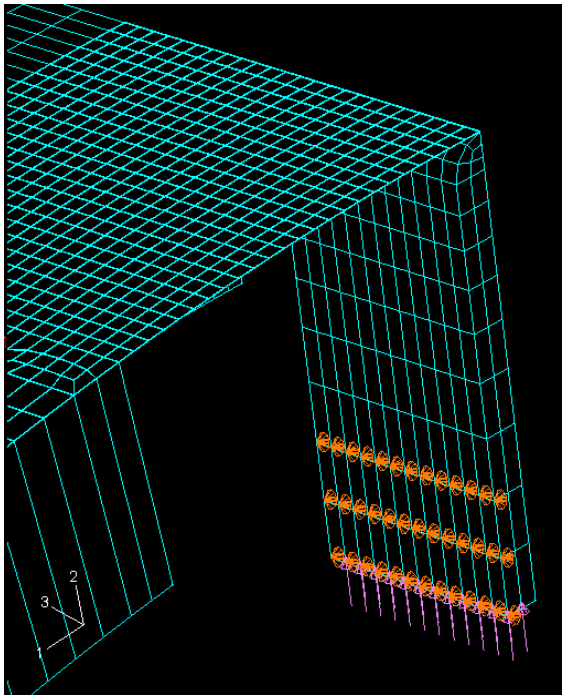

FIGURE 5-6b. BOUNDARY CONDITIONS IMPOSED AT THE BOTTOM OF THE BLUNT NOSE

Two sets of contact surfaces are defined and used in the model. The first is between the fabric and the steel cylinder. The second is between the blunt nose and the fabric. A finite-sliding interaction, which is the most general and allows for arbitrary separation, sliding, and rotation of the participating surfaces, is assigned in both contact cases. The formulation is well-suited to geometrically nonlinear analysis. No friction between the contact surfaces is considered.

The loading from the blunt nose is applied as uniformly distributed loading on the bottom of the blunt nose. The loading is applied in increments to track and construct the load versus blunt nose tip displacement graph.

In the following sections, the results from the FE analyses are presented and compared to the experimentally obtained values that contain an unknown amount of slack. As a result, the experimental load-deflection graphs are shifted horizontally so that the linear portion of the experimental and FE simulation graphs are close to each other.

5.3.1 One-Layer Kevlar Model.

Figure 5-7 and table 5-3 show the comparison between the static test and the results obtained from the FE analysis (FEA).

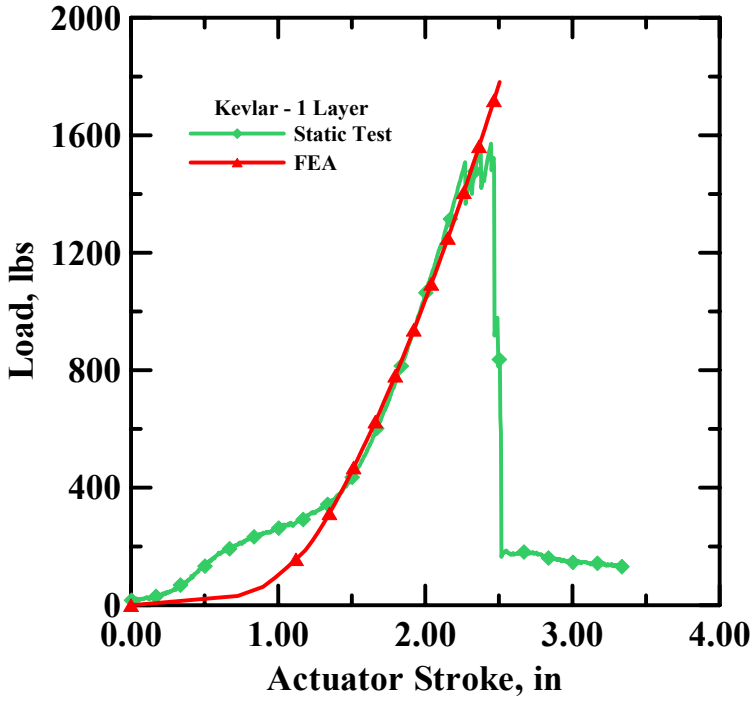

FIGURE 5-7. COMPARISON OF THE LOAD-DISPLACEMENT GRAPHS FOR A ONE-LAYER KEVLAR TEST

TABLE 5-3. STATIC TEST—FEA COMPARISON FOR A ONE-LAYER KEVLAR TEST

	Static Test Kring1_5	FEA
Peak load (lb)	1571	1782
Displacement at peak load (in.)	2.35	2.51

The experimental curve was slack-shifted by 0.65″.

Observations for one-layer Kevlar simulation:

1. Largest strain range (%)

    - Tensile 8 to 10
    - Compressive 2 to 6

2. Reason for termination of the analysis

    - Overclosure of contact surfaces of the fabric and blunt nose, convergence judged unlikely.

3. Strain ranges (%)

    - Near the blunt nose 6 to 10
    - Near the clamps 1.3 to 2.5
    - In between 1.3 to 2.5

4. Contact between the fabric and the ring at the end of the simulation

    - Angle of contact (°) 299.7
    - Arc length of contact (in.) 83.7

The FE and experimental peak load and displacement values are quite close. The FE load-deflection graph follows the experimental graph very closely, except for the initial portion. The FE simulation overpredicts the peak load. This behavior occurs with some of the simulations and is due to the fact that the finite elements where the ultimate strain has been exceeded are still a part of the FE model. Since these elements are not deleted, they still provide some finite stiffness to the overall response. However, it should be noted that these strain zones are very localized (see figures 5-8 and 5-9).

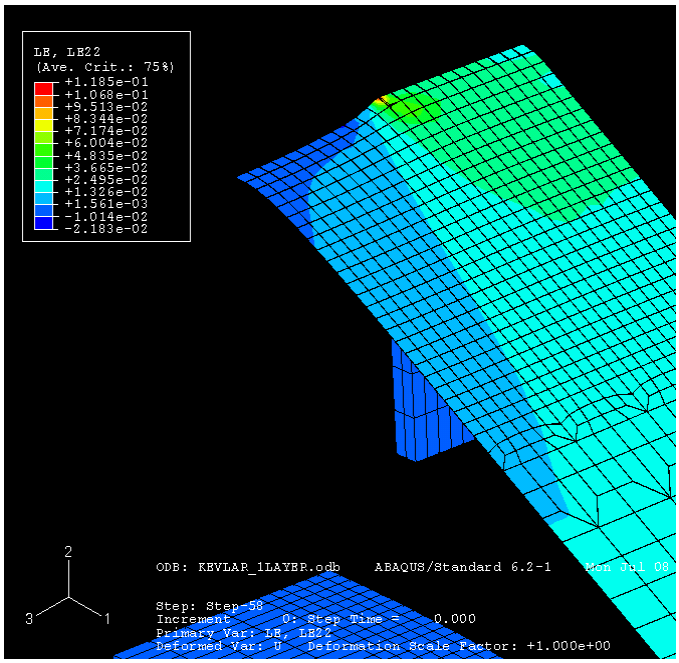

FIGURE 5-8. ONE-LAYER KEVLAR—PLOT OF IN-PLANE STRAIN ε_1 SUPERIMPOSED ON DEFORMATION AT THE END OF THE LAST LOAD STEP

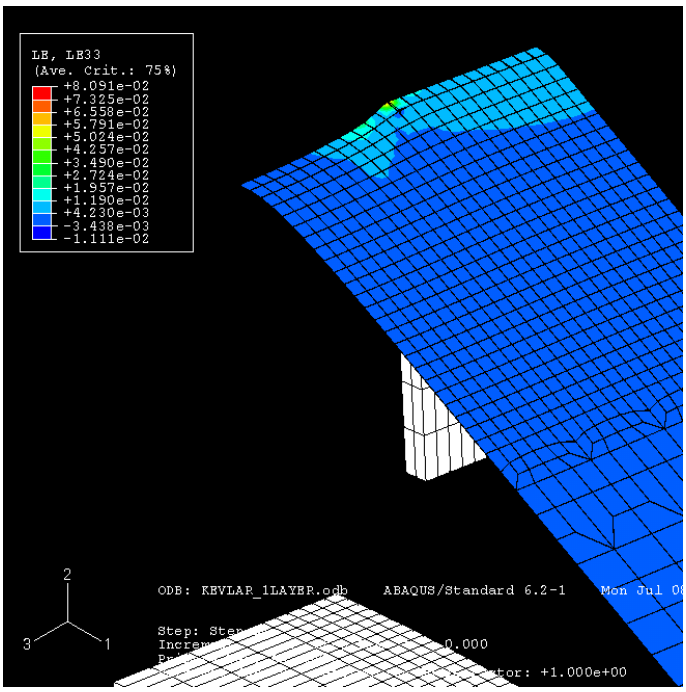

FIGURE 5-9. ONE-LAYER KEVLAR—PLOT OF IN-PLANE STRAIN ε_2 SUPERIMPOSED ON DEFORMATION AT THE END OF THE LAST LOAD STEP

5.3.2 Two-Layer Kevlar Model.

Figure 5-10 and table 5-4 show the comparison between the static test and the results obtained from the FEA. The two layers of Kevlar are modeled with one layer of finite elements with the thickness twice that of one layer of Kevlar fabric.

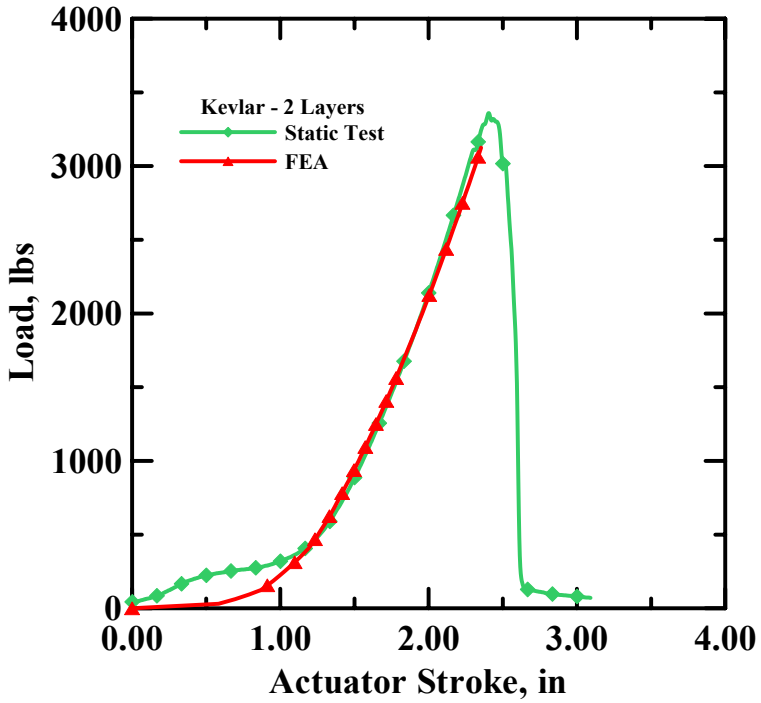

FIGUR E 5-10. COMPARISON OF THE LOAD-DISPLACEMENT GRAPHS FOR A TWO-LAYER KEVLAR TEST

TABLE 5-4. STATIC TEST—FEA COMPARISON FOR A TWO-LAYER KEVLAR TEST

	Static Test Kring2_1	FEA
Peak load (lb)	3360	3125
Displacement at peak load (in.)	2.41	2.35

The experimental curve was slack-shifted by 0.9″.

Observations for two-layer Kevlar simulation:

1. Largest strain range (%)

- Tensile 7.6 to 12.4
- Compressive 0.8 to 2

2. Reason for termination of the analysis

- End of load steps, analysis completed successfully.

3. Strain ranges (%)

- Near the blunt nose 6.4 to 12.4
- Near the clamps 1.6 to 2.7
- In between 1.6 to 2.7

4. Contact between the fabric and the ring at the end of the simulation

- Angle of contact (°) 301.3
- Arc length of contact (in.) 84.1

Once again, the FE and experimental peak load and displacement values are quite close. As with the one-layer model, the FE load-deflection graph follows the experimental graph very closely except for the initial portion. However, the FE simulation under predicts the peak load. This is because the FE model is inherently stiff. See figures 5-11 and 5-12.

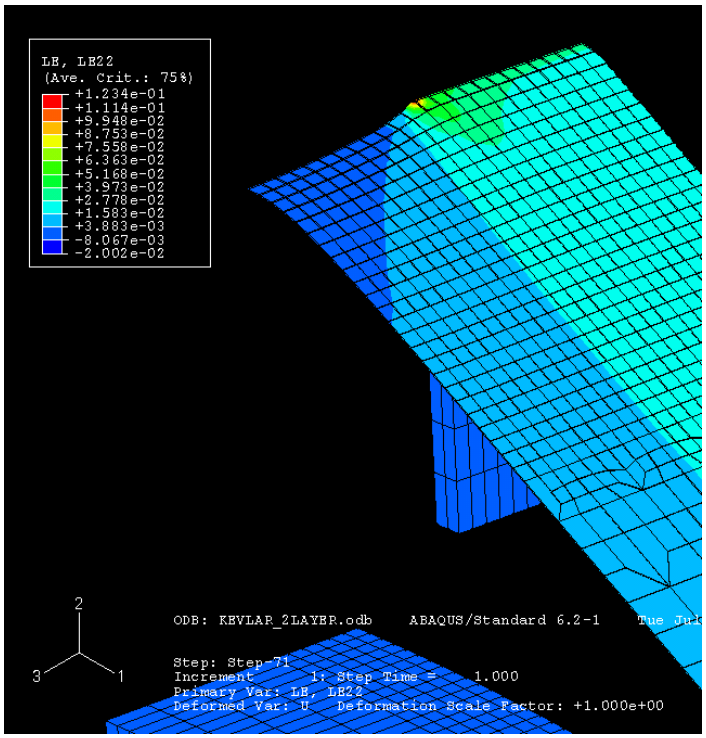

FIGURE 5-11. TWO-LAYER KEVLAR—PLOT OF IN-PLANE STRAIN ε_1 SUPERIMPOSED ON DEFORMATION AT THE END OF THE LAST LOAD STEP

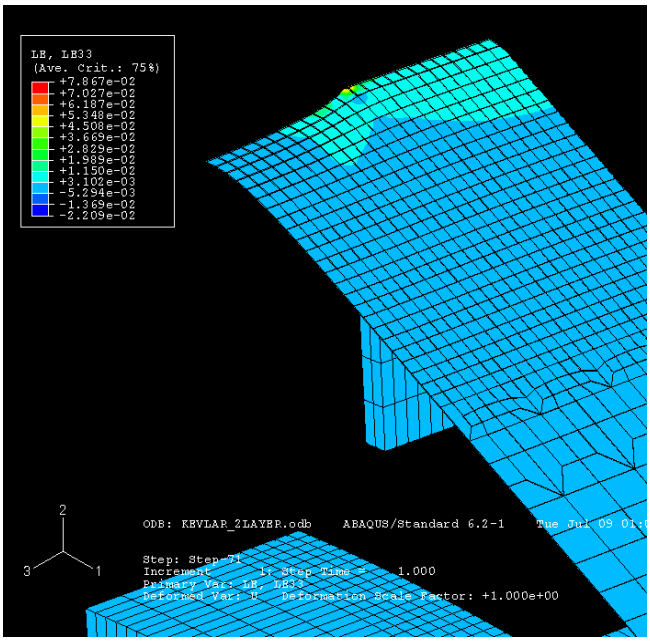

FIGURE 5-12. TWO-LAYER KEVLAR—PLOT OF IN-PLANE STRAIN ε_2 SUPERIMPOSED ON DEFORMATION AT THE END OF THE LAST LOAD STEP

5.3.3 Four-Layer Kevlar Model.

Figure 5-13 and table 5-5 show the comparison between the static test and the results obtained from the FEA. The four layers of Kevlar are modeled as one layer of finite elements with the thickness four times that of one layer of Kevlar fabric.

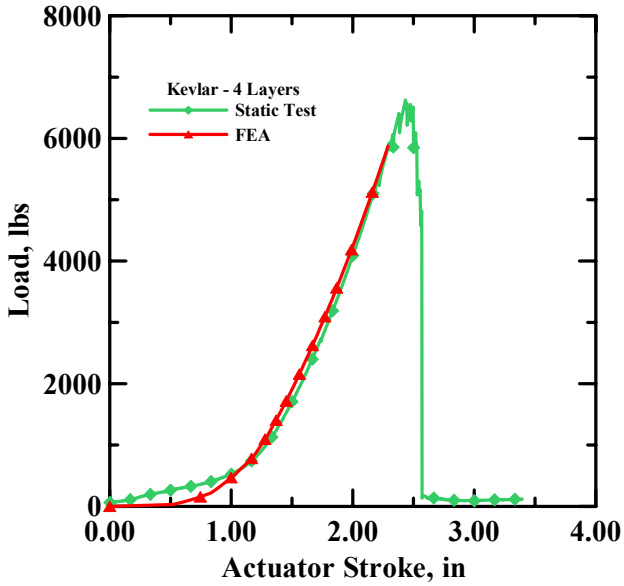

FIGURE 5-13. COMPARISON OF THE LOAD-DISPLACEMENT GRAPHS FOR A FOUR-LAYER KEVLAR TEST

TABLE 5-5. STATIC TEST—FEA COMPARISON FOR A FOUR-LAYER KEVLAR TEST

	Static Test Kring4_1	FEA
Peak load (lb)	6624	5875
Displacement at peak load (in.)	2.41	2.29

The experimental curve was slack-shifted by 0.8″.

Observations for Kevlar four-layer simulation:

1. Largest strain range (%)

   - Tensile 8 to 15
   - Compressive 0.7 to 2.1

2. Reason for termination of the analysis

   - Overclosure of contact surfaces of the fabric and nose, convergence judged unlikely.

3. Strain ranges (%)

   - Near the blunt nose 4 to 15
   - Near the clamps 0.7 to 0.73
   - In between 0.7 to 0.73

4. Contact between the fabric and the ring at the end of the simulation

   - Angle of contact (°) 302
   - Arc length of contact (in.) 84.3

The four-layer model follows the trends exhibited with the one- and two-layer models. The FE and experimental peak load and displacement values are quite close. The FE load-deflection graph follows the experimental graph very closely, including the initial portion of the experimental graph where there is less of a knee. The FE simulation underpredicts the peak load. See figures 5-14 and 5-15.

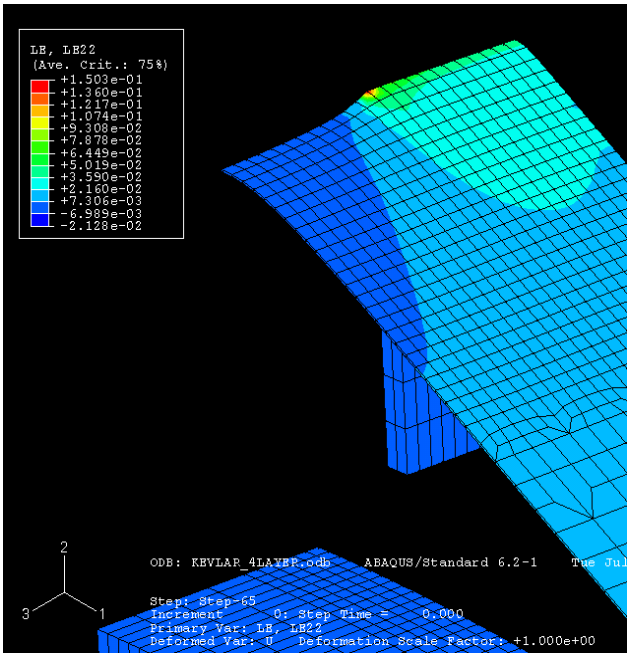

FIGURE 5-14. FOUR-LAYER KEVLAR—PLOT OF IN-PLANE STRAIN ε_1 SUPERIMPOSED ON DEFORMATION AT THE END OF THE LAST LOAD STEP

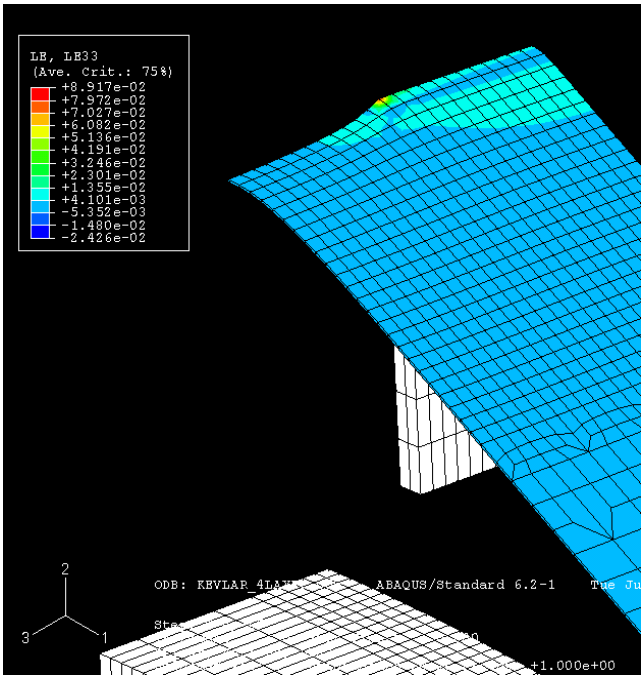

FIGURE 5-15. FOUR-LAYER KEVLAR—PLOT OF IN-PLANE STRAIN ε_2 SUPERIMPOSED ON DEFORMATION AT THE END OF THE LAST LOAD STEP

5.3.4 Eight-Layer Kevlar Model.

Figure 5-16 and table 5-6 show the comparison between the static test and the results obtained from the FE analysis. The eight layers of Kevlar are modeled as one layer of finite elements with the thickness eight times that of one layer of Kevlar fabric.

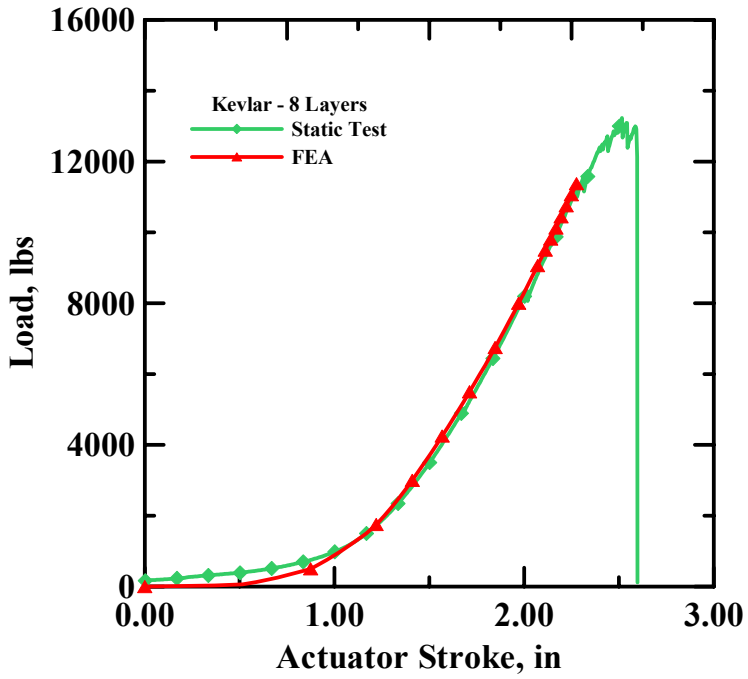

FIGURE 5-16. COMPARISON OF THE LOAD-DISPLACEMENT GRAPHS FOR AN EIGHT-LAYER KEVLAR TEST

TABLE 5-6. STATIC TEST—FEA COMPARISON FOR AN EIGHT-LAYER KEVLAR TEST

	Static Test Kring8_1	FEA
Peak load (lb)	13231	11375
Displacement at peak load (in.)	2.52	2.28

The experimental curve was slack-shifted by 1.1″.

Observations for eight-layer Kevlar simulation:

1. Largest strain range (%)

- Tensile 4 to 18
- Compressive 1.5 to 3

2. Reason for termination of the analysis

   - Overclosure of contact surfaces of the fabric and nose, convergence judged unlikely.

3. Strain ranges (%)

   - Near the blunt nose 2 to 18
   - Near the clamps 0.3 to2
   - In between 0.3 to 2

4. Contact between the fabric and the ring at the end of the simulation

   - Angle of contact (°) 302.2
   - Arc length of contact (in.) 84.4

The eight-layer model follows the previous trends exhibited with the one-, two- and four-layer models. The FE and experimental peak load and displacement values are quite close. As with the four-layer model, the FE load-deflection graph follows the experimental graph very closely, including the initial portion of the experimental graph where there is less of a knee. The FE simulation underpredicts the peak load. It appears that not only the required amount of slack adjustment to bring the two graphs close to each other increases with the number of fabric layers, but also that there is less of a discrepancy between the two curves in the initial portion of the graph. See figures 5-17 and 5-18.

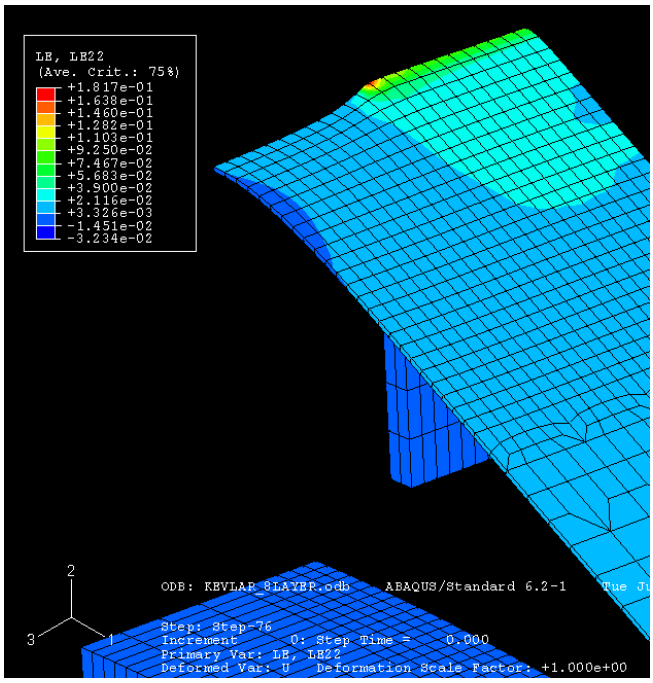

FIGURE 5-17. EIGHT-LAYER KEVLAR—PLOT OF IN-PLANE STRAIN ε_1 SUPERIMPOSED ON DEFORMATION AT THE END OF THE LAST LOAD STEP

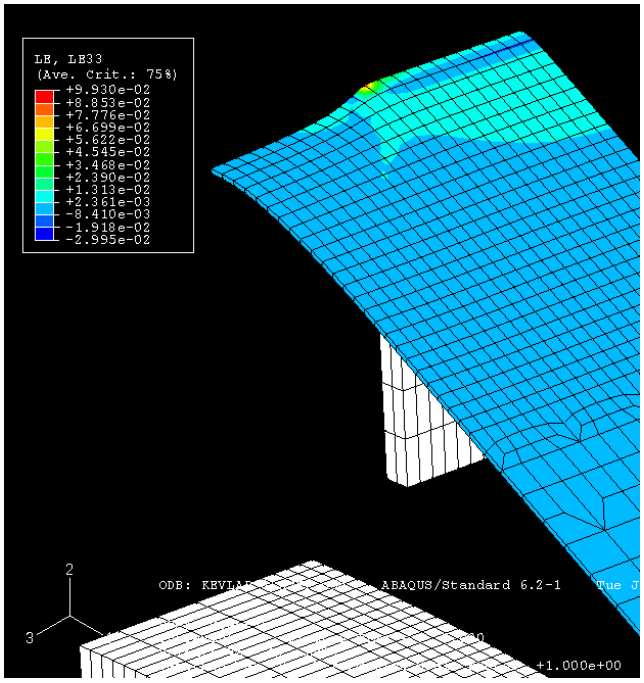

FIGURE 5-18. EIGHT-LAYER KEVLAR—PLOT OF IN-PLANE STRAIN ε_2 SUPERIMPOSED ON DEFORMATION AT THE END OF THE LAST LOAD STEP

5.3.5 Twenty-Four-Layer Kevlar Model.

Figure 5-19 and table 5-7 show the comparison between the static test and the results obtained from the FEA. The twenty-four layers of Kevlar are modeled as three layers of finite elements with the thickness of each layer eight times that of one layer of Kevlar fabric.

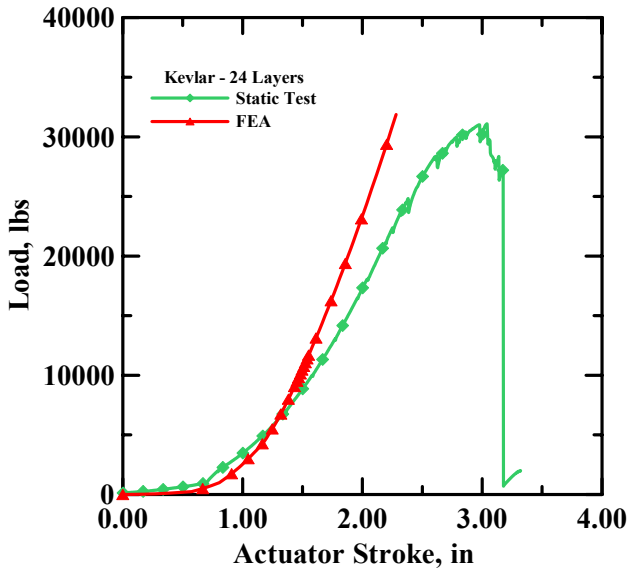

FIGURE 5-19. COMPARISON OF THE LOAD-DISPLACEMENT GRAPHS FOR A 24-LAYER KEVLAR TEST

TABLE 5-7. STATIC TEST—FEA COMPARISON FOR A 24-LAYER KEVLAR TEST

	Static Test Kring24_2	FEA
Peak load (lb)	31131	31875
Displacement at peak load (in.)	3.04	2.28

The experimental curve was slack-shifted by 0.3″.

Observations for 24-layer Kevlar simulation:

1. Largest strain range (%)

   - Tensile 7 to 21
   - Compressive 0.4 to 4

2. Reason for termination of the analysis

   - Negative eigenvalues appear at the end of the load step, and the solution starts to diverge.

3. Strain ranges (%)

   - Near the blunt nose 3 to 21
   - Near the clamps 3.2 to 6.8
   - In between 3.2 to 6.8

4. Contact between the fabric and the ring at the end of the simulation

   - Angle of contact (°) 302.1
   - Arc length of contact (in.) 84.4

The 24-layer model follows some of the previous trends exhibited with the one-, two-, four-, and eight-layer models. The FE and experimental load and displacement values are quite close till about 15,000 lb. While the peak loads are close, the FE peak displacement is much less than the experimentally obtained value. Since the FE is much stiffer in this case, the FE results show that a larger value of load is needed to achieve the same level of deformation. The amount of slack adjustment to bring the two graphs close to each other is much less in this case, since in the experimental setup, the fabric was directly wrapped on the steel ring. See figures 5-20 and 5-21.

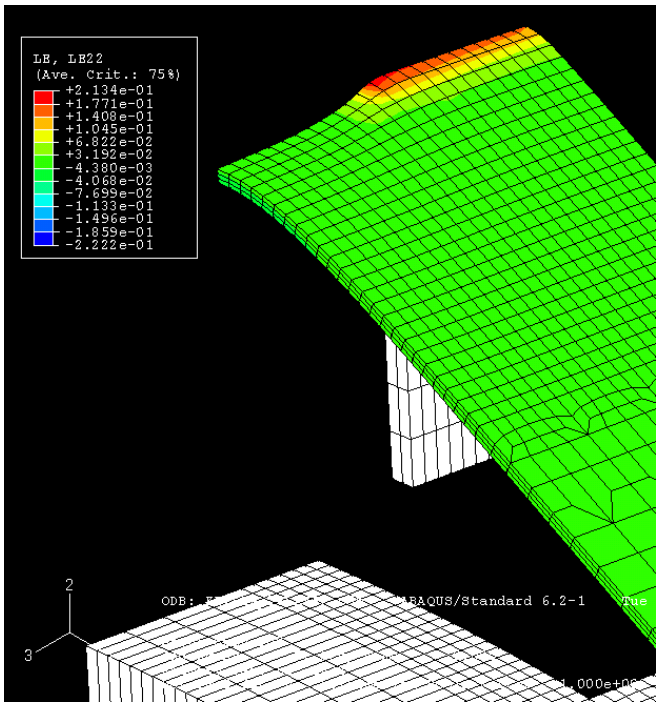

FIGURE 5-20. TWENTY-FOUR-LAYER KEVLAR—PLOT OF IN-PLANE STRAIN ε_1 SUPERIMPOSED ON DEFORMATION AT THE END OF THE LAST LOAD STEP

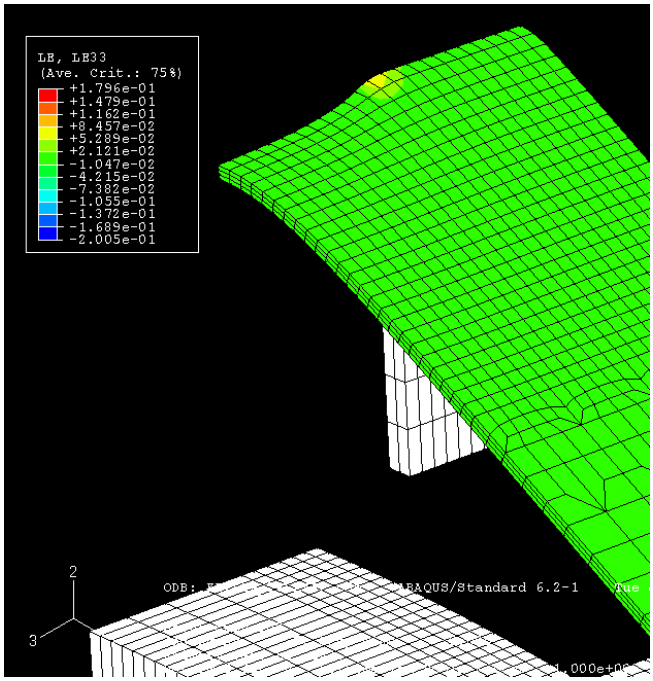

FIGURE 5-21. TWENTY-FOUR-LAYER KEVLAR—PLOT OF IN-PLANE STRAIN ε_2 SUPERIMPOSED ON DEFORMATION AT THE END OF THE LAST LOAD STEP

5.3.6 One-Layer Zylon Model.

Figure 5-22 and table 5-8 show the comparison between the static test and the results obtained from the FEA.

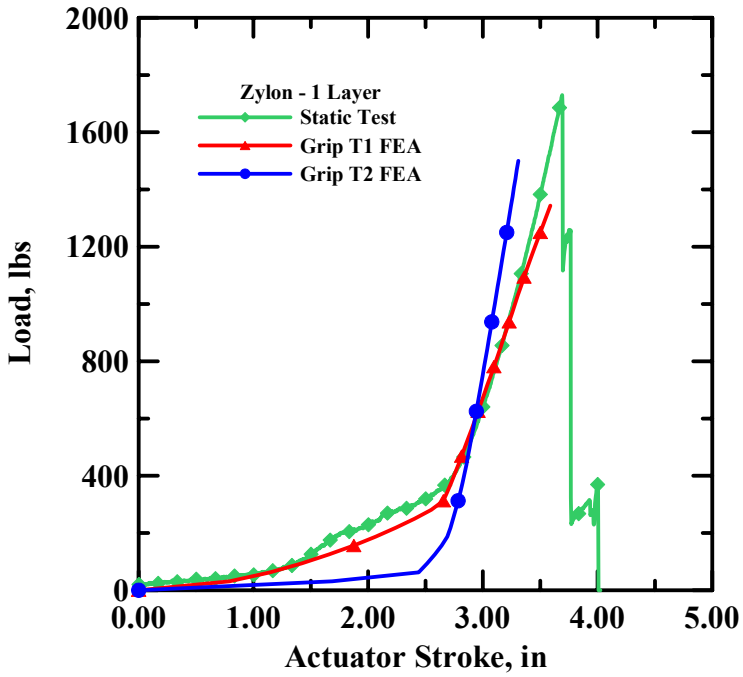

FIGURE 5-22. COMPARISON OF THE LOAD-DISPLACEMENT GRAPHS FOR A ONE-LAYER ZYLON TEST

TABLE 5-8. STATIC TEST—FEA COMPARISON FOR A ONE-LAYER ZYLON TEST

	Static Test Zring1_2	Grip T1 FEA	Grip T2 FEA
Peak load (lb)	1730	1344	1500
Displacement at peak load (in.)	3.69	3.59	3.31

The experimental curve was slack-shifted by 1″.

Observations for one-layer Zylon simulation:

Grip T1 FEA model:

1. Largest strain range (%)

   - Tensile 7 to 30
   - Compressive 0 to 0.4

2. Reason for termination of the analysis

   - End of load steps, analysis completed successfully.

3. Strain ranges (%)

   - Near the blunt nose 6.7 to 30
   - Near the clamps 6.7 to 9.3
   - In between 6.7 to 9.3

4. Contact between the fabric and the ring at the end of the simulation

   - Angle of contact (°) 289.5
   - Arc Length of contact (in.) 80.9

Grip T2 FEA model:

1. Largest strain range (%)

   - Tensile 7 to 12
   - Compressive 0 to 0.4

2. Reason for termination of the analysis

   - Negative eigenvalues appear at the end of the load step, the solution starts to diverge.

3. Strain ranges (%)

   - Near the blunt nose 4 to 12
   - Near the clamps 0.6 to 3
   - In between 3 to 6

4. Contact between the fabric and the ring at the end of the simulation

   - Angle of contact (°) 291.5
   - Arc length of contact (in.) 81.5

The FE and experimental peak load and displacement values as well as the load-deflection graphs are quite close for Grip T1 model. Both the FE simulations underpredict the peak load. Once again, this is because the FE model is inherently stiff. The fabric-draping effect is much more pronounced with these models when compared to the Kevlar models. Figures 5-23 and 5-24 show FEA results of Grip T1. Figures 5-25 and 5-26 show FEA results of Grip T2.

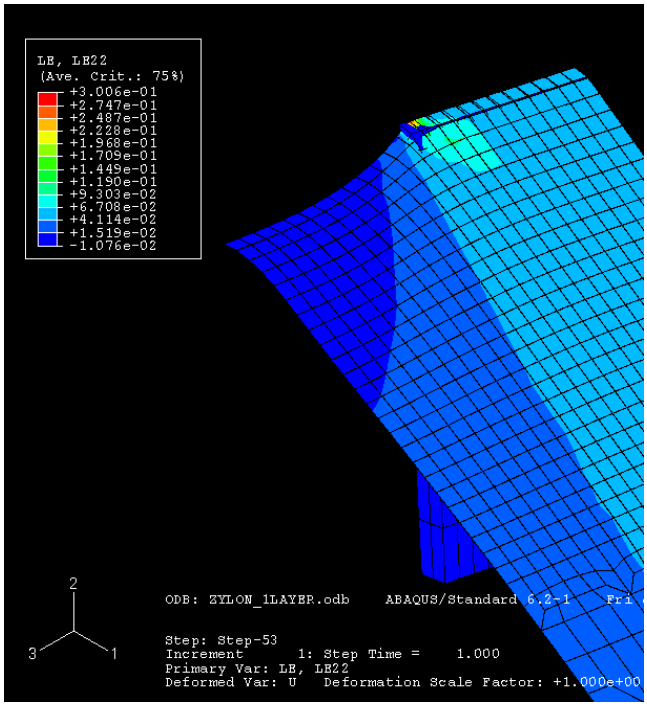

FIGURE 5-23. ONE-LAYER ZYLON—PLOT OF IN-PLANE STRAIN ε_1 SUPERIMPOSED ON DEFORMATION AT THE END OF THE LAST LOAD STEP (GRIP T1)

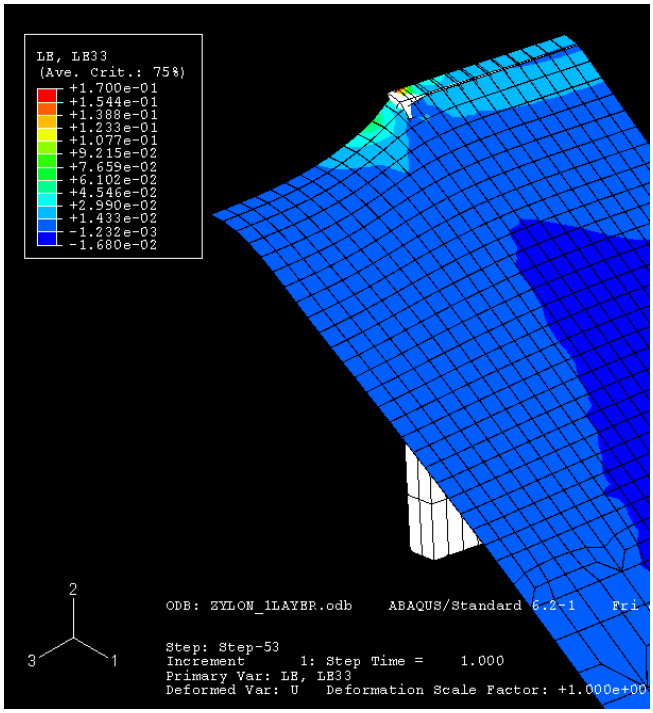

FIGURE 5-24. ONE-LAYER ZYLON—PLOT OF IN-PLANE STRAIN ε_2 SUPERIMPOSED ON DEFORMATION AT THE END OF THE LAST LOAD STEP (GRIP T1)

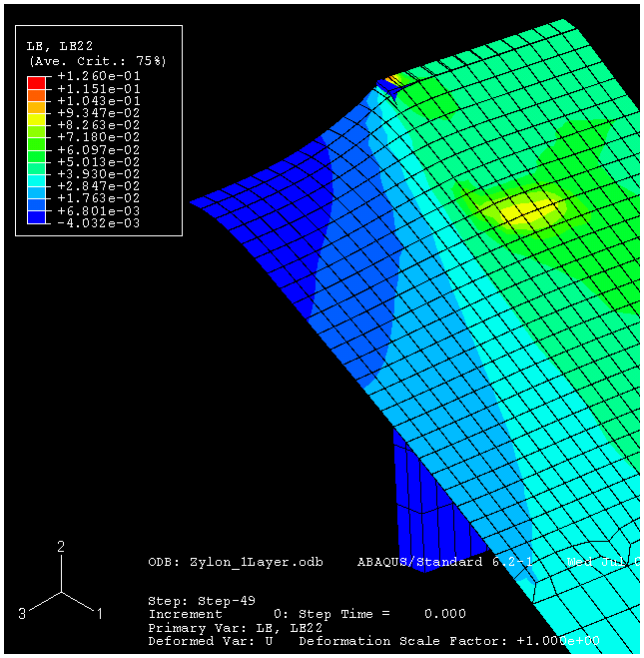

FIGURE 5-25. ONE-LAYER ZYLON—PLOT OF IN-PLANE STRAIN ε_1 SUPERIMPOSED ON DEFORMATION AT THE END OF THE LAST LOAD STEP (GRIP T2)

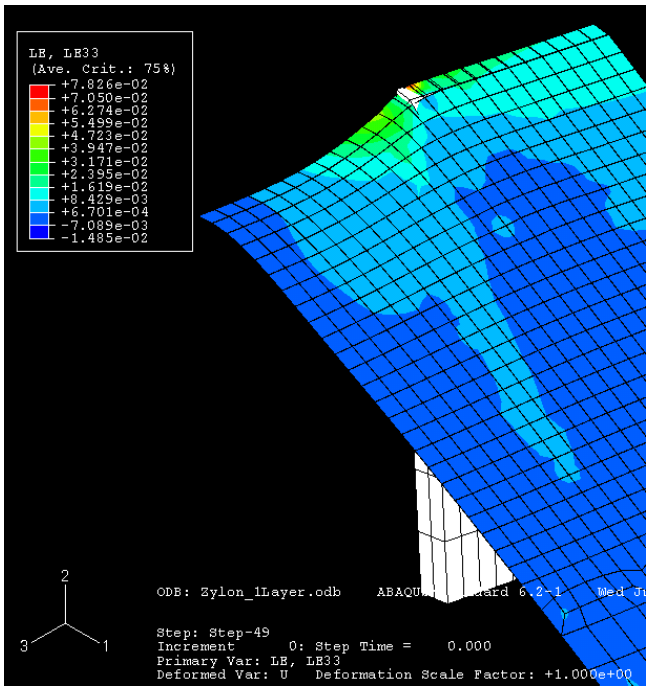

FIGURE 5-26. ONE-LAYER ZYLON—PLOT OF IN-PLANE STRAIN ε_2 SUPERIMPOSED ON DEFORMATION AT THE END OF THE LAST LOAD STEP (GRIP T2)

5.3.7 Two-Layer Zylon Model.

Figure 5-27 and table 5-9 show the comparison between the static test and the results obtained from the FEA. The two layers of Zylon are modeled as one layer of finite elements with the thickness twice that of one layer of Zylon fabric.

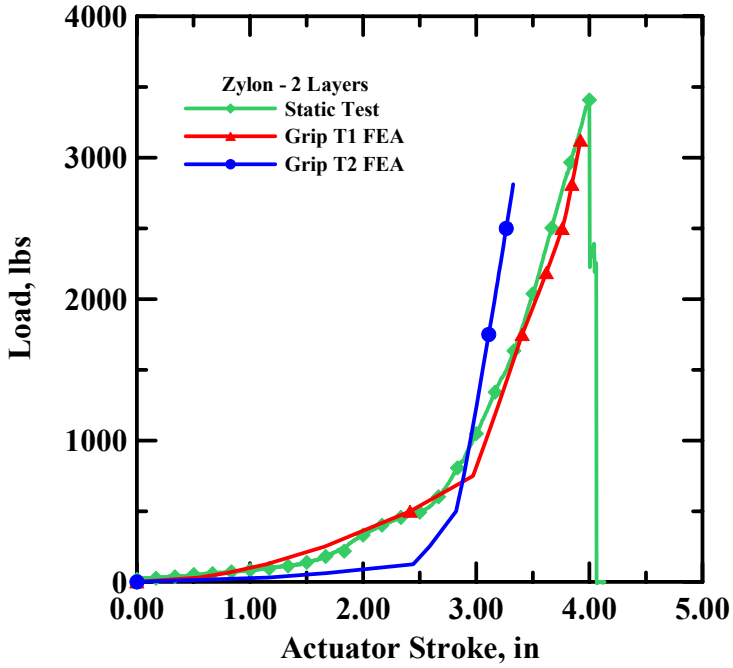

FIGURE 5-27. COMPARISON OF THE LOAD-DISPLACEMENT GRAPHS FOR A TWO-LAYER ZYLON TEST

TABLE 5-9. STATIC TEST—FEA COMPARISON FOR A TWO-LAYER ZYLON TEST

	Static Test Zring2_1	Grip T1 FEA	Grip T2 FEA
Peak load (lb)	3408	3125	2813
Displacement at peak load (in.)	4.00	3.92	3.33

The experimental curve was slack-shifted by 0.47″.

Observations for two-layer Zylon simulation:

Grip T1 FEA model:

1. Largest strain range (%)

   - Tensile 12 to 25
   - Compressive 0.03 to 0.6

2. Reason for termination of the analysis

   - Negative eigenvalues appear at the end of the load step, the solution starts to diverge.

3. Strain ranges (%)

   - Near the blunt nose 8 to 24
   - Near the clamps 6 to 8
   - In between 6 to 8

4. Contact between the fabric and the ring at the end of the simulation

   - Angle of contact (°) 286.9
   - Arc length of contact (in.) 80.1

Grip T2 FEA model:

1. Largest strain range (%)

   - Tensile 9 to 16
   - Compressive 0 to 0.6

2. Reason for termination of the analysis

   - Negative eigenvalues appear at the end of the load step, the solution starts to diverge.

3. Strain ranges (%)

   - Near the blunt nose 5 to 16
   - Near the clamps 2.2 to 5
   - In between 3.7 to 5

4. Contact between the fabric and the ring at the end of the simulation

   - Angle of contact (°) 291.8
   - Arc length of contact (in.) 81.5

Once again, the FE and experimental peak load and displacement values are quite close with the Grip T1 model. The Grip T2 model is stiffer. Less slack adjustment is required to match the initial linear slopes of the experimental and the FE graphs compared to the corresponding Kevlar models. Figures 5-28 and 5-29 show FEA with Grip T1. Figures 5-30 and 5-31 show FEA with Grip T2.

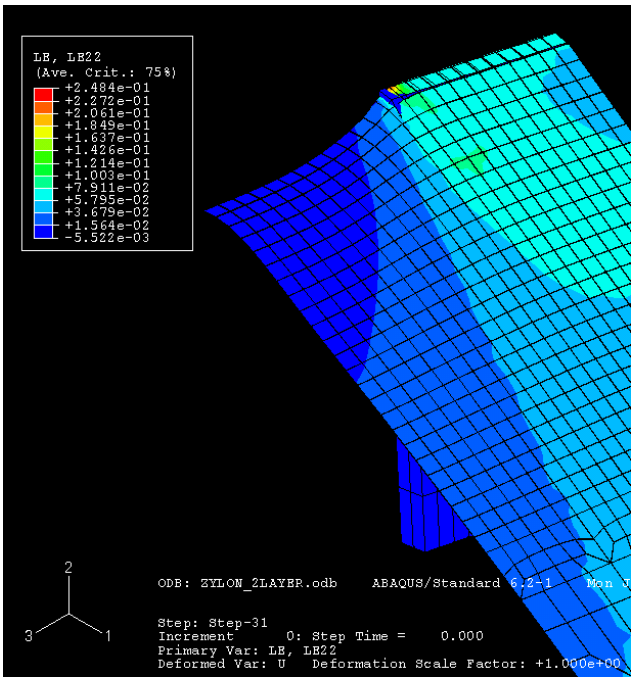

FIGURE 5-28. TWO-LAYER ZYLON—PLOT OF IN-PLANE STRAIN ε_1 SUPERIMPOSED ON DEFORMATION AT THE END OF THE LAST LOAD STEP (GRIP T1)

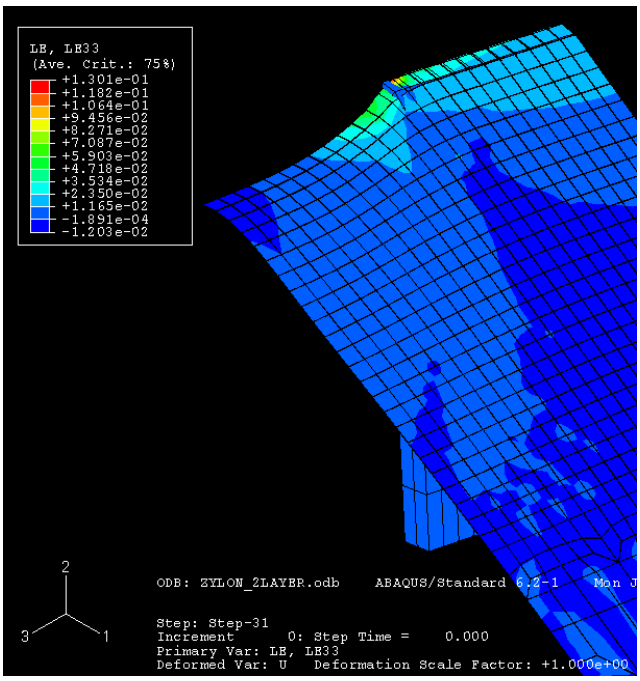

FIGURE 5-29. TWO-LAYER ZYLON—PLOT OF IN-PLANE STRAIN ε_2 SUPERIMPOSED ON DEFORMATION AT THE END OF THE LAST LOAD STEP (GRIP T1)

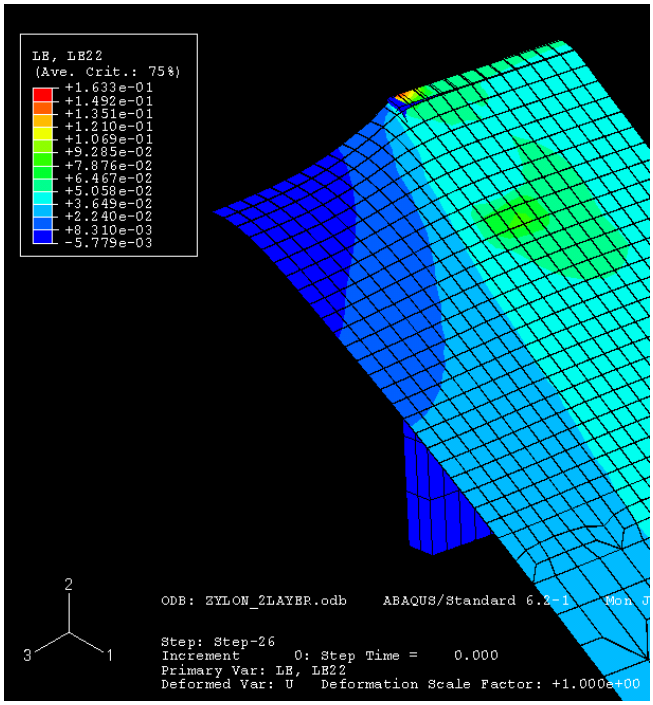

FIGURE 5-30. TWO-LAYER ZYLON—PLOT OF IN-PLANE STRAIN ε_1 SUPERIMPOSED ON DEFORMATION AT THE END OF THE LAST LOAD STEP (GRIP T2)

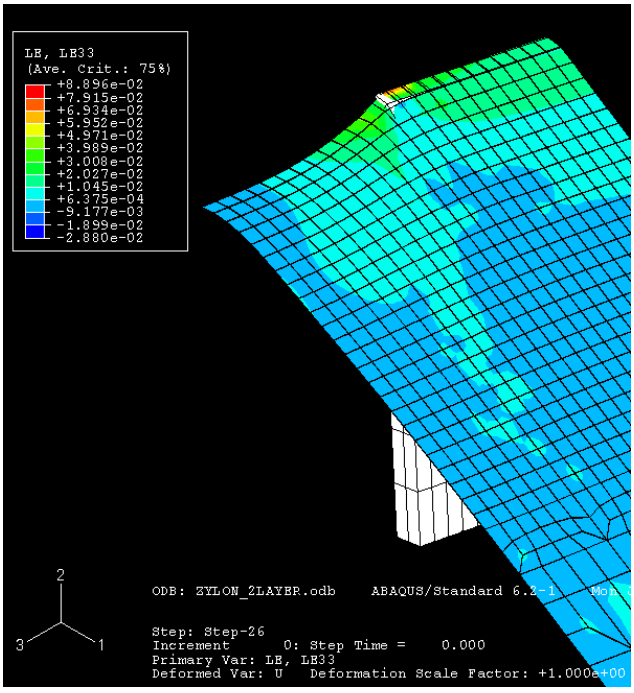

FIGURE 5-31. TWO-LAYER ZYLON—PLOT OF IN-PLANE STRAIN ε_2 SUPERIMPOSED ON DEFORMATION AT THE END OF THE LAST LOAD STEP (GRIP T2)

5.3.8 Four-Layer Zylon Model.

Figure 5-32 and table 5-10 shows the comparison between the static test and the results obtained from the FEA. The four layers of Zylon are modeled as one layer of finite elements with the thickness four times that of one layer of Zylon fabric.

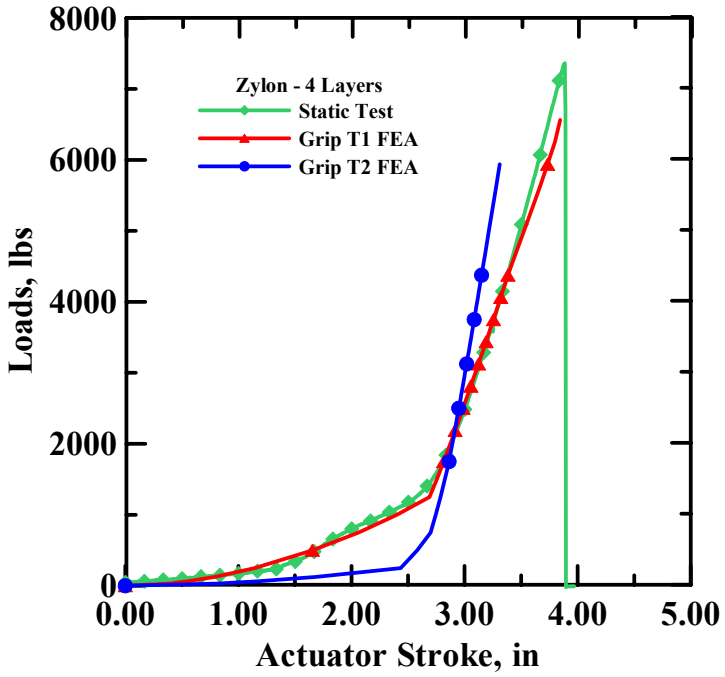

FIGURE 5-32. COMPARISON OF THE LOAD-DISPLACEMENT GRAPHS FOR A FOUR-LAYER ZYLON TEST

TABLE 5-10. STATIC TEST—FEA COMPARISON FOR A FOUR-LAYER ZYLON TEST

	Static Test Zring4_2	Grip T1 FEA	Grip T2 FEA
Peak load (lb)	7363	6563	5938
Displacement at peak load (in.)	3.88	3.85	3.31

The experimental curve was slack-shifted by 0.50″.

Observations for four-layer Zylon simulation:

Grip T1 FEA model:

1. Largest strain range (%)

   - Tensile 9 to 33
   - Compressive 0 to 1.8

2. Reason for termination of the analysis

   - Negative eigenvalues appear at the end of the load step, the solution starts to diverge.

3. Strain ranges (%)

   - Near the blunt nose 7 to 33
   - Near the clamps 7 to 10
   - In between 7 to 10

4. Contact between the fabric and the ring at the end of the simulation

   - Angle of contact (°) 287.5
   - Arc length of contact (in.) 80.3

Grip T2 FEA model:

1. Largest strain range (%)

   - Tensile 8 to 30
   - Compressive 0.004 to 3

2. Reason for termination of the analysis

   - Negative eigenvalues appear at the end of the load step, the solution starts to diverge, and there are distorted elements near the blunt nose.

3. Strain ranges (%)

   - Near the blunt nose 5 to 30
   - Near the clamps 3 to 5
   - In between 3 to 5

4. Contact between the fabric and the ring at the end of the simulation

   - Angle of contact (°) 291.7
   - Arc length of contact (in.) 81.5

The trends observed with the one- and two-layer models continue. The FE and experimental peak load and displacement values are quite close with the Grip T1 model. The Grip T2 model is stiffer. Once again, there is less slack adjustment that is required to match the initial linear slopes of the experimental and the FE graphs compared to the corresponding Kevlar models. Figures 5-33 and 5-34 show FEA with Grip T1. Figures 5-35 and 5-36 show FEA with Grip T2.

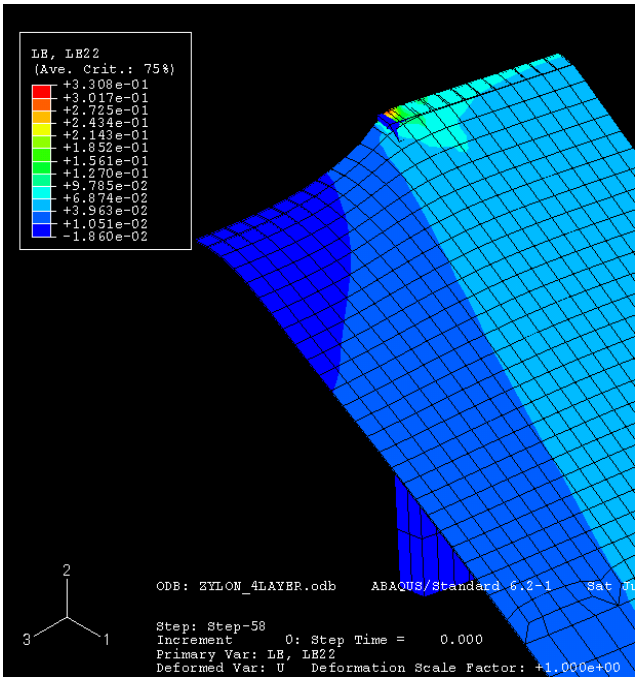

FIGURE 5-33. FOUR-LAYER ZYLON—PLOT OF IN-PLANE STRAIN ε_1 SUPERIMPOSED ON DEFORMATION AT THE END OF THE LAST LOAD STEP (GRIP T1)

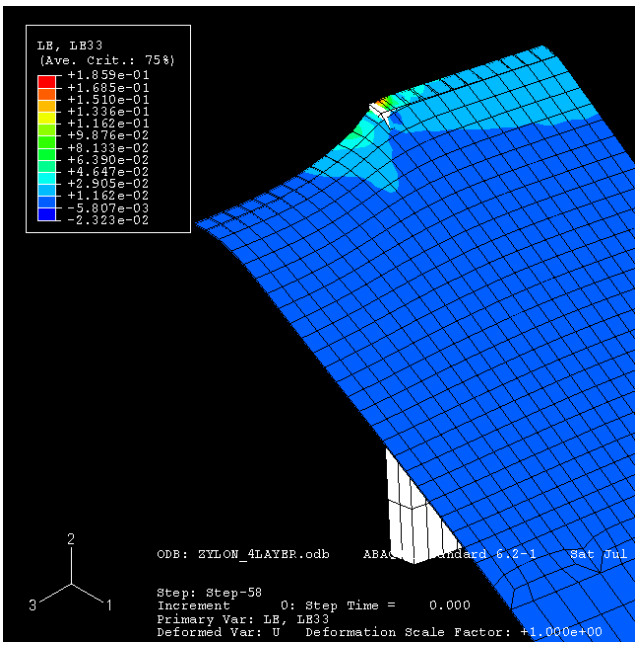

FIGURE 5-34. FOUR-LAYER ZYLON—PLOT OF IN-PLANE STRAIN ε_2 SUPERIMPOSED ON DEFORMATION AT THE END OF THE LAST LOAD STEP (GRIP T1)

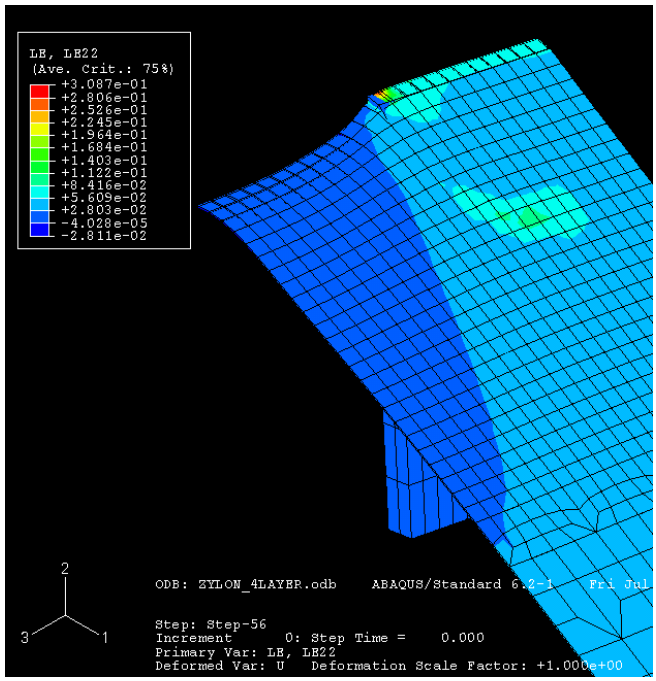

FIGURE 5-35. FOUR-LAYER ZYLON—PLOT OF IN-PLANE STRAIN ε_1 SUPERIMPOSED ON DEFORMATION AT THE END OF THE LAST LOAD STEP (GRIP T2)

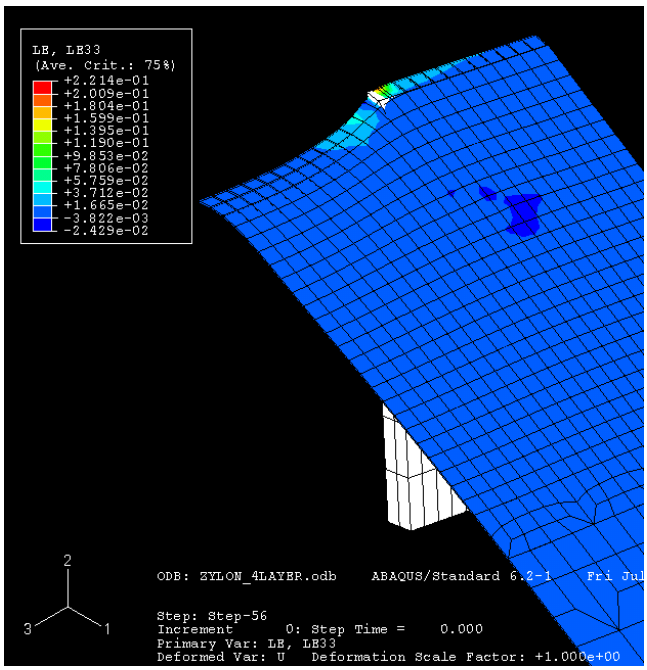

FIGURE 5-36. FOUR-LAYER ZYLON—PLOT OF IN-PLANE STRAIN ε_2 SUPERIMPOSED ON DEFORMATION AT THE END OF THE LAST LOAD STEP (GRIP T2)

5.3.9 Eight-Layer Zylon Model.

Figure 5-37 and table 5-11 show the comparison between the static test and the results obtained from the FEA. The eight layers of Zylon are modeled as one layer of finite elements with the thickness eight times that of one layer of Zylon fabric.

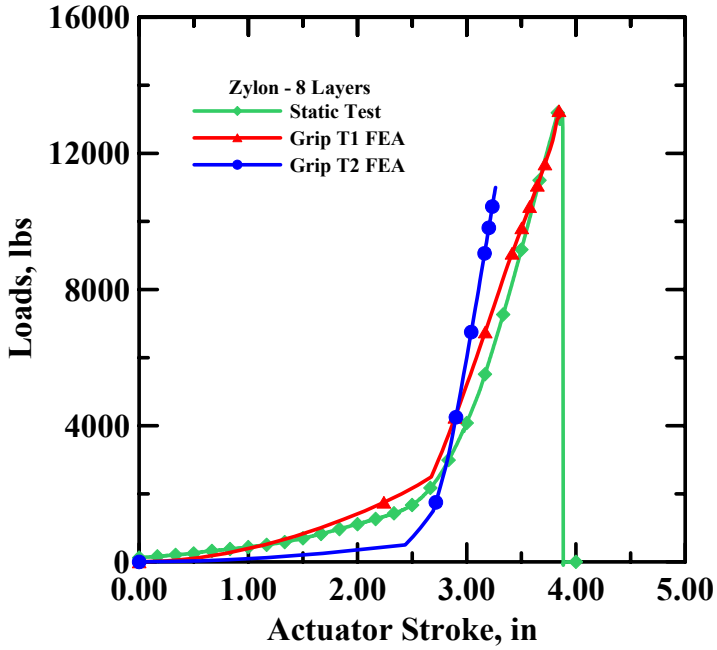

FIGURE 5-37. COMPARISON OF THE LOAD-DISPLACEMENT GRAPHS FOR AN EIGHT-LAYER ZYLON TEST

TABLE 5-11. STATIC TEST—FEA COMPARISON FOR AN EIGHT-LAYER ZYLON TEST

	Static Test Zring8_2	Grip T1 FEA	Grip T2 FEA
Peak load (lb)	13290	13250	11000
Displacement at peak load (in.)	3.72	3.84	3.26

The experimental curve was slack-shifted by 0.84″.

Observations for eight-layer Zylon simulation:

Grip T1 FEA model:

1. Largest strain range (%)

   - Tensile 10 to 35
   - Compressive 0 to 2.3

2. Reason for termination of the analysis

   - End of load steps, analysis completed successfully.

3. Strain ranges (%)

   - Near the blunt nose 7 to 35
   - Near the clamps 7 to 10
   - In between 7 to 10

4. Contact between the fabric and the ring at the end of the simulation

   - Angle of contact (°) 287.5
   - Arc length of contact (in.) 80.3

Grip T2 FEA model:

1. Largest strain range (%)

   - Tensile 9 to 20
   - Compressive 1.5 to 2

2. Reason for termination of the analysis

   - Negative eigenvalues appear at the end of the load step, the solution starts to diverge.

3. Strain ranges (%)

   - Near the blunt nose 5 to 20
   - Near the clamps 2 to 5
   - In between 3.5 to 5.5

4. Contact between the fabric and the ring at the end of the simulation

   - Angle of contact (°) 292.3
   - Arc length of contact (in.) 81.6

The trends observed with the one-, two-, and four-layer models continue. The FE and experimental peak load and displacement values are quite close with the Grip T1 model. The Grip T2 model is stiffer. Figures 5-38 and 5-39 show FEA with Grip T1. Figures 5-40 and 5-41 show FEA with Grip T2.

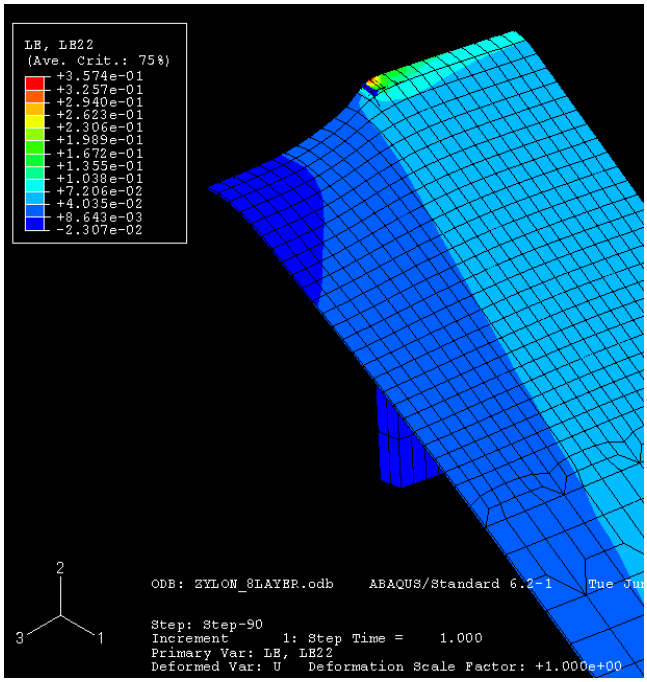

FIGURE 5-38. EIGHT-LAYER ZYLON—PLOT OF IN-PLANE STRAIN ε_1 SUPERIMPOSED ON DEFORMATION AT THE END OF THE LAST LOAD STEP (GRIP T1)

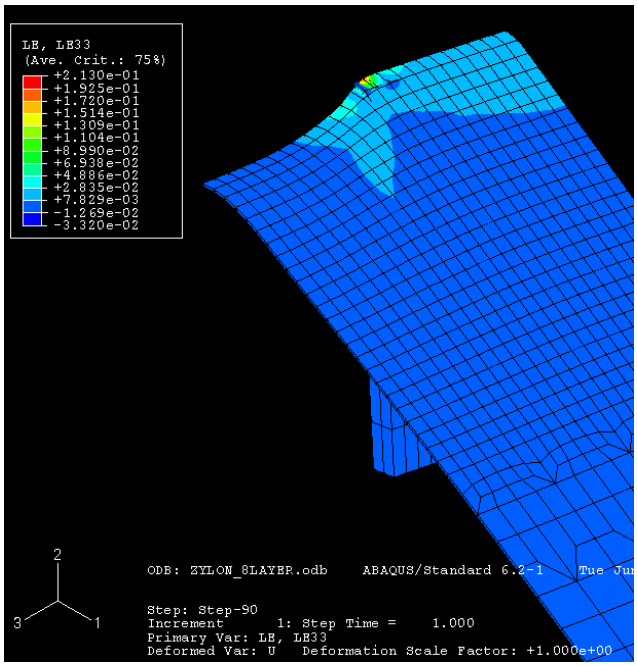

FIGURE 5-39. EIGHT-LAYER ZYLON—PLOT OF IN-PLANE STRAIN ε_2 SUPERIMPOSED ON DEFORMATION AT THE END OF THE LAST LOAD STEP (GRIP T1)

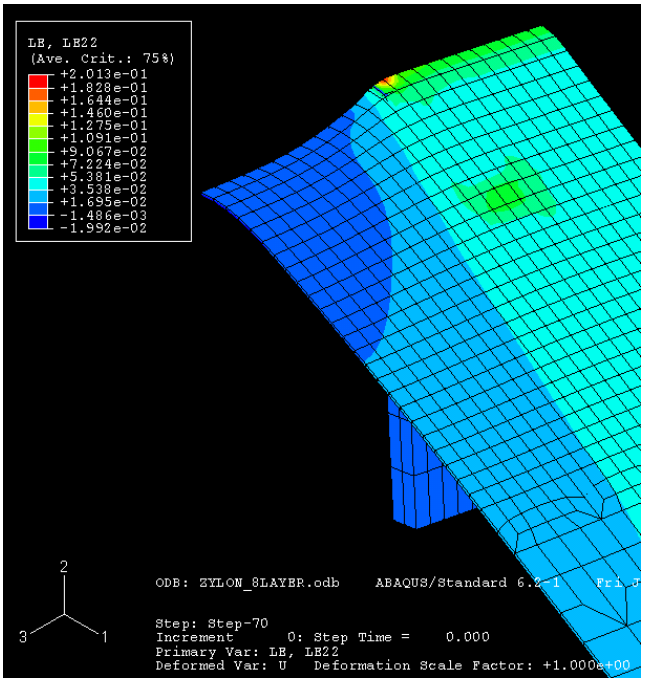

FIGURE 5-40. EIGHT-LAYER ZYLON—PLOT OF IN-PLANE STRAIN ε_1 SUPERIMPOSED ON DEFORMATION AT THE END OF THE LAST LOAD STEP (GRIP T2)

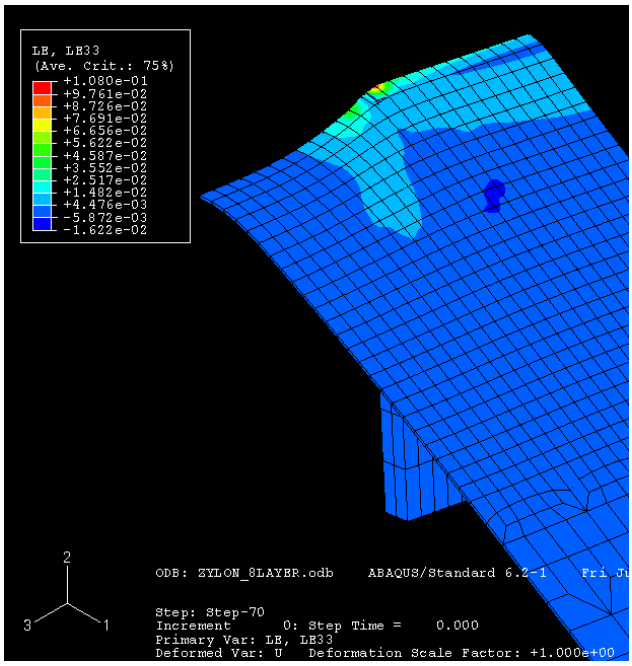

FIGURE 5-41. EIGHT-LAYER ZYLON—PLOT OF IN-PLANE STRAIN ε_2 SUPERIMPOSED ON DEFORMATION AT THE END OF THE LAST LOAD STEP (GRIP T2)

5.3.10 Twenty-Four-Layer Zylon Model.

Figure 5-42 and table 5-12 show the comparison between the static test and the results obtained from the FEA. The twenty-four layers of Zylon are modeled with three layers of finite elements with the thickness of each layer being eight times that of one layer of Zylon fabric. The experimental curve was slack-shifted by 0.2″. Both Grip T1 and Grip T2 FEA underpredicted the peak load. This was because of the limitations of the nonlinear FEA that is discussed at the end of this section. See figures 5-43 through 5-46.

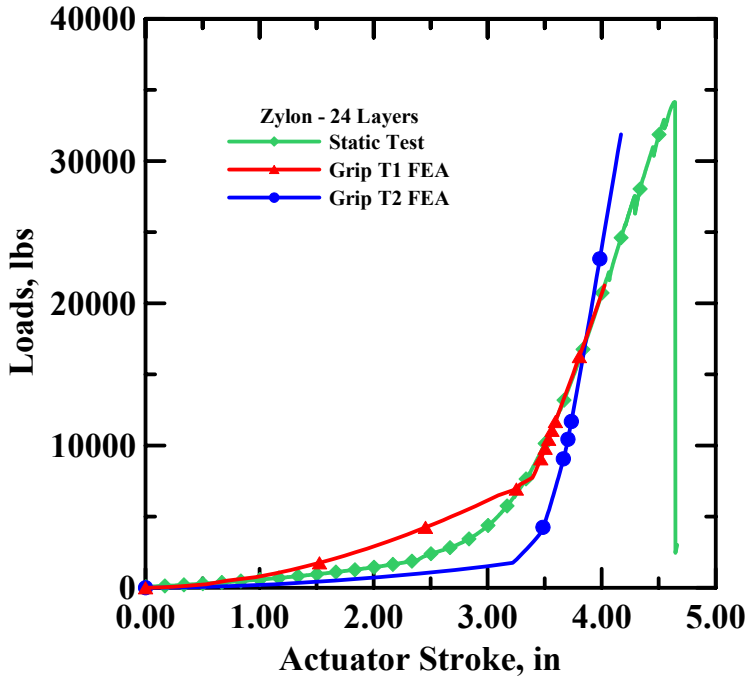

FIGURE 5-42. COMPARISON OF THE LOAD-DISPLACEMENT GRAPHS FOR A 24-LAYER ZYLON TEST

TABLE 5-12. STATIC TEST—FEA COMPARISON FOR A 24-LAYER ZYLON TEST

	Static Test Zring24_1	Grip T1 FEA	Grip T2 FEA
Peak load (lb)	34149	21250	31875
Displacement at peak load (in.)	4.64	4.03	4.17

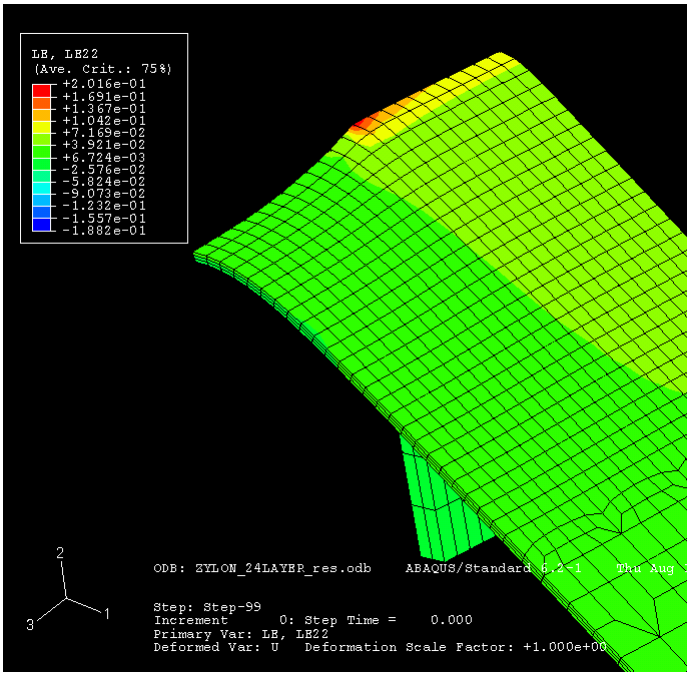

FIGURE 5-43. TWENTY-FOUR-LAYER-ZYLON—PLOT OF IN-PLANE STRAIN ε_1 SUPERIMPOSED ON DEFORMATION AT THE END OF THE LAST LOAD STEP (GRIP T1)

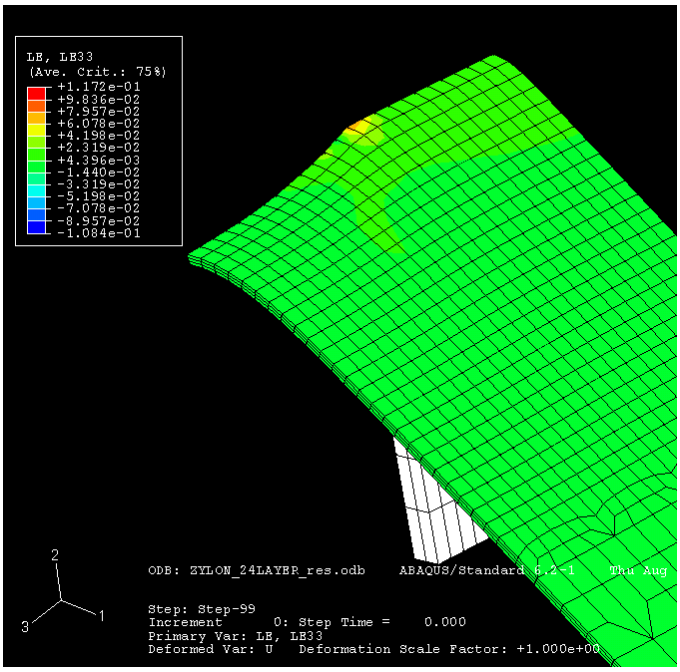

FIGURE 5-44. TWENTY-FOUR-LAYER-ZYLON—PLOT OF IN-PLANE STRAIN ε_2 SUPERIMPOSED ON DEFORMATION AT THE END OF THE LAST LOAD STEP (GRIP T1)

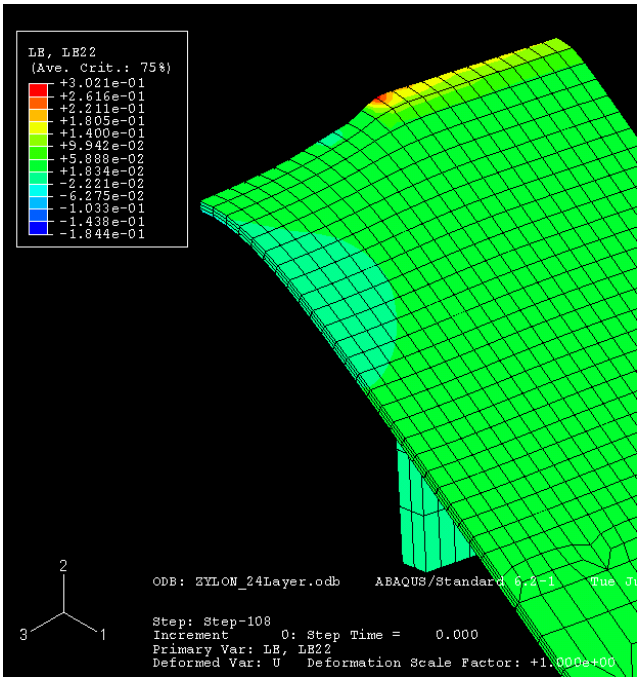

FIGURE 5-45. TWENTY-FOUR-LAYER ZYLON—PLOT OF IN-PLANE STRAIN ε_1 SUPERIMPOSED ON DEFORMATION AT THE END OF THE LAST LOAD STEP (GRIP T2)

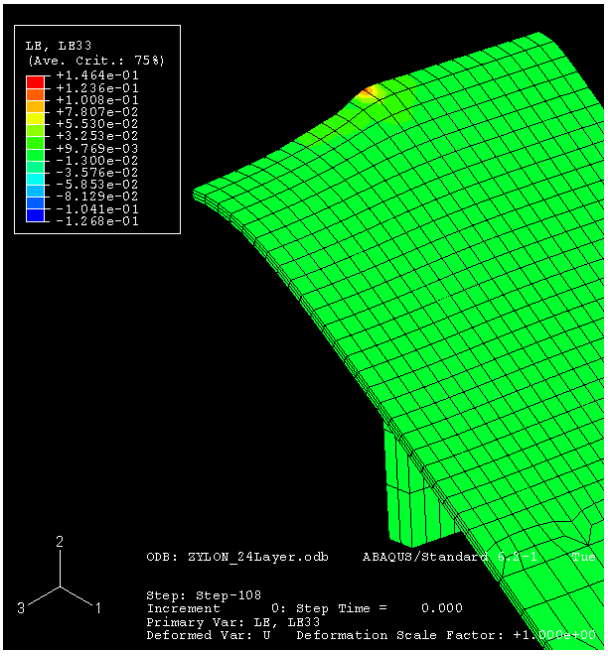

FIGURE 5-46. TWENTY-FOUR-LAYER ZYLON—PLOT OF IN-PLANE STRAIN ε_2 SUPERIMPOSED ON DEFORMATION AT THE END OF THE LAST LOAD STEP (GRIP T2)

Observations for 24-layer Zylon simulation:

Grip T1 FEA model:

1. Largest strain range (%)

    - Tensile 16 to 20
    - Compressive 1.5 to 4.4

2. Reason for termination of the analysis

    - Overclosure of contact surfaces, convergence judged unlikely.

3. Strain ranges (%)

    - Near the blunt nose 7 to 20
    - Near the clamps 6 to 7
    - In between 6 to 7

4. Contact between the fabric and the ring at the end of the simulation

    - Angle of contact (°) 286
    - Arc length of contact (in.) 79.9

Grip T2 FEA model:

1. Largest strain range (%)

    - Tensile 14 to 30
    - Compressive 0 to 3

2. Reason for termination of the analysis

    - Negative eigenvalues appear at the end of the load step, the solution starts to diverge, and distorted elements occur near the blunt nose.

3. Strain ranges (%)

    - Near the blunt nose 6 to 30
    - Near the clamps 6 to 10
    - In between 6 to 10

4. Contact between the fabric and the ring at the end of the simulation

    - Angle of contact (°) 285
    - Arc length of contact (in.) 79.6

For all the Kevlar and Zylon simulations, the following observations were made.

1. The maximum tensile strain in the fabric occurs at the area in contact with the edge of the blunt nose. This is consistent with the failure mode that is observed (during the static tests) to initiate at and around the blunt nose contact region. The strain gradient is very high near the edges of the blunt nose and decreases very rapidly away from the blunt nose. Strain values greater than the ultimate strain value are found in all the FE simulations. This is because finite elements are not deleted when the ultimate strain values are exceeded. However, this high strain zone is very localized.

2. The highest compressive strains occur in the fabric at (a) the end diametrically opposite to the blunt nose and (b) at the edge of the fabric near the blunt nose. These compressive strains are prominent only after the postpeak stiffness value was reached. A fabric-draping effect is seen in the deformed plot that is more prominent with Zylon specimens than with Kevlar specimens.

3. The FE load-displacement curves track the experimentally obtained curve quite nicely, up until the peak load. In the case of Zylon, the stress-strain curve from the T1 test performs better than the T2-generated curve. When the multiple-layer results are compared to the FE-obtained curves, the FE results indicate a stiffer model or behavior. This is probably because, in the FEA, only one equivalent fabric layer is modeled.

4. Termination of the FEA takes place when the (a) solution starts diverging due to the presence of negative eigenvalues in the system stiffness matrix (matrix is not positive definite) or (b) contact surface between the fabric and the blunt nose cannot be resolved at large displacement values.

5.4 ENERGY ABSORPTION COMPARISONS.

The energy absorption data obtained from the analysis of static tests and FE simulation are tabulated in table 5-13. It should be noted that the energy-absorbed values only represent the load-deflection curve until the peak load, as the simulation cannot be carried beyond the peak load.

TABLE 5-13. SUMMARY OF ENERGY ABSORPTION DATA (PREPEAK) FOR STATIC TEST AND FE SIMULATIONS

Specimen	No. of Layers	Energy-Absorbed Data (lb-in.)		
		Static Test	FEA Simulation	
Kevlar 17x17	1	1260	1227	
	2	2371	1992	
	4	4503	3611	
	8	9907	6877	
	24	37434	19548	
Zylon 35x35			Grip T1	Grip T2
	1	1323	1048	574
	2	2906	2520	1039
	4	6105	5577	2250
	8	9499	11178	3954
	24	32526	24390	14120

The differences in the energy absorption values are mainly due to (1) premature termination of the FEA before the peak load value is reached and (2) the FE model being inherently stiffer. Figures 5-47 to 5-52 show the comparison of the energy-absorbed values of static tests and the simulations.

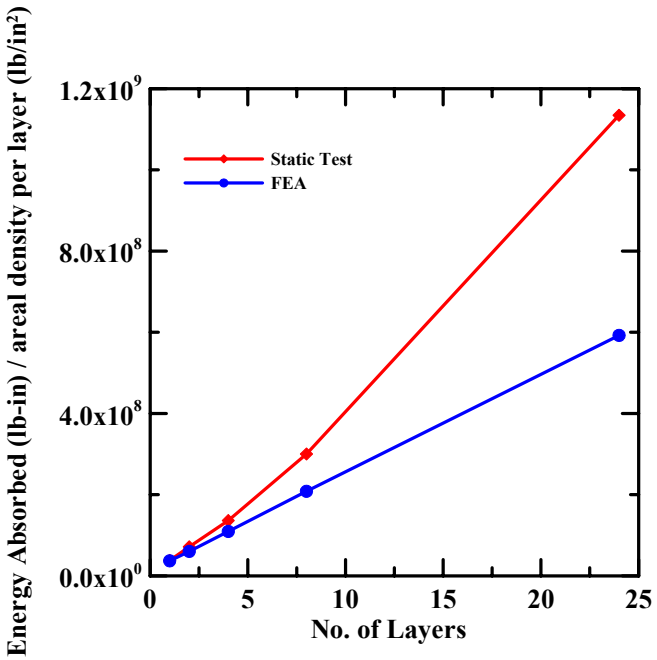

FIGURE 5-47. ENERGY-ABSORBED/AREAL DENSITY GRAPHS FOR 1-, 2-, 4-, 8-, AND 24-LAYER KEVLAR SAMPLES

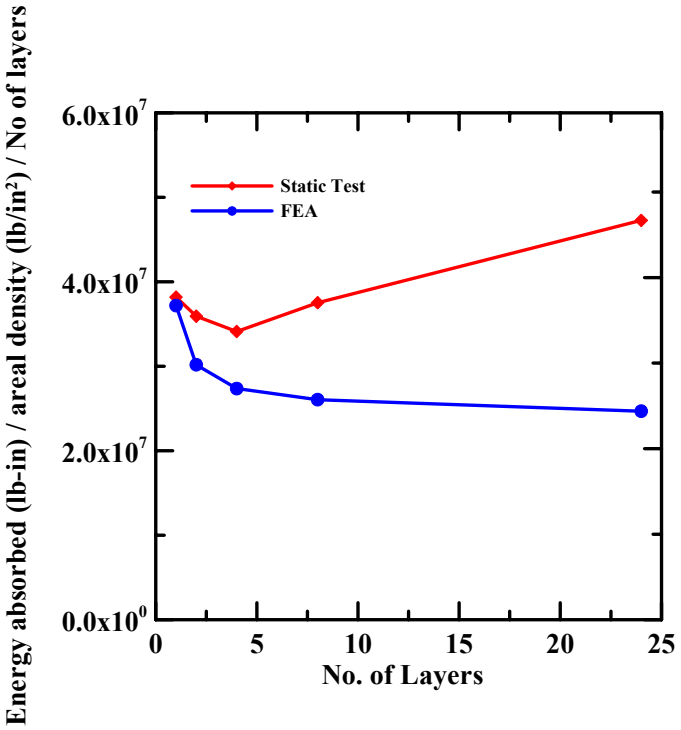

FIGURE 5-48. ENERGY-ABSORBED/AREAL DENSITY GRAPHS OF 1-, 2-, 4-, 8-, AND 24-LAYER KEVLAR NORMALIZED BY THE NUMBER OF LAYERS

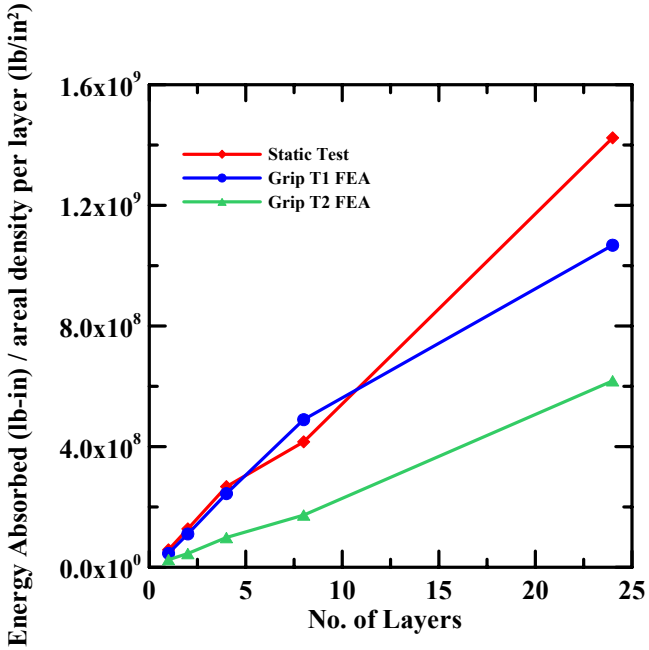

FIGURE 5-49. ENERGY-ABSORBED/AREAL DENSITY GRAPHS FOR 1-, 2-, 4-, 8-, AND 24-LAYER ZYLON SAMPLES

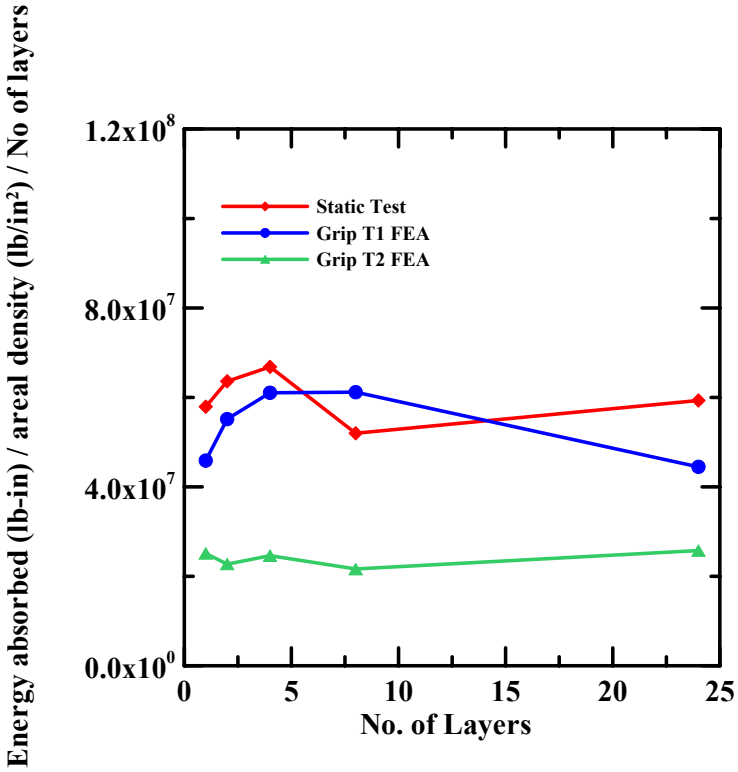

FIGURE 5-50. ENERGY-ABSORBED/AREAL DENSITY GRAPHS OF 1-, 2-, 4-, 8-, AND 24-LAYER ZYLON NORMALIZED BY THE NUMBER OF LAYERS

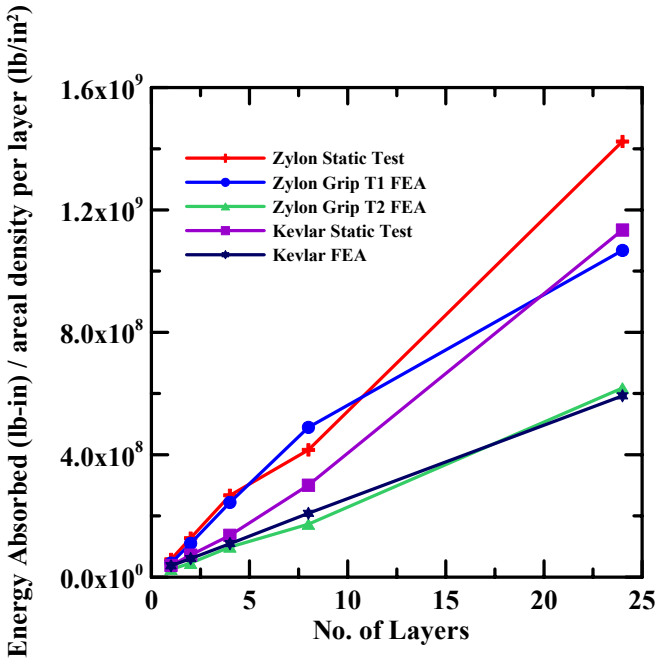

FIGURE 5-51. ENERGY-ABSORBED/AREAL DENSITY GRAPHS FOR ALL KEVLAR AND ZYLON SAMPLES

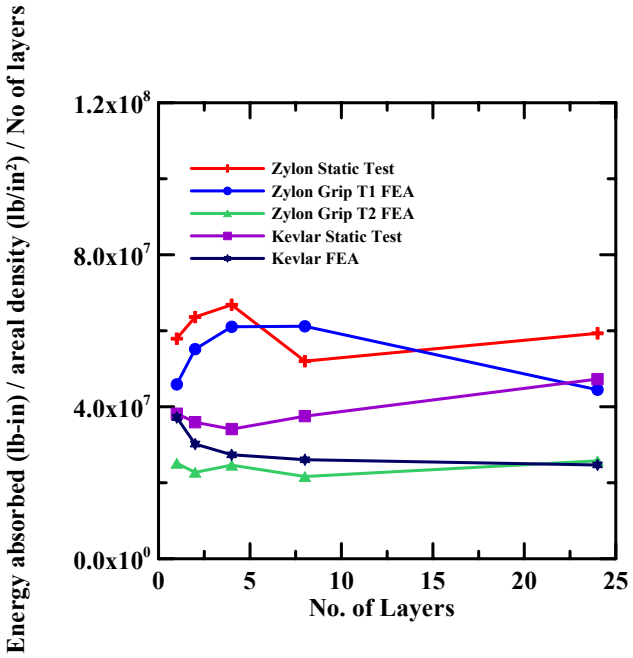

FIGURE 5-52. ENERGY-ABSORBED/AREAL DENSITY GRAPHS FOR ALL KEVLAR AND ZYLON SAMPLES NORMALIZED BY THE NUMBER OF LAYERS

The following deficiencies exist in the FE modeling and simulations.

1. The material model is essentially driven by the results from simple tension tests. The modulus of elasticity along the principal material direction was obtained from the tests, and all the other material constants were adjusted based on this value. Tests could be conducted to obtain additional material constants. This approach can then be combined with more sophisticated analytical/numerical approaches in constructing the material model for different weaves and ply counts without resorting to expensive testing procedures. Bridging the gap between the microfabric model and the macrofabric model suitable for use in an FEA was a challenge.

2. The FEA does not account for damage accumulation and progressive failure. It would be desirable to delete elements from the model that represent broken yarns. This may explain why some of the FE results overpredicted the strength of the test specimen.

3. Dry fabrics do not have any appreciable compressive strength. However, the compressive behavior was taken to be similar to the last linear segment tensile behavior.

4. The FE results for the 8 and 24 layers indicated that the FE model is stiffer than the experiments. This was to be expected, since FE models are inherently stiff to begin with. Modeling changes could be made to improve the results such as using a finer mesh, etc.

While the results obtained in this research program were extremely encouraging, further improvements to the FE modeling are recommended.

6. CONCLUSIONS.

The simple tension tests were performed on a number of Kevlar® and Zylon® fabrics to determine the stress-strain relationship in the principal material direction. Response of fabrics to adhesion was determined in the splice tests. It was found that adhesion was a problem especially for Zylon. Hence, it was decided to clamp the fabric specimens to the steel ring in the static ring tests. These tests facilitated an understanding of the performance in terms of strength, stiffness, and energy absorption capacity for Kevlar and Zylon in terms of single- and multiple-layers of fabrics. User-defined materially nonlinear, large displacement, multiple-contact surface finite element analyses were carried out in ABAQUS to compare the finite element simulation results with those obtained experimentally.

The finite element modeling and the results are extremely encouraging. This is the first time large-scale experimental results (mimicking the use of dry fabrics in engine containment systems) have been compared to results obtained from a finite element analysis. However, as noted earlier in the report, there is a need for improvements both in the experiments and the finite element simulations.

7. REFERENCES.

1. ABAQUS, INC., ABAQUS Version 6.2, Providence, R.I., 2002.
2. ABAQUS, INC., ABAQUS/Standard User Manual, Volume III, Providence, RI, 2002.

APPENDIX A—STATIC TEST RESULTS

Additional graphs (load-deflection curves) and pictures of the specimens after the tests are shown in figuresA-1 through A-30.

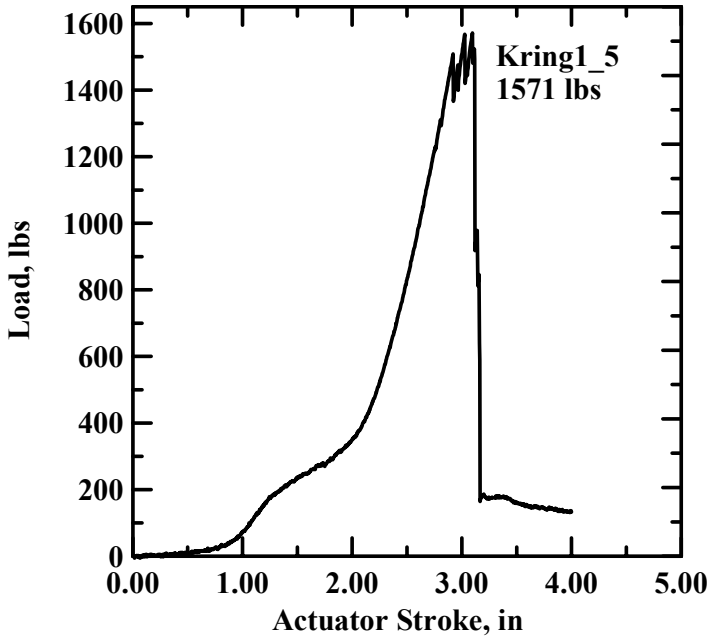

FIGURE A-1. LOAD DEFORMATION RESPONSE OF A ONE-LAYER KEVLAR SAMPLE

FIGURE A-2. FAILURE AROUND THE BLUNT NOSE CONTACT POINT, PARTIAL PENETRATION OF NOSE AT TOP (Kring1_5)

FIGURE A-3. REMOTE FAILURE AT THE CLAMP POSITION (Kring1_5)

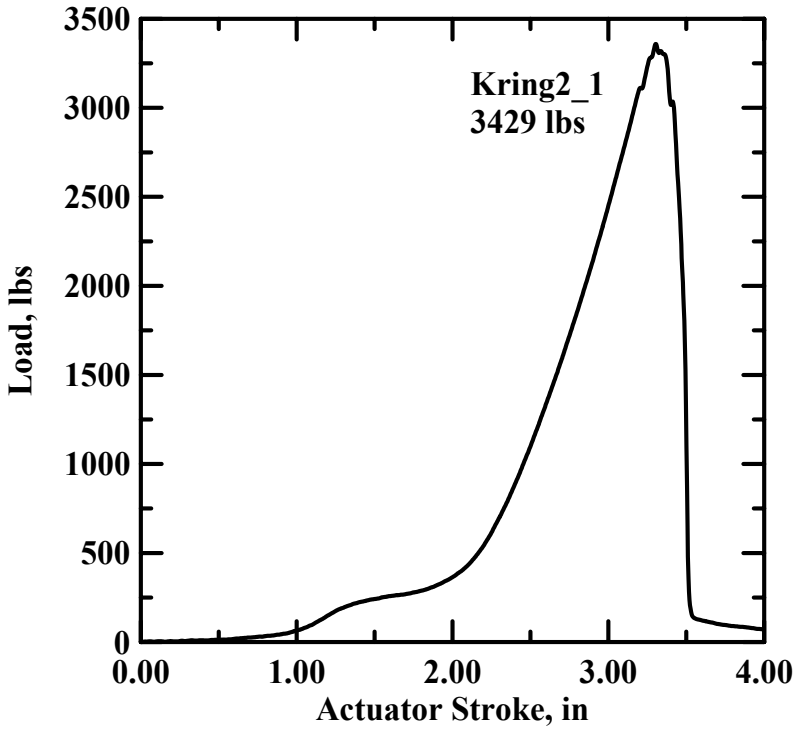

FIGURE A-4. LOAD DEFORMATION RESPONSE OF A TWO-LAYER KEVLAR SAMPLE

FIGURE A-5. FAILURE AROUND THE BLUNT NOSE CONTACT POINT, PARTIAL PENETRATION OF NOSE AT THE TOP (Kring2_1)

FIGURE A-6. REMOTE FAILURE AT CLAMP POSITION (Kring2_1)

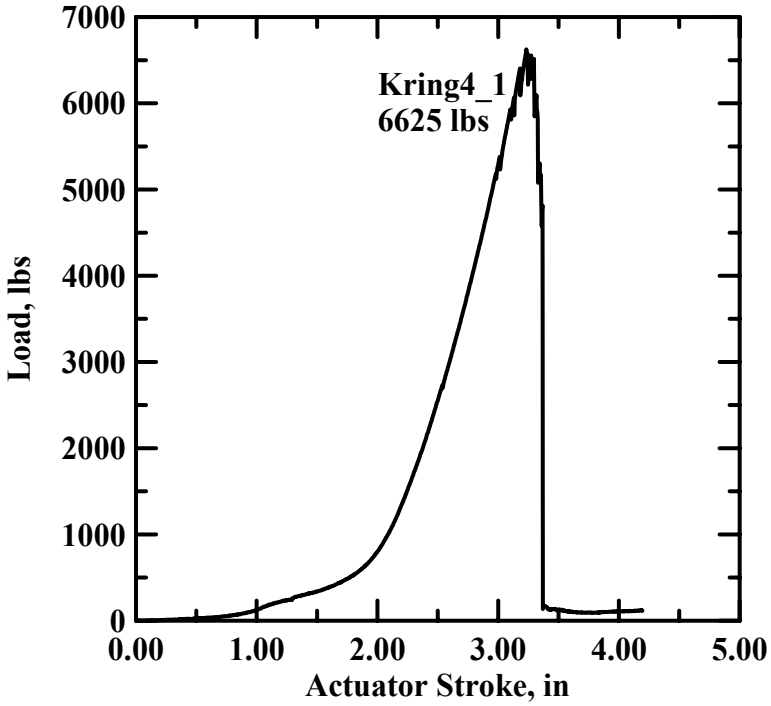

FIGURE A-7. LOAD DEFORMATION RESPONSE OF A FOUR-LAYER KEVLAR SAMPLE

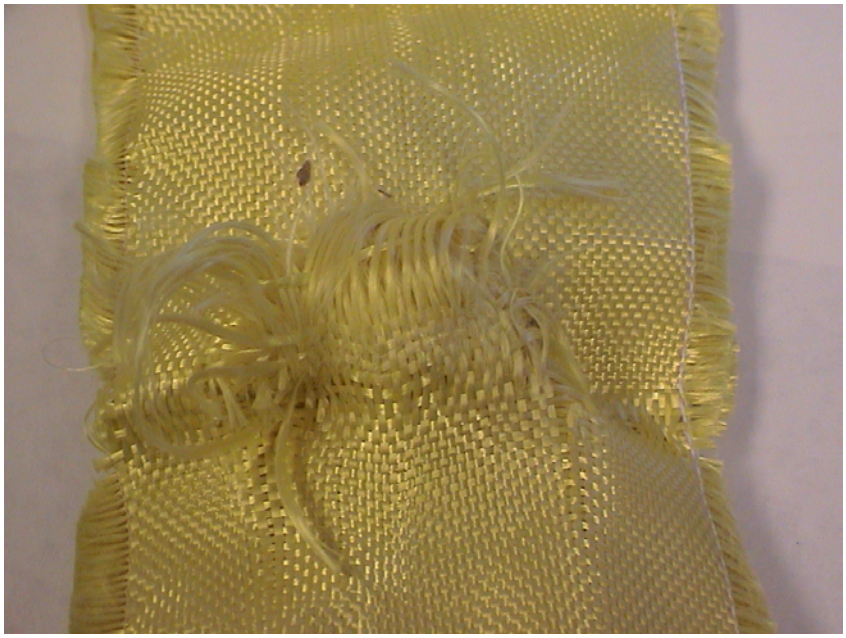

FIGURE A-8. FAILURE AROUND THE BLUNT NOSE CONTACT POINT, PARTIAL PENETRATION OF NOSE AT THE TOP (Kring4_1)

FIGURE A-9. REMOTE FAILURE AT CLAMP POSITION (Kring4_1)

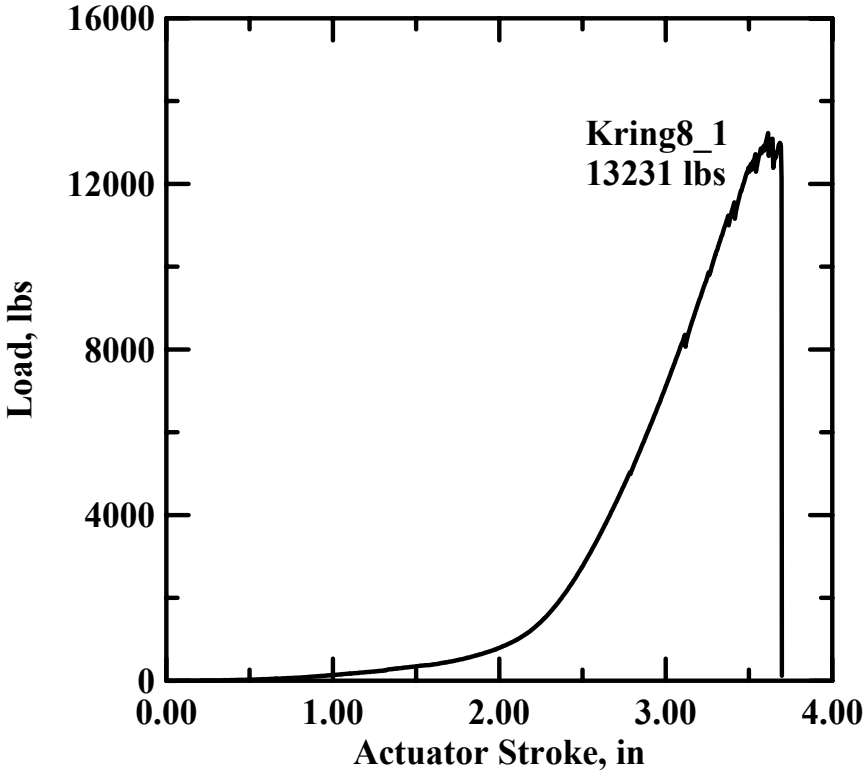

FIGURE A-10. LOAD DEFORMATION RESPONSE OF AN EIGHT-LAYER KEVLAR SAMPLE

FIGURE A-11. FAILURE AROUND THE BLUNT NOSE CONTACT POINT, PARTIAL PENETRATION OF NOSE AT THE TOP (Kring8_1)

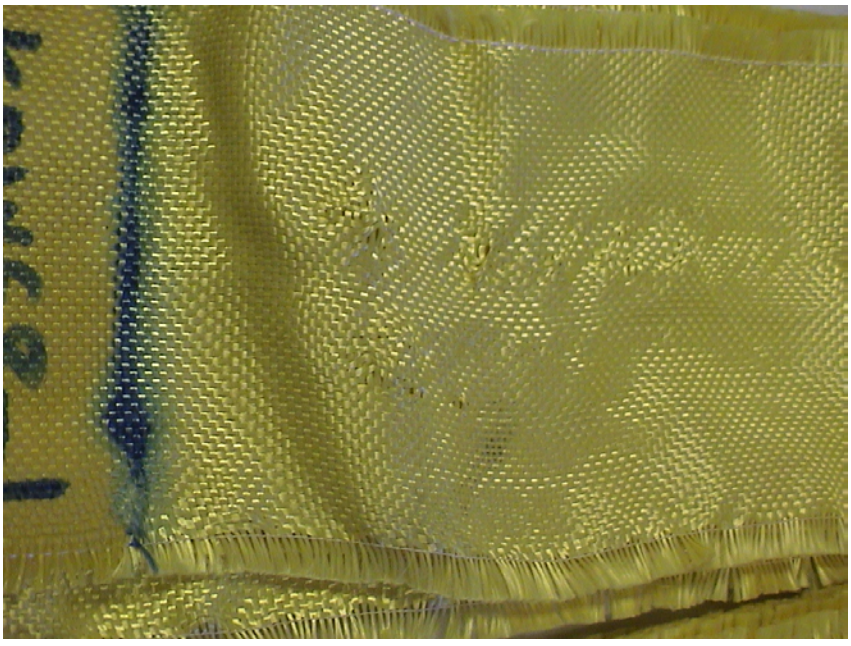

FIGURE A-12. REMOTE FAILURE AT CLAMP POSITION (Kring8_1)

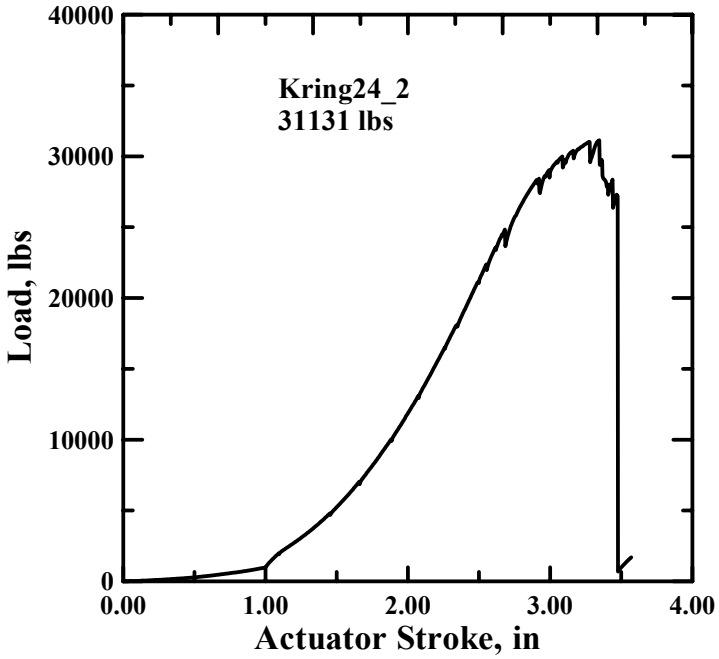

FIGURE A-13. LOAD DEFORMATION RESPONSE OF A 24-LAYER KEVLAR SAMPLE

FIGURE A-14. FAILURE AROUND THE BLUNT NOSE CONTACT POINT PARTIAL PENETRATION OF NOSE AT THE TOP (Kring24_2)

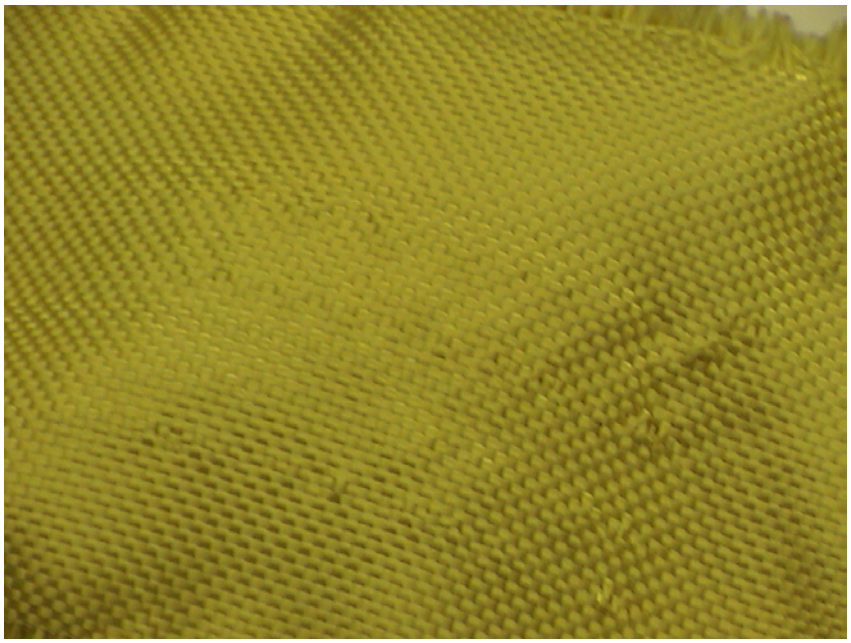

FIGURE A-15. REMOTE FAILURE AT CLAMP POSITION (Kring24_2)

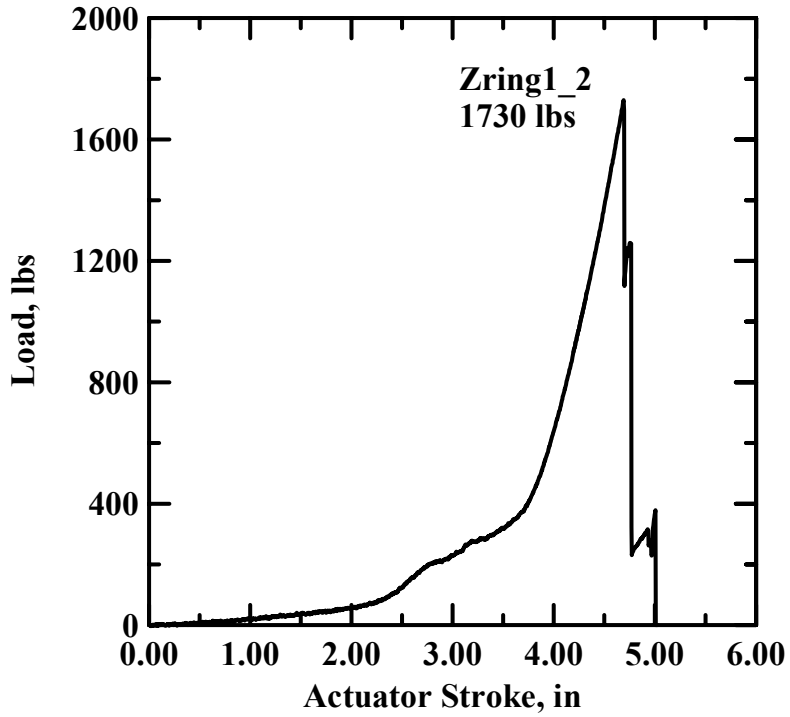

FIGURE A-16. LOAD DEFORMATION RESPONSE OF A ONE-LAYER ZYLON SAMPLE

FIGURE A-17. COMPLETE NOSE PENETRATION (Zring1_2)

FIGURE A-18. YARN PULLOUT ALONG THE CIRCUMFERENCE AT THE EDGE OF THE NOSE (Zring1_2)

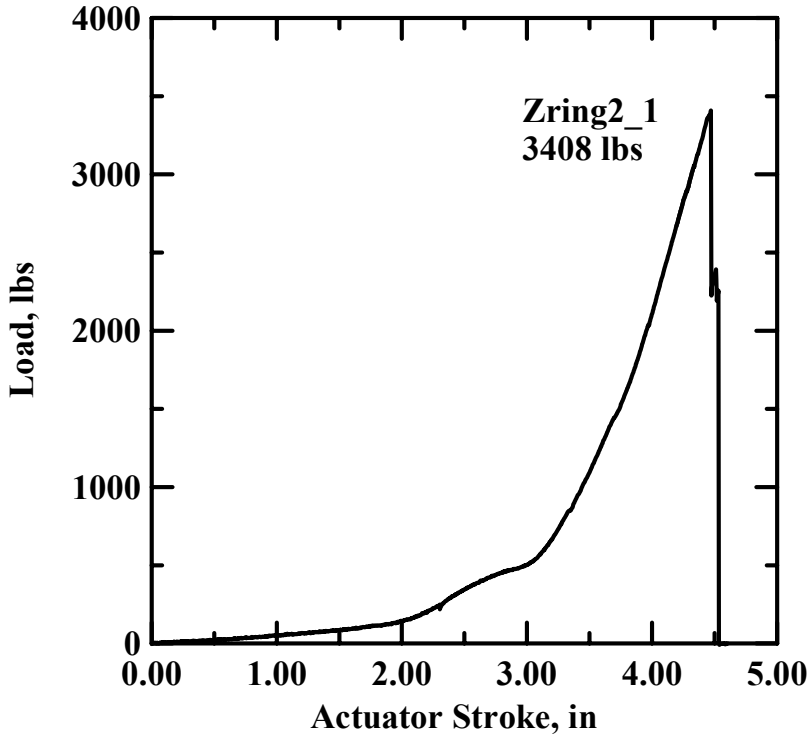

FIGURE A-19. LOAD DEFORMATION RESPONSE OF A TWO-LAYER ZYLON SAMPLE

FIGURE A-20. COMPLETE NOSE PENETRATION (Zring2_1)

FIGURE A-21. OVERLAP PEEL-OFF (Zring2_1)

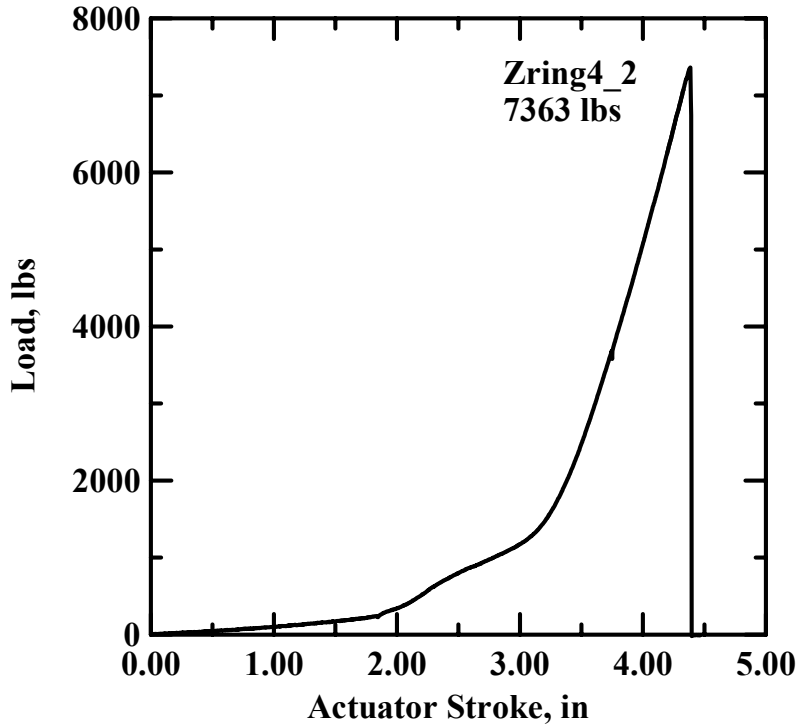

FIGURE A-22. LOAD DEFORMATION RESPONSE OF A FOUR-LAYER ZYLON SAMPLE

FIGURE A-23. COMPLETE NOSE PENETRATION (Zring4_2)

FIGURE A-24. OVERLAP PEEL-OFF (Zring4_2)

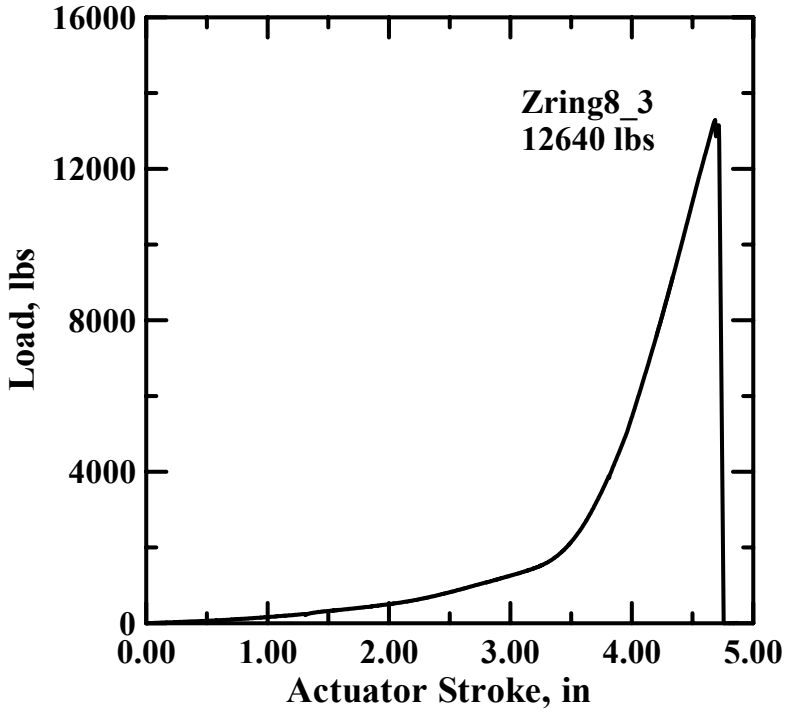

FIGURE A-25. LOAD DEFORMATION RESPONSE OF AN EIGHT-LAYER ZYLON SAMPLE

FIGURE A-26. COMPLETE NOSE PENETRATION (Zring8_3)

FIGURE A-27. FORMATION OF 2″ WIDE BAND VISIBLE ALONG THE EDGE OF THE NOSE THROUGHOUT THE CIRCUMFERENCE (Zring8_3)

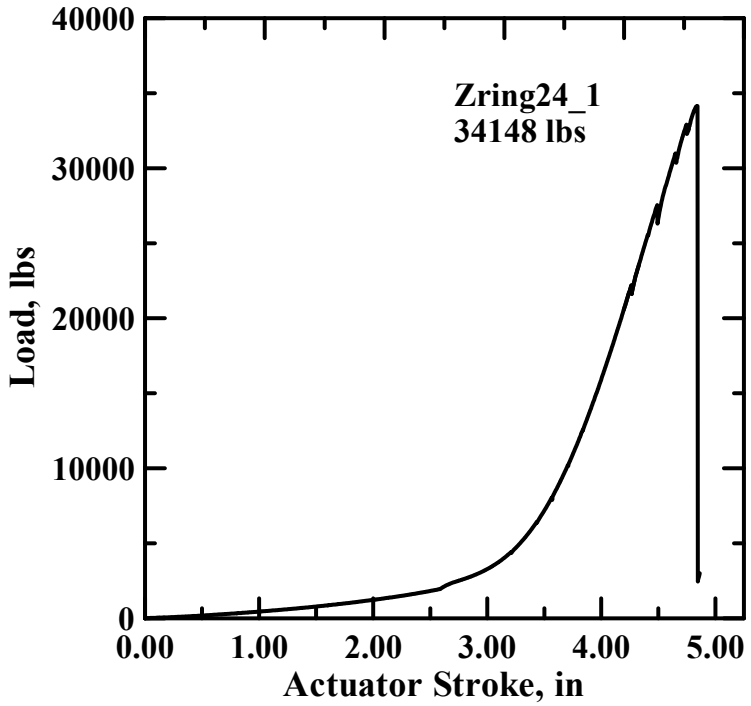

FIGURE A-28. LOAD DEFORMATION RESPONSE OF A 24-LAYER ZYLON SAMPLE

FIGURE A-29. COMPLETE NOSE PENETRATION (Zring24_1)

FIGURE A-30. FORMATION OF 2″ WIDE BAND VISIBLE ALONG THE EDGE OF THE NOSE THROUGHOUT THE CIRCUMFERENCE (Zring24_1)